Dissertation zur Erlangung des Doktorgrades

der Fakultät für Chemie und Pharmazie

der Ludwig-Maximilians-Universität München

Complementary target identification approaches for the identification of protein binding partners of phyllobilins, a family of abundant natural products

Pengyu Wang

aus Zhoukou, Henan, China

2022

Erklärung

Diese Dissertation wurde im Sinne von §7 der Promotionsordnung vom 28. November 2011 von Frau Prof. Dr. Angelika M. Vollmar betreut.

Eidesstattliche Versicherung

Diese Dissertation wurde eigenständig und ohne unerlaubte Hilfe erarbeitet.

München, den 06.05.2022

_____

Pengyu Wang

Dissertation eingereicht am: 09.06.2022
1. Gutachterin: Prof. Dr. Angelika M. Vollmar
2. Gutachter: Prof. Dr. Stefan Zahler
Mündliche Prüfung am: 05.07.2022

To my family

致我的家人

Table of Contents

SUMMARY

1 Summary

Chlorophylls (Chl) are compounds produced by plants and give them their green colour. They act as light harvesting pigments in the process of photosynthesis that converts energy from sunlight to chemical energy. As one of the “pigments of life”, chlorophylls are found in all green plants, cyanobacteria and algae.

The degradation of this green plant pigment in higher plants remained mysterious for many decades, since research on the degradation products expected coloured compounds. However, the first identified catabolite of chlorophyll turned out to be colourless, which finally set the derailed research direction back on track and opened up the stage for the discovery of new chlorophyll degradation products. Since then, more and more of these catabolites, which are now named phyllobilins, were identified and structurally elucidated. With the characteristic tetrapyrrole core and multiple modifiable side chains, phyllobilins showed a large structural diversity. With the expansion of the structural family, phyllobilins started to draw more attention to their potential physiological properties as well as pharmacological applications. Surprisingly, recent research has revealed several biological activities of phyllobilins, including anti-oxidative activity, anti-inflammatory activity and apoptosis inducing activity, contradicting the previous notion of these natural products being only waste products of a detoxification process. With developing isolation and characterization methods, we are convinced that more and more phyllobilins will be identified in different plants, and more importantly, other pharmacological activities of phyllobilins will also be discovered. Thus, phyllobilins have the potential to become established as important phytochemicals in the future.

In this work, using a modified extraction method, we identified Plane tree (*Platanus occidentalis*) as a new source of phyllobilins. With a straightforward chemical modification, we also obtained phyllobilin derivatives with enhanced anti-proliferative activities, further indicating phyllobilins as promising phytochemicals.

To develop a promising compound into a drug, finding target binding proteins is inevitable and also a large challenge. A combination of different target identification methods is thus necessary in many cases to shorten drug target discovery. Here in this work, a newly developed yeast three-hybrid system and classical affinity chromatography were used as complementary approaches to identify target proteins for phyllobilins.

Based on the yeast two-hybrid system, which was built to detect protein-protein interactions, the yeast three-hybrid system allows for the identification of small molecule-protein interaction. One drawback of the system is that the drug of interest has to be derivatized; furthermore, it has to be taken up by the yeast cells in sufficient amount. Here in this study, we established a yeast three-hybrid platform using the *Saccharomyces cerevisiae* ABC9Δ strain as a reporter strain, which features 9 efflux pump deletions and thus has a better uptake for small drugs. For a proof-of-concept screening, we exemplarily chose ethinylestradiol as small molecule candidate and screened for potential binding proteins using the yeast three-hybrid system. Procollagen-lysine 2-oxoglutarate 5-dioxygenase 2 (PLOD2) was identified as a potential target protein of ethinylestradiol, which was then confirmed by complementary affinity chromatography. Moreover, an activity assay revealed that ethinylestradiol affected PLOD2 activity. PLOD2 is responsible for the formation of stable collagen crosslinks and is known to be secreted by cells to remodel the extracellular matrix. Using fluorescence microscopy, we could show that ethinylestradiol had an impact of the formation of collagen fibers around cells.

Having confirmed the availability of our yeast three-hybrid setup, we also applied phyllobilin probes to a yeast three-hybrid screen, and unveiled NPC intracellular cholesterol transporter 2 (NPC2) and promyelocytic leukemia protein (PML) as the potential binding proteins of a phylloxanthobilin (PxB), a late stage phyllobilin with interesting bioactivities. NPC2 binds cholesterol and functions as a cholesterol transfer

protein *in vitro*, whereas PML is a tumor suppressor protein and functions in a wide range of important cellular processes. The interactions of PxB and those proteins were again validated by complementary affinity chromatography.

On the other hand, mass spectrometry-based affinity chromatography was also used to identify target binding proteins for phyllobilins, leading to a number of promising protein candidates, which need to be validated further and will be the focus of future studies.

To sum up, we expanded the source of the phyllobilin family by identifying phyllobilins from Plane tree, and modified a phyllobilin without activity on cancer cells by esterification, which led to an anti-proliferative activity in the micromolar range. To identify target proteins for bioactive phyllobilins, we established a yeast three-hybrid platform and used it to screen the model drug ethinylestradiol. PLOD2 was identified as a novel binding partner of ethinylestradiol. Furthermore, using the yeast three-hybrid system, NPC2 and PML were verified as potential target proteins of PxB and also confirmed by affinity chromatography. At last, mass spectrometry-based classical affinity chromatography revealed promising targets of phyllobilins.

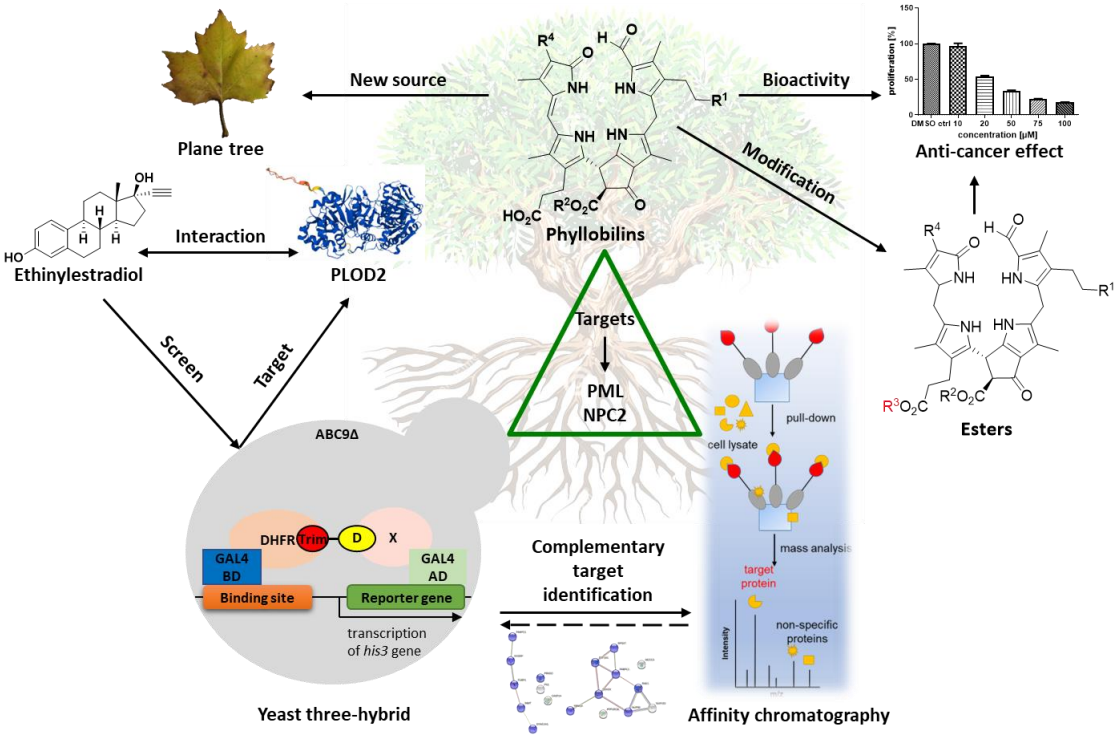

Figure 1. Overview of the project.

Complementary target identification approaches for the identification of protein binding partners of phyllobilins, a family of abundant natural products degraded from chlorophyll.

INTRODUCTION

2 Introduction

2.1 Chlorophyll breakdown

The seasonal disappearance of the green color in plant leaves due to the Chlorophyll (Chl) breakdown has long been fascinating to see as a clear indication for a programmed cell death in plants. As the most abundant pigment on Earth, it is estimated that about one billion tons of Chl are degraded per year [1], which is probably the most visual sign of life on Earth, even observable from outer space [2]. Chl is also a potential phototoxin, and therefore it has to be broken down in the course of a detoxification process [3]. Even though this Chl breakdown process is very important for understanding the basic biology of plants, the effort to find residuals of the green pigment remained obscure for a considerable amount of time, since the idea that the degradation products of colored Chl should also be colorful was the main guiding principle [4]. The breakthrough was therefore only achieved in 1991 when a colourless tetrapyrrole was identified as the first non-green catabolite of Chl [2]. The structure of this colourless and non-fluorescent Chl catabolite (NCC) of barley (*Hordeum vulgare*), termed *Hv*-NCC-1, also named rusty pigment 14 (due to its HPLC retention time) as it can be easily oxidized further, could be identified and clarified (Figure 2).

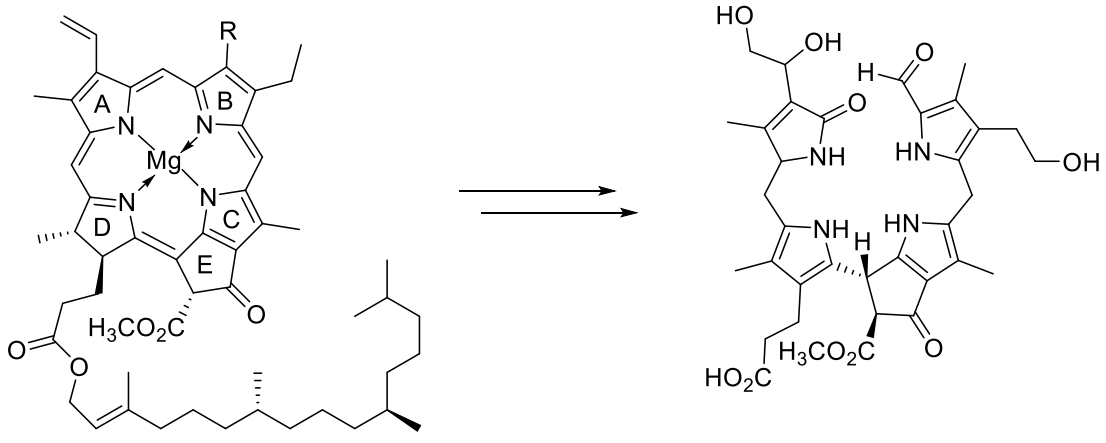

Chl *a*: R = CH_3 **Chl *b*:** R = CHO

***Hv*-NCC-1**

Figure 2. Structural formula of the first identified Chl breakdown product.

From senescent leaves of barley (*Hordeum vulgare*), the first non-fluorescent Chl catabolite (NCC), which was named phylloleucobilin (PleB) later, was identified by Kräutler and co-

workers [2], revealing a linear tetrapyrrole core structure and an additional cyclopentanone unit with a methoxycarbonyl moiety which is Chl-characteristic. The broad relevance of the tetrapyrrolic PleBs as products of Chl breakdown in higher plants was also confirmed by later studies [5, 6].

Following the initial identification of *Hv*-NCC-1 as the first verified non-fluorescent Chl catabolite (NCC), which is now named phylloleucobilin (PleB), systematic isolation from a variety of vascular plant sources, and subsequent structural work, have pathed the way for a series of structural identifications of catabolites in other plants [7], which allowed for a better understanding of the Chl breakdown process. Although there are differences in the side groups of the identified catabolites among plant species, they are all related to this breakdown process [5]. Moreover, it is now clear that the final products of this tightly controlled detoxification process are linear tetrapyrrolic catabolites - the phyllobilins (PBs).

2.2 Phyllobilins -- a family of natural products generated in the process of chlorophyll breakdown

Chl catabolites were named as phyllobilins since they are derived from chlorophyll and demonstrate a remarkable structural similarity to the much more known heme-derived bilins [8]. The common nomenclature of the phyllobilins usually uses a prefix indicating the plant source with the initials of the Latin name of the plant, and a suffix indicating the polarity (either in subsequent numbers within a plant species or using the retention time from a reversed-phase HPLC gradient used for the analysis of the plant extract), *e.g.*, *Hv*-PleB-1 for the most polar PleB from barley (*Hordeum vulgare*). The elucidation of phyllobilin structures and important enzymes contributing to Chl degradation has revealed this breakdown process to be a strictly controlled catabolic program.

2.2.1 Phyllobilins in the early stage of chlorophyll breakdown

The early phase of the Chl breakdown pathway happens in senescent chloroplasts [3]. Except for a PleB from *Arabidopsis thaliana* feathering a hydroxymethyl group at C2 [9], all of the so-far identified phyllobilins turned out to carry a typical methyl unit, indicating them to be derived from Chl *a*. However, an *in vivo* deuterium labeling experiment by Folley et al. [10] revealed that Chl *b* is converted into Chl *a* before degradation in a two-step reaction catalyzed by Chl *b* reductases (Figure 3). Since Chl *b* was shown to be biosynthesized by chlorophyllide *a* oxygenase (CAO) from chlorophyllide *a* [11], which is also an immediate precursor of Chl *a* in the biosynthetic path [12], it is this so-called Chl cycle, the Chl *a/b* interconversion, that regulates the relative levels of Chl *a* and Chl *b* throughout the development of the plant, as well as in the first step of Chl breakdown in senescent plant tissues [13].

To start, Chl *a* is converted in several steps to pheophorbide *a* (Pheo *a*) in the chloroplasts by removing the magnesium ion and hydrolysis of the phytyl ester [14]. Afterwards, the Chl breakdown continues via the today called PaO/PB pathway [6] because it involves the key enzyme pheophorbide *a* oxygenase (PaO) [15] and generates phyllobilins (PBs). By oxygenolytic opening of the macrocycle with PaO, a red Chl catabolite (RCC) is generated from Pheo *a*. RCC comprises the first 1-formyl-19-oxophyllobilin structure and is therefore the progenitor of all phyllobilins generated later during Chl breakdown [16]. RCC is then further metabolized in enzyme-bound form to a fleetingly observed intermediate, the primary fluorescent Chl catabolite (*p*FCC) [17, 18], which was also named primary phyllolumibilin (*p*PluB) later. The reduction of the C15/16 double bond of RCC is catalyzed by the RCC reductase (RCCR) [19], which has 2 isoforms and therefore induces a new stereocenter at C16 of *p*PluB, resulting in the '*n*' or '*epi*' configuration, depending on the plant species [18]. In the last step of the early stage of Chl breakdown, *p*PluB or *epi*-*p*PluB is transferred out of the chloroplast to the cytosol for further degradation (Figure 3).

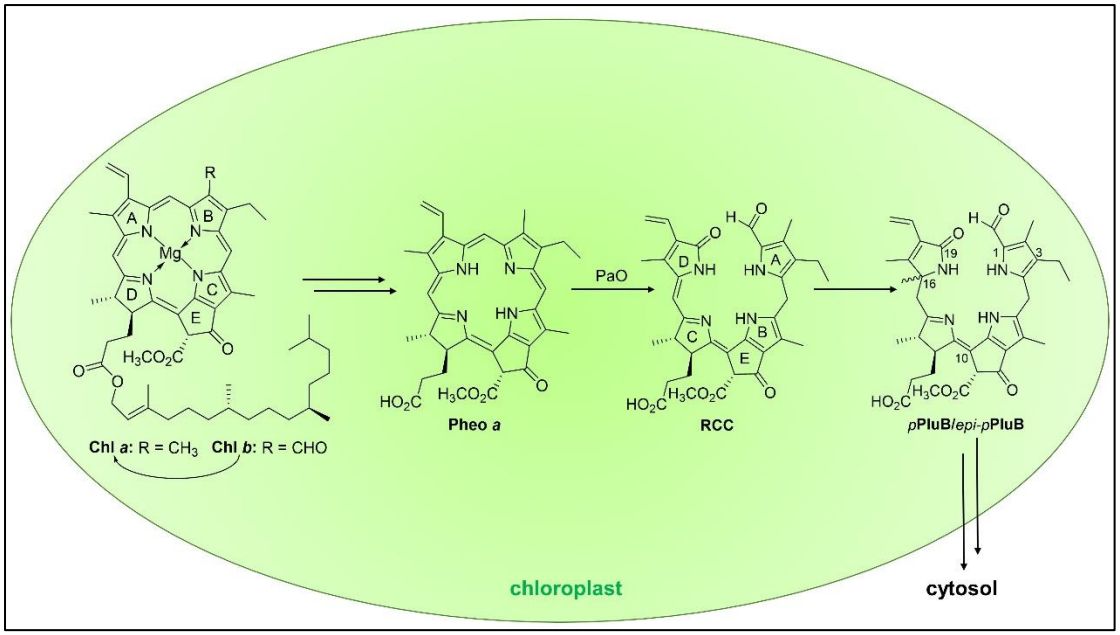

Figure 3. Chl is de-greened rapidly in a strictly regulated process to colourless, fluorescent Chl catabolites (*p*PluBs).

Overview of early stages of Chl breakdown in the chloroplast. The initial step of Chl breakdown is the degradation of Chl *a* and Chl *b* to Pheo *a* in several steps [14], followed by the key step of the so-called PaO/PB pathway to convert Pheo *a* to the PB precusor RCC by the enzyme pheophorbide *a* oxygenase (PaO) [15]. RCC is then reduced to *p*PluB or *epi-p*PluB depending on the source of the reduction enzyme [18]. At last, *p*PluBs are transferred to the cytosol for downstream modifications.

2.2.2 Phyllobilins in the later stage of chlorophyll breakdown -- type-I and type-II phyllobilins

After being transferred into the cytosol, *p*PluBs are degraded in so-far known three different ways: they are converted to modified PluBs (*m*PluBs) and directly transferred into the vacuole to generate type-I phyllobilins (1-formyl-19-oxobilin); in a different branch, they can be oxidatively deformylated at C1 [20], which generates the type-II phyllobilins (1,19-dioxobilin) lacking the original formyl moiety; or in a third pathway, they can be further modified to hypermodified PluBs (*hm*PluBs) rendering these catabolites more persistent (Figure 4).

2.2.2.1 Type I phyllobilins

In the type I phyllobilin pathway, *m*PluBs are transferred into the vacuole and isomerized to the type I phylloleucobilins (PleBs) spontaneously and rapidly due to the acidic environment in the vacuole. Surprisingly, the analysis of the nuclear Overhauser effect spectra and circular dichroism (CD) spectra of all structurally characterized known natural PleBs demonstrated the same pattern at this newly formed C10 stereocenter as an (*R*) - configuration (Figure 4) [21, 22]. PleBs are the best characterized and well-studied phyllobilins so far [23]. Compared to the phyllobilins in the early stage of Chl breakdown, one or several decorations are introduced (Figure 4). Among all those investigated modifications, the most abundant PleB so far is a 'simple' catabolite, which carries a hydroxyethyl group (R^1) at ring A [24].

Before the first insight into colored pigments from Chl breakdown was gained by Moser et al. in 2008 [25], PleBs were long considered the final products of Chl breakdown. The yellow Chl catabolites (YCCs), now named phylloxanthobilins (PxBs), were revealed to feature a C15/16 double bond and could be obtained via partial synthesis by oxidation of the PleBs. This double bond forms a conjugated π-electron system extended over ring C and D, which results in the intense yellow colour and contributes to the fall colour of senescent leaves [25]. PxBs are only found in several plant species so far [26-30], and the amount is usually lower compared to their PleB precursors, with some exceptions [29].

At the last stage of the so far investigated Chl breakdown process, pink Chl catabolites (PiCCs), which were named phylloroseobilins (PrBs) recently, were also identified. The structure elucidation of a PrB extracted from the senescent leaves of the deciduous tree *Cercidipyllum japonicum* (Katsura tree) revealed it to be the oxidation product of *Cj*-PxB, featuring an additional double bond at C10/11 position [31]. *Cj*-PrB is the only naturally found PrB so far. However, an oxidation of the corresponding PxB by

complexation with Zn(II)-ions and subsequent de-complexation was successfully performed to obtain PrB [32].

2.2.2.2 Type II phyllobilins

The first stage of the type II phyllobilin pathway is the oxidative deformylation of *p*PluBs to DPluBs. After that, similar to type I phllobilins, there are also three known stages for type II phyllobilins, featuring dioxobilin-type phylloleucobilins (DPleBs), phylloxanthobilins (DPxBs) and phylloroseobilins (DPrBs) (Figure 4). Among them, DPleBs are also the most abundant ones in the vacuoles of various plants. In the model plant *Arabidopsis thaliana*, in particular, 90% of all found phyllobilins are DPleBs [20, 33, 34].

The formation of subsequent DPxBs is considered to result from the endogenous oxidative activity [35]. Several DPxBs have been identified naturally, *e.g.*, in senescent leaves of grapevine [36] and de-greening savoy cabbage [37].

No reference has yet been found for DPrBs in nature. Only one DPrB was synthesized in the lab with the same metal complexing method as performed for the PrB by Li and co-workers [35].

2.2.2.3 *Hypermodified* phyllolumibilins

Although all studied higher plants turned out to break down Chl via a common Chl degradation pathway to generate PleBs or DPleBs, which were considered earlier as the typical end products of Chl breakdown in leaves, this process appeared to be derailed in bananas, which are one of the most important commercial fruits. In the peels of ripening bananas (*Musa acuminata*, 'cavendish' cultivar), abundant PluBs were found to accumulate [38], which are usually fleetingly existent intermediates of Chl breakdown and hardly detectable in other higher plants. These 'stabilized' *Mc*-PluBs were shown to be hypermodified to carry an ester functionality, thereby masking

the $C8^2$ propionic acid, which is responsible for rapid and stereospecific isomerization of PluBs to PleBs [22]. Apart from banana peels, PluBs were also found in banana leaves [39], whereas PleBs, the typically more abundant Chl catabolites in leaves, could not be detected.

In the meantime, abundant PluBs were further discovered in yellow leaves of the *Spathiphyllum wallisii* [40], *Arabidopsis thaliana* [41] and *Vitis vinifera* [36].

Why plants actively retain PluBs from being converted to their PleB counterparts is still unclear. These ‘persistent’ *hypermodified* PluBs, however, may prove to be natural molecular markers of senescence, which open a new noninvasive view into cellular processes in leaves and fruit.

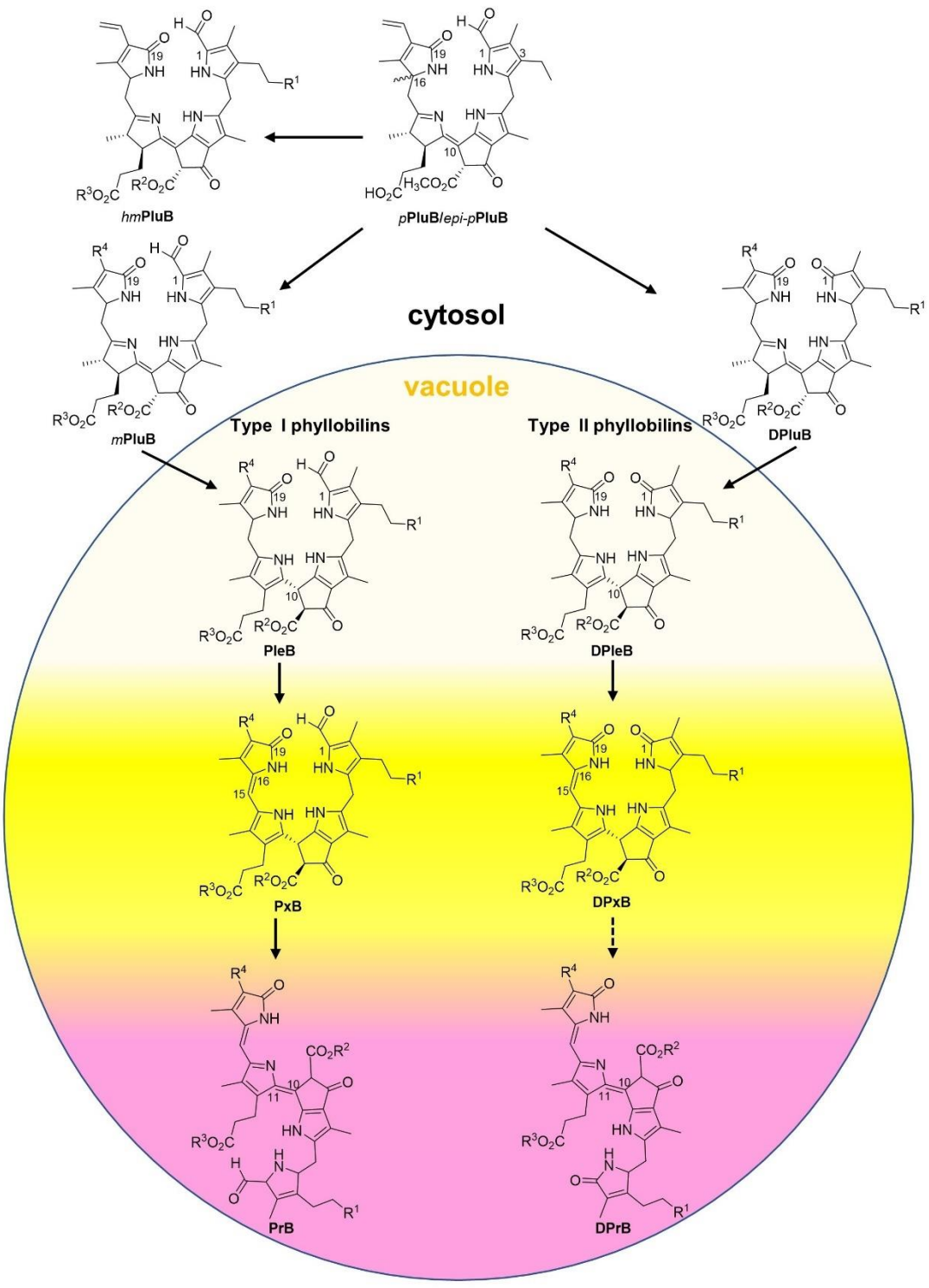

Figure 4. Overview of the later stages of Chl breakdown.

Although earlier stages appear to be identical in all higher plants investigated so far, the program branches out at later stages, giving rise to different kinds of phyllobilins. Starting from the *p*PluB stage, one branch leads to *hypermodified* PluBs in the cytosol; another branch generates type I phyllobilins in which the formyl group of ring A is retained, whereas it is

converted in yet another branch to a dioxo-bilin type structure of type II phyllobilins. Further degradation branches might still be discovered. So far, the stage of a PrB is the 'last' characterized catabolite for the type-I phyllobilins. A type-II DPrB could recently be synthesized by oxidation of its DPxB precursor [35], but has not yet been found to occur naturally.

2.3 Natural Diversity of phyllobilins

Phyllobilins were found to not only occur in leaves of deciduous trees, but also in fruit and vegetables, and more importantly, medicinal plants. In the late steps of the Chl breakdown procedure, a large structural diversity of phyllobilins was observed due to modification of different side groups depending on the plant species (Figure 5).

Phyllobilins at all stages (except the PrB level, for which only a formyloxobilin-type is known to occur naturally) occur as either formyloxobilin- or dioxobilin-type, furnishing a formyl group and a γ-lactam at ring A, respectively. Type I and type II phyllobilins are typically modified at $C3^2$ and at C18. Modifications of the western hemisphere at ring D appear as vinyl or dihydroxyethyl side chain, except for a PleB identified in leaves of plum tree (*Prunus domestica*) carrying a dihydroxyethyl-group at C18, which is further glycosylated at the $C18^2$ position [42]. Several modifications could be identified at the $C3^2$ position, from a simple hydroxyl group to O-β-D-glycosyl, O-malonyl, or O-β-D-glycosyl-malonyl units. Typical for phyllobilins from *Arabidopsis thaliana*, among others, is an ethyl group at ring A. Special modification motifs of ring A in *Arabidopsis thaliana* are additional hydroxymethyl moieties at C2 or C4 or a hydroxymethyl group instead of the typical methyl unit at C2 [9]. PleBs and PluBs arise as two epimeric forms at C16, the normal (*n*-type) and the epimeric (*epi*-type) form. Generally, ring E of the phyllobilin core structure is modified by a methyl ester unit, however, a free carboxyl moiety could be identified for PleBs in spinach (*Spinacia oleracea*) [43], among others. Exotic modifications of the propionic acid side chain at ring C were found for PluBs in peels and leaves of banana [38, 39] as well as for phyllobilins in leaves of wych elm [28] and grapevine [35], for which an intramolecular glycosidic

bridge between the propionic acid side chain and the hydroxyl group at C3[2] could be identified. An unprecedented carbon skeleton was discovered in fern, lacking the carboxyl group at ring E and featuring a novel chemical constitution of ring A, B and E [36].

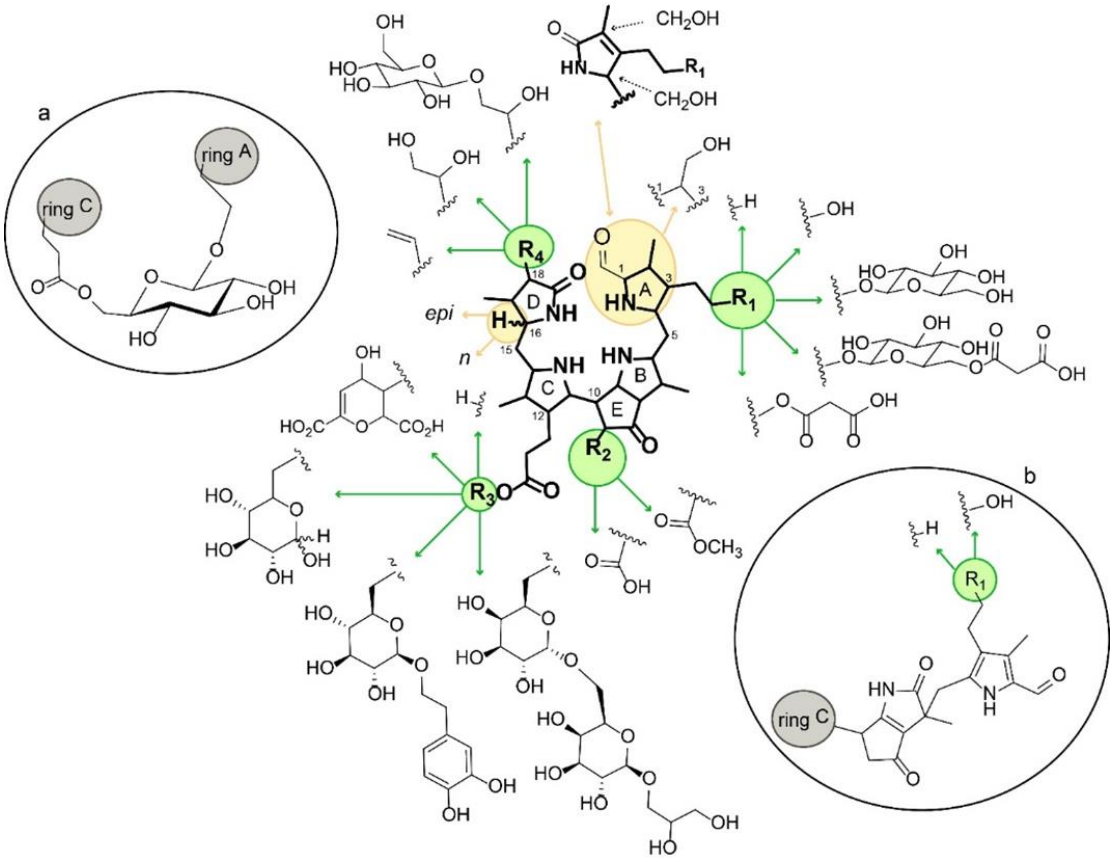

Figure 5. Overview of structural diversity in peripheral modifications of phyllobilins.

Double bonds of the basic chemical phyllobilin structure have been omitted for better illustration. Not all of the modifications are found in all different phyllobilin states (PluB, PleB, PxB, PrB). a large structural diversity of phyllobilins was observed due to modification of different side groups depending on the plant species.

This structural diversity provides access to various new natural compounds and opens up the possibility of influencing polarity, solubility, and therefore cellular characteristics of phyllobilins, probably affecting cellular uptake, tissue targeting, or protein affinities. Hence, it creates a starting point for exploiting the vast source of phyllobilins as natural

compound class and compare potential physiological properties as well as pharmacological applications.

2.4 Pharmacological potential of phyllobilins

The structural diversity of phyllobilins, which is mainly due to modifications on different side chains depending on the plant species, makes it more interesting to elucidate potential pharmacological activities of phyllobilins, which are related to structure, and could differ dramatically. Interestingly, phyllobilins show striking structural similarities to the catabolites of heme, the bilins [44, 45]. Apart from their similar tetrapyrrolic structure, both families of natural products were long thought to be waste products of detoxification processes. However, several studies have proven that bilins possess interesting pharmacologically relevant activities [46-48]. Research on phyllobilins so far focused more on the elucidation of the structural diversity, but especially the similarities to the bilins indicate that they are also an interesting class of compounds for pharmaceutical approaches. Recently, more and more research has pointed towards relevant pharmacological effects of phyllobilins.

One of the PleBs isolated from freshly cut yellow peels of ripe pears was confirmed to have a slightly inferior anti-oxidative activity to that of bilirubin [49], which is not only a strong antioxidant, but also a cytoprotective component relevant in the reduction of coronary heart diseases, retinal damage and cancer mortality, among others [50]. At the PxB level, 6 different PxBs were isolated from the extract of the medicinal plant *Echinacea purpurea* and all of them were shown to have a potential *in vitro* and *in cellulo* anti-oxidative activity [29]. 5 out of 6 *Ep*-PxBs even exhibited a stronger *in vitro* anti-oxidative potential relative to caffeic acid, which is a known anti-oxidative constituent of *Echinacea* extracts [51]. A DPxB isolated from de-greened leaves of savoy cabbage (*Brassica Oleracea var. sabauda*) was revealed to have even higher anti-oxidative qualities than bilirubin and Trolox [37]. The implication of phyllobilins as

anti-oxidative plant components, occurring in fruit and vegetable that play a role in human nutrition, is very promising for future investigations.

Besides, a PxB which was isolated from fresh leaves of nettle (*Urtica dioica*) was shown to possess anti-oxidative and anti-inflammatory properties comparable to known nettle phytochemicals [30].

Furthermore, first analysis of herbivore-infested and fungal-infected basil leaves have revealed a significant increase of phyllobilins in the areas of pest infestation [52], indicating that pathogen attack could potentially induce Chl degradation. Hence, phyllobilins might also play a role in possible plant defense or signaling mechanisms.

In conclusion, phyllobilins have been overlooked for far too long, and have now emerged as natural product class with relevant pharmacological roles that could have broad implications for phytotherapy, due to the ubiquitous occurrence of phyllobilins in the plant kingdom. Thus, phyllobilins have the potential of becoming established as important phytochemicals in the future.

With the so-far established pharmacological properties of phyllobilins, it's already more than necessary to find potential target binding proteins for phyllobilins and gain more knowledge about the role that phyllobilins play in the life system of plants and, more importantly, in human nutrition.

2.5 Complementary target identification approaches for the identification of protein binding partners of small molecules

In traditional target-based identification of bioactive small molecules, libraries of small molecules are typically screened against a selected (disease related) target [53, 54]. However, cell-based screenings of new biologically active small molecules are increasingly employed recently as a 'bottom-up' strategy. In order to develop small molecules as potential lead structures for novel therapeutics, gaining knowledge of the identity of the target protein is the key step [55]. However, identification of a molecular

target for a bioactive compound has always been quite challenging. This time-consuming and labor-intensive process is one of the rate-limiting steps in drug development [56]. To completely explain the biological effects of a small molecule and understand the mechanisms which lead to observed effects, up/down-stream signaling pathways and involved networks are often the missing part.

Although various methods have been successfully utilized for target identification, the combination of complementary approaches is required for success in many cases. Current approaches for target identification mainly reply on chemical proteomics and genetic mutant screens [57]. Among these approaches, affinity chromatography is probably the most widely used.

2.5.1 Mass spectrometry-based affinity chromatography

Affinity chromatography represents an un-biased method that allows for identification of a direct binding partner of small molecules [58]. For this approach, a molecule of interest has to be conjugated to a solid phase and then incubated with total cell lysate to fish for potential binding proteins [59]. In contrast to high-throughput screening efforts, which often only focus on selected sub-proteomes such as kinases, the compound of interest is exposed to the entire variety of cellular proteins including all naturally occurring post-translational modifications and activation states.

Although it is one of the most extensively used target identification approaches, affinity chromatography also has some drawbacks. First, the method selects for high abundance proteins, whereas proteins that are only expressed at low levels are easily missed. Besides, being an *in vitro* approach, it requires the derivatization of the active molecule onto solid phase [60, 61].

The biotin-tagged affinity chromatography is a classical method for identifying the target proteins of biologically active small molecules [62]. Biotin-tagged small molecules are first immobilized onto streptavidin beads and then incubated with whole

cell lysate for bound proteins. A washing step is performed afterwards to remove most unbound proteins. Bound proteins are then analyzed by SDS-PAGE and identified by detection methods like Western blot or mass spectrometry (Figure 6).

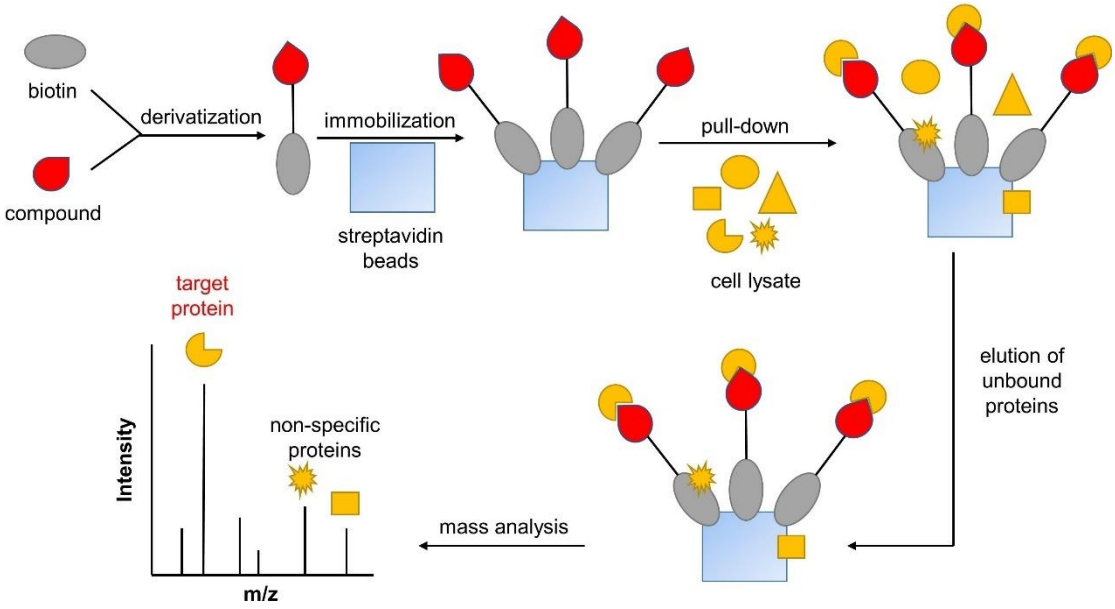

Figure 6. Overview of the biotin-based affinity chromatography.

In a biotin-based pull-down, the compound of interest is coupled with biotin and immobilized on streptavidin beads. Protein containing whole cell lysate are added for incubation and most of the non-specific proteins are then eluted. At last, bound proteins are detected and characterized by mass spectrometry.

Over the last several years, efforts have been made to improve those previously mentioned disadvantages. Most importantly, advances in mass spectrometry and statistical analysis methods have improved the sensitivity of detection and quantification of targets from affinity purification [63, 64].

2.5.2 Yeast three-hybrid (Y3H) system

The yeast three-hybrid (Y3H) system builds on the yeast two-hybrid (Y2H) system, which is used to screen for protein-protein interactions of a selected organism in baker's yeast [65]. In the Y2H system, a protein of interest is expressed as fusion

protein to a DNA binding domain of a split transcription factor as the “bait”, whereas a pool of potential binding proteins or cDNA libraries (‘preys’) are expressed as fusion proteins of the DNA activation domain. The transcription of a reported gene and the subsequent survival of the yeast cells on selective plates will only happen if an interaction takes place [66].

In the Y3H system, however, a small molecule-ligand hybrid is added to the Y2H setup (Figure 7) [67]. The small molecule of interest is chemically derivatized with a linker molecule, which can be a small molecule substrate with high affinity to the enzyme it inhibits as the anchor, such as the methotrexate-dihydrofolate reductase interaction pair [68, 69], or the substrate of a protein tag such as SNAP tag [70].

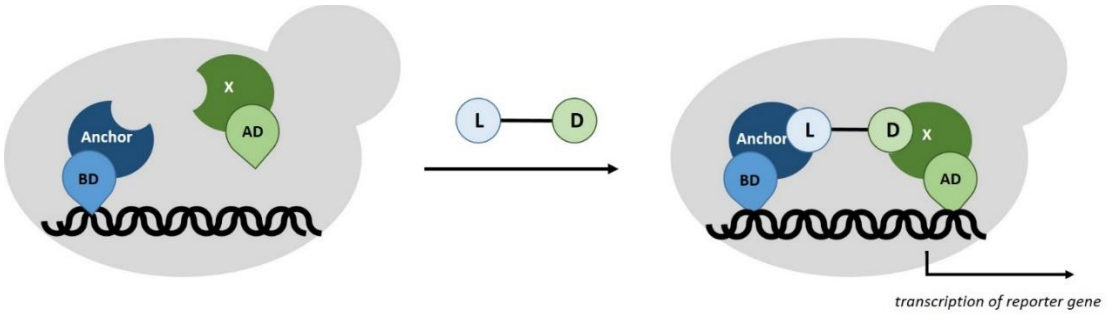

Figure 7. Setup of a yeast three-hybrid system.

A small molecule (D) is coupled to a linker (L) that allows for binding to an anchor protein coupled with the DNA binding domain of a split transcription factor (BD). In this setup, the small molecule is screened against a library of potential binding partners (X) fused to the activation domain of a split transcription factor (AD). Transcription of a reporter gene and thus survival of the yeast cell on selective plates only occurs upon interaction of the small molecule (D) with a protein (X).

Compared to affinity based target identification, the Y3H system offers several advantages, such as its application in living cells; besides, the Y3H system is based on cDNA libraries, hence allows for the identification of proteins underrepresented in cell lysates used for affinity chromatography due to low expression levels; furthermore, no high end mass spectrometry or other costly device is necessary; the identity of the

protein of interest can be obtained by standard DNA sequencing, for which ample service providers are available at very low costs.

2.6 Aims of the study

Phyllobilins are a family of abundant natural products which are derived from the degradation of Chl and observed in leaves of deciduous trees, fruits, vegetables, and, more importantly, medicinal plants. Recently, some of these natural products were shown to possess bioactivities relevant for human health, such as anti-oxidative activity and anti-inflammatory activity. These results point towards important pharmacological effects of phyllobilins. With developing isolation and characterization methods, we are convinced that more and more phyllobilins will be identified in different plants, and more importantly, other relevant pharmacological roles that phyllobilins play could have broad implications for phytotherapy, due to the ubiquitous occurrence of phyllobilins in the plant kingdom. Thus, phyllobilins have the potential of becoming established as important phytochemicals in the future.

As is the case for the majority of newly discovered natural products, phyllobilins have only been subjected to limited testing for biological activities. The true potential of phyllobilins and the majority of natural products as drugs or unique lead compounds, which can interfere with specific biological pathways, is still unexplored. Improving this mismatch between the diversity of promising small molecules and the limited knowledge about their targets and mechanisms of action is and will still be one of the greatest challenges in the war against diseases. Therefore, identification and validation of targets for bioactive small molecules are important to all of chemical biology and drug development. To further understand the role that phyllobilins play in biological systems, identification of potential target binding proteins for phyllobilins are more than necessary and important, given the so-far established biological properties

of phyllobilins. To achieve that, a combination of complementary target identification approaches is the most promising.

The aims of the study can be summarized as below:

1. Isolation, identification and structural characterization of new phyllobilins in different plant sources, and elucidation of their potential biological activities, anti-cancer activity in particular.
2. Establishment of a reliable yeast three-hybrid system for the target identification of small molecules.
3. Identification of potential binding proteins for phyllobilins using complementary target identification approaches.
4. Validation of the identified target protein as the binding partners of phyllobilins.

MATERIALS AND METHODS

3 Materials and Methods

3.1 Materials

3.1.1 Compounds

Compound	Producer
THK15	Thomas Klaßmüller (Prof. Dr. Franz Bracher, LMU Munich)
THK42	Thomas Klaßmüller (Prof. Dr. Franz Bracher, LMU Munich)

Table 1. Compounds

3.1.2 Reagents

Reagent	Producer
Acetic acid (AcOH)	VWR, Ismaning, Germany
Acetonitrile (ACN) HPLC grade	VWR, Ismaning, Germany
Adenine	Sigma-Aldrich, Taufkirchen, Germany
Agar-Agar	Carl Roth, Karlsruhe, Germany
Agarose	Sigma-Aldrich, Taufkirchen, Germany
Ammonium acetate (NH_4AcO)	Merck, Darmstadt, Germany
Ammonium bicarbonate (NH_4HCO_3)	Sigma-Aldrich, Taufkirchen, Germany
Ampicillin	Carl Roth, Karlsruhe, Germany
Anti-Mouse IgGk light chain BP secondary antibody	Santa Cruz Biotechnology, Heidelberg, Germany
Anti-PLOD2/LH2 antibody	Abcam, Berlin, Germany
Anti-GAL4 AD antibody	Abcam, Berlin, Germany
Ascorbic acid	Sigma-Aldrich, Taufkirchen, Germany
Benzotriazol-1-yloxytripyrrolidinophosphonium hexafluorophosphate (PyBOP)	Sigma-Aldrich, Taufkirchen, Germany
Biotin-PEG_7-NH_2	Sigma-Aldrich, Taufkirchen, Germany
Biotin-PEG_3-N_3	Sigma-Aldrich, Taufkirchen, Germany
Bovine serum albumin (BSA)	Sigma-Aldrich, Taufkirchen, Germany
Calcium chloride ($CaCl_2$)	Sigma-Aldrich, Taufkirchen, Germany
Collagen Type I	Thermo Fisher Scientific, Schwerte, Germany

Reagent	Producer
Collagen Type I-FITC Conjugate	Sigma-Aldrich, Taufkirchen, Germany
Complete®	Roche Diagnostics, Penzberg, Germany
Competent DH5α-*E. coli*	New England BioLabs, Frankfurt a.M., Germany
Copper(II) sulfate pentahydrate ($CuSO_4 \times 5H_2O$)	Sigma-Aldrich, Taufkirchen, Germany
Crystal violet	Carl Roth, Karlsruhe, Germany
Dichloromethane (DCM)	VWR, Ismaning, Germany
Dimethyl sulfoxide (DMSO)	Sigma-Aldrich, Taufkirchen, Germany
d_6-DMSO	Sigma-Aldrich, Taufkirchen, Germany
Dithioerythritol (DTE)	Sigma-Aldrich, Taufkirchen, Germany
Dithiothreithol (DTT)	SERVA Electrophoresis, Heidelberg, Germany
D-glucose	Sigma-Aldrich, Taufkirchen, Germany
Dulbecco's Modified Eagle Medium (DMEM)	Pan Biotech, Aidenbach, Germany
Dynabeads™ M-280 Streptavidin	Thermo Fisher Scientific, Schwerte, Germany
Ethanol (EtOH)	Carl Roth, Karlsruhe, Germany
Ethinylestradiol	Sigma-Aldrich, Taufkirchen, Germany
Ethylendiaminetetraacetic acid (EDTA)	Sigma-Aldrich, Taufkirchen, Germany
Ethylenediaminetetracetic acid disodium (EDTA-2Na)	Sigma-Aldrich, Taufkirchen, Germany
Ethylene glycol-bis(2-aminoethylether)-N,N,N′,N′-tetraacetic acid (EGTA)	Sigma-Aldrich, Taufkirchen, Germany
FastAP Thermosensitive Alkaline Phosphatase	Thermo Fisher Scientific, Schwerte, Germany
Ferrous chloride ($FeCl_2$)	Sigma-Aldrich, Taufkirchen, Germany
Fetal calf serum (FCS)	Pan Biotech, Aidenbach, Germany
Formic acid (LC-MS grade)	Thermo Fisher Scientific, Schwerte, Germany
Glass beads	Sigma-Aldrich, Taufkirchen, Germany
Glycerol	AppliChem, Darmstadt, Germany
Goat anti-Rabbit IgG secondary antibody	Dianova, Hamburg, Germany
HEPES	Sigma-Aldrich, Taufkirchen, Germany

Reagent	Producer
High-Fidelity (HF) restriction enzymes	New England BioLabs, Frankfurt a.M., Germany
Hoechst 33342	Sigma-Aldrich, Taufkirchen, Germany
Hydrochloric acid (HCl)	VWR, Ismaning, Germany
Hydroxybenzotriazole (HOBT)	Sigma-Aldrich, Taufkirchen, Germany
$[IKG]_3$ peptide	Thermo Fisher Scientific, Schwerte, Germany
Imidazole	Sigma-Aldrich, Taufkirchen, Germany
Iodoacetamide	Sigma-Aldrich, Taufkirchen, Germany
α-Ketoglutaric acid	Carl Roth, Karlsruhe, Germany
Lithium acetate	BioScience GmbH, Dümmer,Germany
Magnesium chloride ($MgCl_2$)	AppliChem, Darmstadt, Germany
Magnesium sulfate ($MgSO_4$)	Sigma-Aldrich, Taufkirchen, Germany
Methanol (MeOH) HPLC grade	VWR, Ismaning, Germany
Minoxidil	Sigma-Aldrich, Taufkirchen, Germany
N-(3-Dimethylaminopropyl)-N′-ethylcarbodiimide hydrochloride (EDCl)	Sigma-Aldrich, Taufkirchen, Germany
Page Ruler™ Plus Prestained Protein Ladder	Thermo Fisher Scientific, Schwerte, Germany
Penicillin/Streptomycin	PAN Biotech, Aidenbach, Germany
Phenylmethylsulfonyl fluoride (PMSF)	Sigma-Aldrich, Taufkirchen, Germany
Phusion High-Fidelity DNA Polymerase	Thermo Fisher Scientific, Schwerte, Germany
PLOD2 (Human) Recombinant Protein Abnova™	Thermo Fisher Scientific, Schwerte, Germany
Polyethylene glycol (PEG) 50%	Takara Bio, CA, USA
Potassium chloride (KCl)	Carl Roth, Karlsruhe, Germany
Potassium phosphate dibasic (K_2HPO_4)	Sigma-Aldrich, Taufkirchen, Germany
Potassium phosphate monobasic (KH_2PO_4)	Sigma-Aldrich, Taufkirchen, Germany
Primers	Metabion, Planegg, Germany
Purvalanol B	Biomol, Hamburg, Germany
Pyridine	Sigma-Aldrich, Taufkirchen, Germany
Pyronin Y	Sigma-Aldrich, Taufkirchen, Germany
Rhodamin phalloidin	Sigma-Aldrich, Taufkirchen, Germany

Reagent	Producer
Roti®-Quant (5x) Bradford solution	Carl Roth, Karlsruhe, Germany
Silica gel 60	VWR, Ismaning, Germany
Sodium ascorbate	Sigma-Aldrich, Taufkirchen, Germany
Sodium chloride (NaCl)	Sigma-Aldrich, Taufkirchen, Germany
Sodium deoxycholate	Sigma-Aldrich, Taufkirchen, Germany
Sodium dodecyl sulfate (SDS)	Carl Roth, Karlsruhe, Germany
Sodium hydroxide (NaOH)	VWR, Ismaning, Germany
Sorbitol	Merck, Darmstadt, Germany
Taq DNA Polymerase (5U/µl)	Thermo Fisher Scientific, MA, USA
Triethylamine (Et_3N)	Sigma-Aldrich, Taufkirchen, Germany
Tris-Base	Sigma-Aldrich, Taufkirchen, Germany
Tris-HCl	Sigma-Aldrich, Taufkirchen, Germany
Tris[(1-benzyl-1H-1,2,3-triazol-4-yl)methyl]amine (TBTA)	Carl Roth, Karlsruhe, Germany
Triton-X 100	Sigma-Aldrich, Taufkirchen, Germany
Trypsin	PAN Biotech, Aidenbach, Germany
Trypsin (Sequencing grade)	Promega GmbH, Walldorf, Germany
Tryptophan	Sigma-Aldrich, Taufkirchen, Germany
Tween 20	Sigma-Aldrich, Taufkirchen, Germany
Yeast nitrogen base	Sigma-Aldrich, Taufkirchen, Germany
Yeast synthetic drop-out medium supplements	Sigma-Aldrich, Taufkirchen, Germany
α-ketoglutarate	Sigma-Aldrich, Taufkirchen, Germany
β-mercaptoethanol	Sigma-Aldrich, Taufkirchen, Germany
3-amino-1,2,4-triazole (3-AT)	Sigma-Aldrich, Taufkirchen, Germany
10× PCR Buffer without Mg	Thermo Fisher Scientific, MA, USA
10 mM dNTP Mix	Thermo Fisher Scientific, MA, USA
50 mM $MgCl_2$	Thermo Fisher Scientific, MA, USA

Table 2. Reagents

3.1.3 Kits

Kit	Producer
cDNA Reverse Transcription Kit	Applied Biosystems, Waltham, USA
EZ-10 Spin Column Yeast Plasmid DNA Mini-Preps Kit	Biozol, Eching, Germany
High-Capacity cDNA Reverse Transcription Kit	Applied Biosystems, Waltham, USA
QIAGEN Maxiprep Kit	QIAGEN, Hilden, Germany
QIAprep® Spin Miniprep Kit (250)	QIAGEN, Hilden, Germany
QIAquick® Gel Extraction Kit (250)	QIAGEN, Hilden, Germany
RNeasy® Mini Kit (250)	QIAGEN, Hilden, Germany
Succinate-Glo™ JmjC Demethylase/Hydroxylase Assay Kit	Promega GmbH, Walldorf, Germany

Table 3. Kits

3.1.4 Consumables

Consumable	Producer
Cell culture flasks	TPP, Trasadingen, Switzerland
Disposable pipettes	Greiner Bio, Frickenhausen, Germany
Falcon tubes	VWR, Ismaning, Germany
Ibidi Treat µ-slides	Ibidi GmbH, Munich, Germany
Parafilm	American National Can, Chicago, USA
Petri dishes, polystyrene	Sigma-Aldrich, Taufkirchen, Germany
SepPak Plus C18 cartridges	Waters Associates, Milford, USA
Nitrocellulose membrane (0.2 µm)	Hybond-ECL™, Amersham Bioscience, Freiburg, Germany
Polyvinylidene difluoride (PVDF) membrane (0.2 µm)	Hybond-ECL™, Amersham Bioscience, Freiburg, Germany
Thin layer chromatography (TLC) plates	VWR, Ismaning, Germany

Table 4. Consumables

3.1.5 Technical equipment

Device	Producer
Agilent 1260 Infinity II LC system	Agilent Technologies Germany GmbH & Co. KG, Waldbronn, Germany
Büchi Pure C-830	BÜCHI Labortechnik GmbH, Essen, Germany
ChemiDoc™ Touch Imaging System	Bio-Rad Laboratories GmbH, Munich, Germany
Eppendorf Eporator	Merck, Darmstadt, Germany
Eppendorf ThermoMixer	Merck, Darmstadt, Germany
Heracell CO_2 Incubator 150i	Thermo Fisher Scientific, MA, USA
Heraeus Megafuge 1.0 RS centrifuge	Kendro Laboratory Products, Hanau, Germany
IKA RV 3 Rotary Evaporator	IKA®-Werke GmbH & Co. KG, Staufen, Germany
Leica Dmil microscope	Leica Microsystems, Wetzlar, Germany
Leica TCS SP8 confocal laser scanning microscope	Leica Microsystems, Wetzlar, Germany
Mikro 22R centrifuge	Hettich, Tuttlingen, Germany
Millipore Express® PLUS membrane filter	Merck Millipore, Darmstadt, Germany
Nanodrop® Spectrophotometer	PEQLAB Biotechnologie GmbH, Erlangen, Germany
Orion II Microplate Luminometer	Berthold Detection Systems GmbH, Pforzheim, Germany
Christ RVC 2-18 CDplus rotary vacuum concentrator	Martin Christ Gefriertrocknung-sanlagen GmbH, Osterode am Harz, Germany
Tecan SpectraFluor Plus Microplate Reader	Tecan, Crailsheim, Germany
Vi-Cell™ XR	Beckman Coulter, Fullerton, CA, USA

Table 5. Technical equipment

3.1.6 Plant Material

Katsura trees (*Cercidiphyllum japonicum*) were located outside of the botanical garden Munich using the tree-finder app https://www.botmuctrees.de/. Senescent leaves were collected in the Maria-Ward-Straße, Munich, Germany (48°09'41.0"N 11°29'58.8"E). Senescent leaves of Plane trees (*Platanus occidentalis*) were collected from trees in the Feodor-Lynen-Straße at the campus Großhadern of the University of Munich (48°06'48.6"N 11°27'56.2"E).

3.2 Methods

3.2.1 Analytical methods

3.2.1.1 Analytical HPLC

Agilent 1260 Infinity II LC system with a 1260 Infinity Degasser, a 1260 Series quaternary pump and 1260 Series diode array detector; Merck LiChrospher® 100 RP-18 (5 µm) LiChroCART® 125-4, protected by a Merck LiChrospher® 100 RP-18 (5 µm) LiChroCART® 4-4 i.d. pre-column; injection volume: 100 µl (unless stated otherwise). Solvent system: mobile phase A = NH_4AcO buffer 10 mM pH 7, B = ACN, flow 0.5 ml/min; Solvent composition: 0-2 min 5% B, 2-17 min 5% to 100% B, 17-20 min 100% B, 20-22 min 100% to 5% B. Data were processed with OpenLab CDS Data Analysis 2.3.

3.2.1.2 Semi-preparative HPLC

Büchi Pure C-830 with prep HPLC pump 300 bar, fraction collector, and prep sample injection valve. Gynkotek LC-System with manual sampler, M480 pump, Phenomenex DG-301 online degasser, Gynkotek UVD 640 diode array detector and a Rheodyne injection valve with 5 ml loop. Column: Supelco Ascentis® C18, 5 µm, 15 cm x 10 mm, with a Phenomenex pre-column ODS 9 x 16 mm; mobile phase A = NH_4AcO buffer 10 mM pH 7, B = ACN, flow 2.5 ml/min; solvent composition: 0-2 min 12% B, 2-12 min

12% to 20% B, 12-30 min 20% to 80% B, 30-40 min 80% to 100% B. Data were processed with Gynkosoft 5.50 or Büchi Pure software 1.5.

3.2.1.3 Spectroscopy

UV-Vis: λ_{max} in nm (rel. ε); Thermo Spectronic Genesys 5 (336001) UV-Visible spectrophotometer. Concentrations of PleBs and derivatives were calculated using log ε (312 nm) = 4.23 [49], concentrations of PxBs and derivatives were calculated using log ε (426 nm) = 4.51 [25].

HR-ESI-MS were measured on a ThermoScientific QExactive Orbitrap mass spectrometer equipped with an ESI source (positive-ion mode, spray voltage 3.7 kV) at the MS facility of the Department of Chemistry, University of Munich. Data were processed using Xcalibur.

NMR spectra were recorded on an Avance III HD 500 MHz NMR spectrometer from Bruker BioSpin equipped with a CryoProbe™ Prodigy broadband probe holder. NMR data were analysed with Mestre Nova.

3.2.2 Phyllobilins isolation and modification

3.2.2.1 Large scale isolation of PleBs from senescent leaves of Katsura (*Cercidiphyllum japonicum*) and Plane tree (*Platanus occidentalis*)

Phyllobilins were extracted with the following modified method. 300 g of frozen leaves of Katsura or Plane tree were ground in a 5 l stainless steel beaker using a Braun hand blender Model MR 5000 and extracted with 1200 ml hot water. The mixture was filtered through a cotton cloth and the residue was again washed with 500 ml hot water. The mixture was allowed to cool to room temperature (RT) before extracting twice with 200 ml of DCM. The DCM solution was applied to a silica column (50 mm diameter, 300 mm length, 70 g silica gel 60). The column was washed with DCM, and phyllobilins were eluted with increasing MeOH (DCM/MeOH 95/5, 80/20, 50/50). The different

fractions were analyzed by thin layer chromatography (TLC). Phyllobilins containing fractions were combined, and the solvent was evaporated. The obtained residue was dissolved in MeOH/potassium phosphate buffer (pH 7.4) and purified by semi-preparative HPLC. Yields were 50 mg (77.6 µmol) of PleB and 10 mg (15. 6 µmol) of PxB.

3.2.2.2 HPLC analysis of Plane tree phyllobilins

In a co-elution experiment, isolated pure samples of *Po*-PleB with *Po*-PxB, which were isolated from Plane tree leaves, were applied to analytical HPLC. *Cj*-PleB and *Cj*-PxB were also isolated from Katsura tree leaves as described above and were analyzed the same way. In addition, a 1:1 mixture of *Po*-PleB and *Cj*-PleB, and of *Po*-PxB and *Cj*-PxB, were analyzed by HPLC.

3.2.2.3 Solid-phase synthesis of PxB by oxidation of *Cj*-PleB or *Po*-PleB

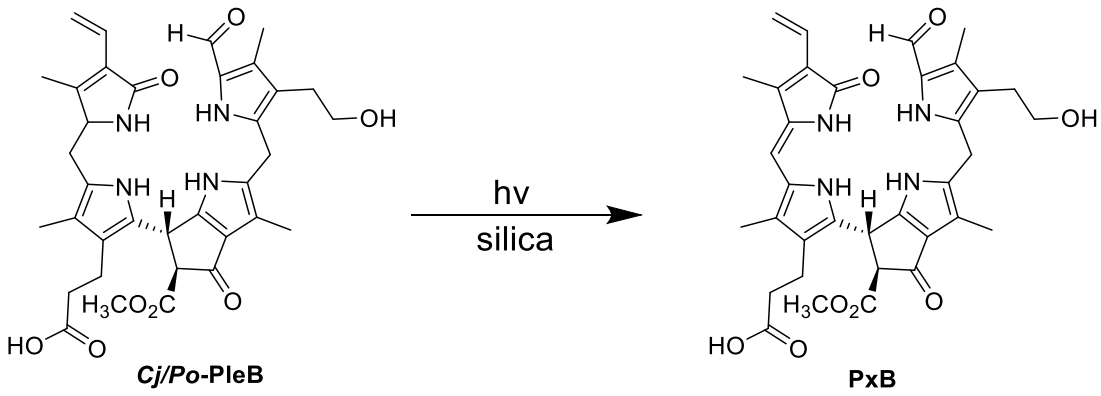

10 mg *Cj*-PleB or *Po*-PleB were dissolved in 5 ml of DCM and 1 ml of MeOH and added to 7 g of silica. The mixture was carefully dried under vacuum and the powder was stirred overnight under a tungsten light bulb. The complete formation of PxB was confirmed by analytical HPLC. The reaction mixture was eluted with EtOH, filtered through a filter paper and the solvent was evaporated by a rotary evaporator. The crude product was purified by semi-preparative HPLC. PxB containing fractions were pooled and dried by a rotary evaporator. The residue was dissolved in ACN/potassium

phosphate buffer (pH 2.5) 20/80 and stirred overnight. After SPE (Sep-Pak-C18 cartridge 5 g), pure PxB was eluted with ACN and dried under vacuum. 2 mg (3.1 µmol, 20%) of PxB were obtained. DMSO stocks were prepared and stored at -80°C until further use.

3.2.2.4 Esterification of *Cj*-PleB

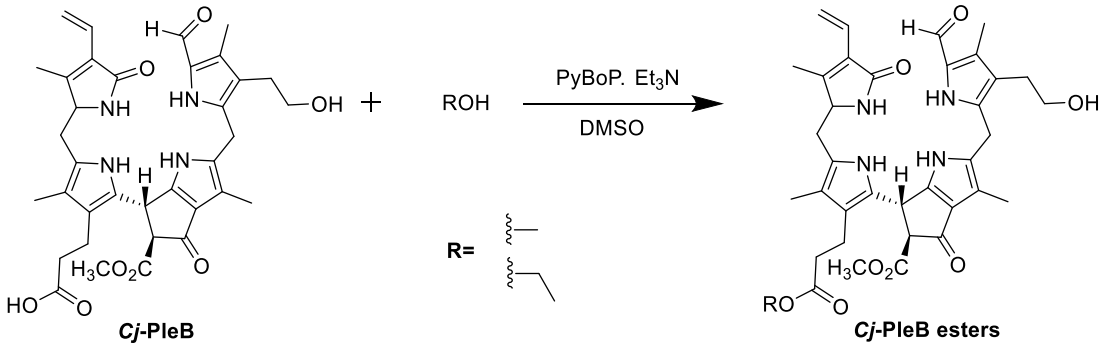

For synthesis of methyl-PleB, 4 mg *Cj*-PleB were dissolved in 1 ml of DMSO and 10 µl of MeOH, 2.5 µl of Triethylamine (Et_3N), and 4.5 mg of PyBoP were added. The mixture was stirred at RT overnight. The formation of methyl-PleB was confirmed by analytical HPLC. The mixture was purified by semi-preparative HPLC, yielding 1.6 mg (2.4 µmol, 40%) of methyl-PleB.

Synthesis of ethyl-PleB was performed according to the protocol of Li and Kräutler[71] with minor modifications (performed by Prof. Dr. Thomas Müller, Department of Organic Chemistry, University of Innsbruck). PyBoP was used instead of BOP. *Cj*-PleB was dissolved in EtOH, followed by addition of the coupling reagents. The formation of the ethyl-PleB was confirmed by analytical HPLC, yielding 0.74 mg (1.1 µmol, 58%) of ethyl-PleB.

3.2.2.5 Oxidation of PleB esters to PxB esters

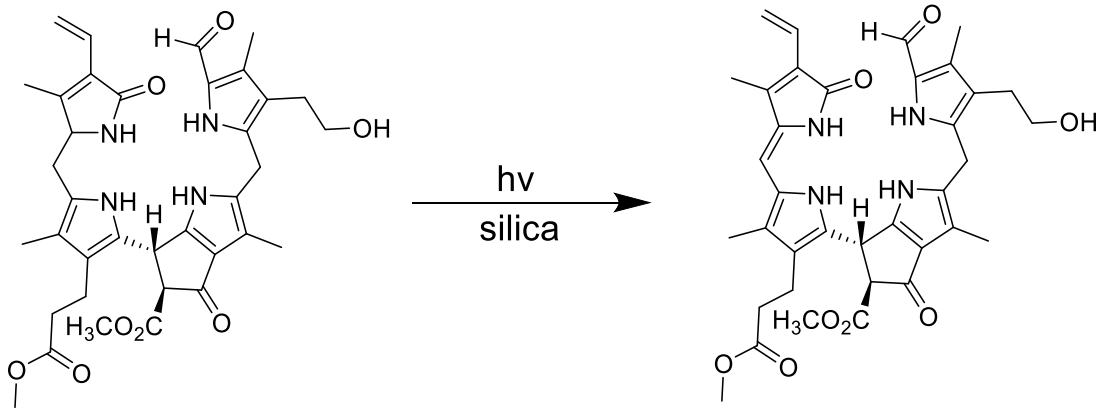

methyl-PleB **methyl-PxB**

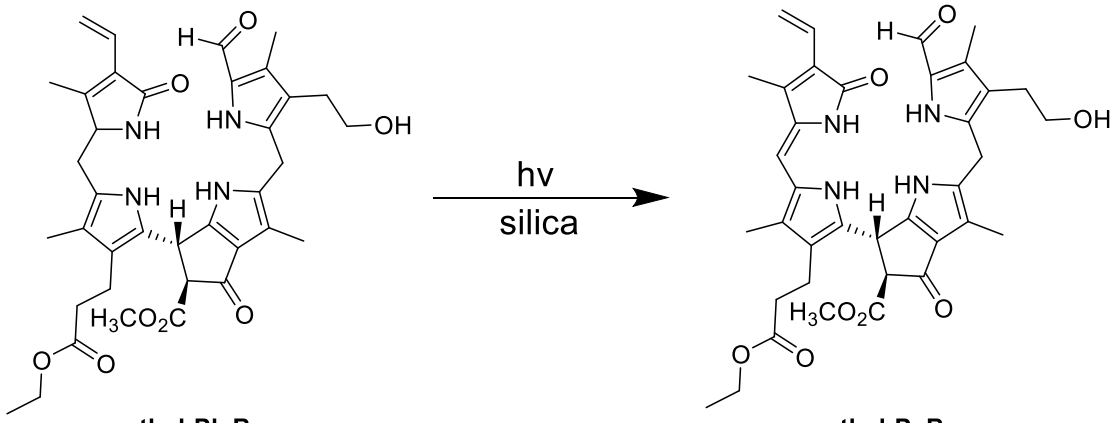

ethyl-PleB **ethyl-PxB**

10 mg methyl-PleB or ethyl-PleB were dissolved in 20 ml of DCM and added to 7 g of silica. The mixture was carefully dried under vacuum and the powder was stirred overnight under a tungsten light bulb. The complete formation of methyl-PxB or ethyl-PxB was confirmed by analytical HPLC and mass spectrometry. The reaction mixture was eluted with MeOH, filtered through a filter paper and the solvent was evaporated by a rotary evaporator. The crude product was purified by semi-preparative HPLC. Methyl-PxB or ethyl-PxB containing fractions were pooled and dried by a rotary evaporator, resulting 2.35 mg (3.58 µmol, 24%) of methyl-PxB or 3.06 mg (4.56 µmol, 31%) of ethyl-PxB. DMSO stocks were prepared and stored at -80°C until further use.

3.2.3 Cell culture

3.2.3.1 Cell culture buffers and solutions

PBS (pH 7.4)	
NaCl	132.2 mM
Na_2HPO_4	10.4 mM
KH_2PO_4	3.2 mM
H_2O	

PBS+Ca^{2+}/Mg^{2+} (pH 7.4)	
NaCl	137 mM
KCl	2.68 mM
Na_2HPO_4	8.10 mM
KH_2PO_4	1.47 mM
$MgCl_2$	0.25 mM
H_2O	

Growth medium	
DMEM	500 ml
FCS	50 ml
Penicillin/Streptomycin	5 ml

Freezing medium	
DMEM	70%
FCS	20%
DMSO	10%

Trypsin/EDTA (T/E)	
Trypsin	0.05%
EDTA	0.02%
PBS	

Table 6. Cell culture buffers and solutions

3.2.3.2 Cell culture

Human bladder cancer cell line T24 and the cervical cancer cell line HeLa were obtained from the Deutsche Sammlung von Mikroorgansimen und Zellkulturen (DSMZ; Braunschweig, Germany) and maintained in DMEM medium supplemented with 10% fetal calf serum (FCS) and 1% penicillin/streptomycin. Cells were cultured at 37°C under 5% CO_2 atmosphere with constant humidity in 75 cm^2 cell culture flasks.

3.2.3.3 Cell Passaging

When cells nearly reached confluency, they were split 1:2-1:10 and sub-cultured in 75 cm^2 cell culture flasks or seeded in multi-well plates or dishes for further experimental use. For passaging, culture medium was aspired, cells were washed with pre-warmed PBS and detached by incubation with pre-warmed trypsin/ethylenediaminetetraacetic acid (EDTA) (T/E) solution for 3-5 min at 37°C. Thereafter, culture medium was added to stop tryptic digestion and T/E solution was removed by centrifugation (*1000 rpm*, 5 min, 20°C) and addition of new culture medium. Cell number was counted with Vi-Cell™ XR.

3.2.3.4 Freezing and thawing

Before freezing, cells were cultured to reach confluency in a 150 cm^2 flask. Washing and cell detachment was conducted as described previously. After centrifugation (*1000 rpm*, 5 min, 20°C), cells were resuspended in ice-cold freezing medium and transferred into cryovials at a cell density of 3×10^6 cells per 1.5 ml aliquot. Following an initial storage at -80°C for at least 24 h, cryovials were transferred into liquid nitrogen tanks (-196°C) for long-term storage.

For thawing, the cryovial content was mixed with pre-warmed culture medium. After DMSO removal by centrifugation (*1000 rpm*, 5 min, 20°C), the cell pellet was resuspended in culture medium and initially transferred into a 25 cm^2 flask for 24 h before cells were cultured in a 75 cm^2 flask.

3.2.4 Cell proliferation assay

Proliferation of phyllobilins treated T24 cells was determined by a crystal violet staining. 2.5×10^3 T24 cells were seeded in 96 well plates and grown for 24 h. Cells were incubated with indicated concentrations of compounds for 72 h, followed by washing with PBS+ and staining with 0.5% crystal violet solution for 10 min. After washing the

cells with water and drying overnight, crystal violet was redissolved with trisodium citrate solution, and absorption at 550 nm was measured with a SpectraFluor Plus plate reader (Tecan, Crailsheim, Germany). The number of viable cells was calculated by subtracting the average of the day 0 control values and normalizing to the corresponding DMSO control.

3.2.5 Establishment of yeast three-hybrid system

3.2.5.1 Cloning of the bait and prey vector for spot test

The *dhfr* gene was amplified from genomic DNA of *E. coli* using Thermo Scientific Phusion High-Fidelity DNA Polymerase and the following primers, which were determined by the *E. coli* DH5-α *dhfr* sequence from NCBI Gene (gene 944790) and contain a restriction site for NdeI:

Forward primer:

5’-CATGGAGGCCCATATGATGATCAGTCTGATTGCGGC-3’

Reverse primer:

5’-GCAGGTCGACCATATGTTACCGCCGCTCCAGAATCT-3’

CDK5 was amplified from a CDK5 containing plasmid for mammalian expression (Plasmid 1870, addgene) using the following primers adding BamHI and EcoRI restriction sites:

Forward primer:

5’-CATGGAGGCCGAATTCATGCAGAAATACGAGAAACTGGAA-3’

Reverse primer:

5’-GCAGGTCGACGGATCCGGATCCGGGCGGACAGAAGTCGGA-3’

The PCR products were analyzed by a 1% agarose gel and purified using a gel extraction kit (Qiagen). The purified inserts, the bait vector pGBKT7, and the prey vector pGADT7 (Takara Bio) were digested with High Fidelity NdeI (New England Biolabs) only to insert DHFR into pGBKT7, and also digested with BamHI and EcoRI

to insert CDK5 into pGADT7. Lower concentrations than indicated in the protocol were used for EcoRI and CDK5, since CDK5 contains a restriction site for EcoRI. The vectors were further dephosphorylated by directly adding 1 µl of FastAP Thermosensitive Alkaline Phosphatase (Thermo Scientific). Vector and insert were again purified using a gel extraction kit. Ligation was carried out in a 1:3 ratio (vector: insert) using the protocol from Thermo Fisher Scientific at RT for 30 min, followed by heat shock transformation of the ligation mixture into competent DH5α-*E. coli*. Plasmid isolation was performed using the QIAprep® Spin Miniprep Kit (Qiagen). They were analyzed by PCR and sequencing using a standard T7 primer (Eurofins Scientific).

3.2.5.2 Synthesis of trimethoprim-PEG-purvalanol B

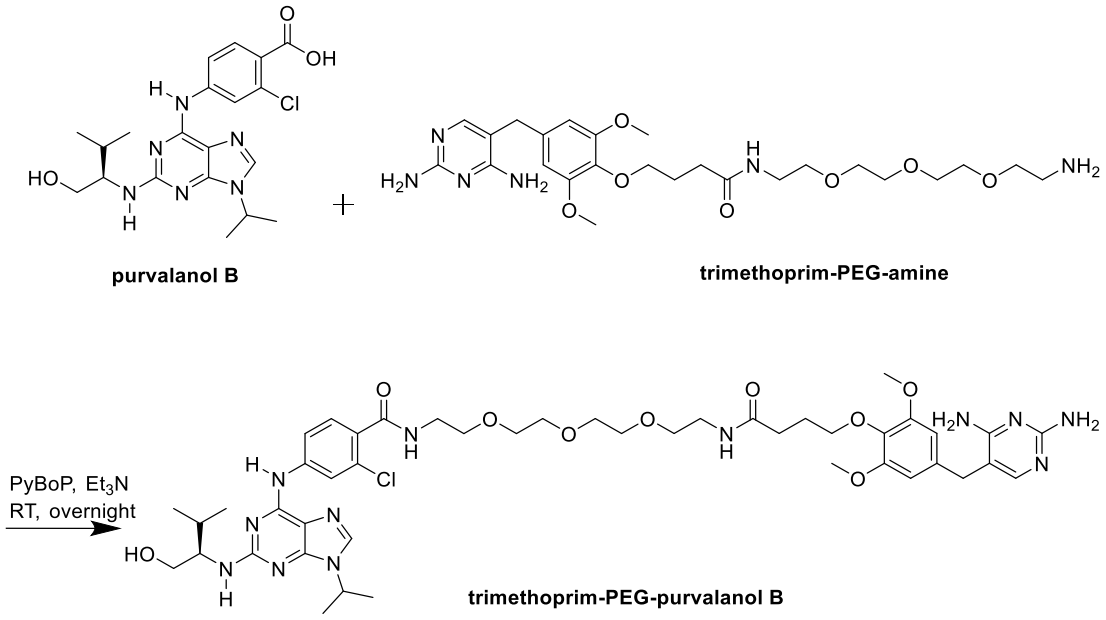

Purvalanol B (3.0 mg, 6.9 µmol) and PyBOP (9.0 mg, 17.3 µmol, 2.5 eq) were dissolved in 0.3 ml of DMSO. Et_3N (3.0 µl, 20.8 µmol, 3 eq) was added and the mixture was stirred for 45 min at RT in the dark. Trimethoprim-PEG-amine (THK42) (4.0 mg, 7.6 µmol, 1.1 eq) was added and the reaction mixture was stirred at RT in the dark overnight. The reaction mixture was purified by semi-preparative HPLC, and solvent was evaporated in vacuo to yield 3.3 mg (3.5 µmol, 50%) of trimethoprim-PEG-purvalanol B.

3.2.5.3 Spot test with trimethoprim-PEG-purvalanol B

The *Saccharomyces cerevisiae* reporter strain ABC9Δ was transformed with bait and prey plasmid in two steps. In the first step, the bait plasmid was introduced into the yeast using the quick & easy protocol from Gietz et al. [72]. The transformation mix was spread on 10 mm plates containing complete minimal medium minus tryptophan (-W). In a second step, the yeast cells containing the bait plasmid were transformed using the high efficiency transformation protocol from Gietz et al. [73]. Selection of transformants was carried out on plates containing complete minimal medium minus leucine tryptophan (-LW). One colony of each transformation was re-streaked on a -LW plate to ensure robust growth. The yeast was then picked from the plate, and suspended in 1× TE in 3 dilutions. A 2 µl portion of each dilution was spotted on -LW plates as growth control, and on plates containing complete minimal medium minus leucine tryptophan histidine (-LWH) and on -LWH plates containing 10 µM trimethoprim-PEG-purvalanol B (in DMSO). The plates were incubated at 30°C and pictures were taken after 4 d.

3.2.6 Y3H system validation with ethinylestradiol as model drug

3.2.6.1 Preparation of the Y3H reporter strains containing cDNA libraries

The mammary gland, pancreas and kidney cDNA library in pACT2 were purchased from Takara Bio (traditional Y2H libraries). Plasmids were isolated after cultivation in Luria-Bertani (LB) medium containing ampicillin using a Qiagen MaxiPrep kit. The ABC9Δ strain containing the bait plasmid (eDHFR in pGBKT7) was transformed by electroporation based on the protocol of Benatuil et al. [74] with modifications: An overnight culture of yeast in -W was diluted 5× to 1 l in two 500 ml baffled flasks. After incubation on a shaker for 5-6 h, the cultures were centrifuged at 4°C (*500 g*) for 2 min. The pellets were washed twice with 200 ml of ice cold MilliQ water each and once with 200 ml of ice cold 1 M sorbitol. The pellet was suspended in 80 ml of 0.1 M lithium

acetate/10 mM DTT and incubated at 30°C for 30 min with shaking. After centrifugation, the pellet was washed with 80 ml of ice cold 1 M sorbitol and centrifuged again. The competent cells were cautiously suspended in 400 µl of ice cold 1 M sorbitol (total volume about 1 ml) and used within 1 h. 1.5 µg of library plasmid were used for electroporation. The electroporation was carried out using an Eppendorf Eporator with the settings for *Saccharomyces cerevisiae*. 1 ml of pre-warmed YPAD medium was added directly after the pulse, and the transformation mixture was incubated at 30°C on a thermoshaker (*400 rpm*). After 1 h, the mixtures were centrifuged (1 min, *10 000 rpm*). The pellets were suspended in -LW medium and incubated at 30°C overnight on a shaker. The cultures were centrifuged and washed twice with one volume of 1× TE. About two pellet volumes of freezing solution (65% glycerol, 100 mM $MgSO_4$, 25 mM Tris-HCl pH 8) were added. The viability of the libraries was determined by plating dilutions on -LW plates to be 2×10^9 cfu/ml for the mammary gland library, 4×10^9 cfu/ml for the pancreas library and 2×10^6 cfu/ml for the kidney library.

3.2.6.2 Synthesis of trimethoprim-PEG-ethinylestradiol

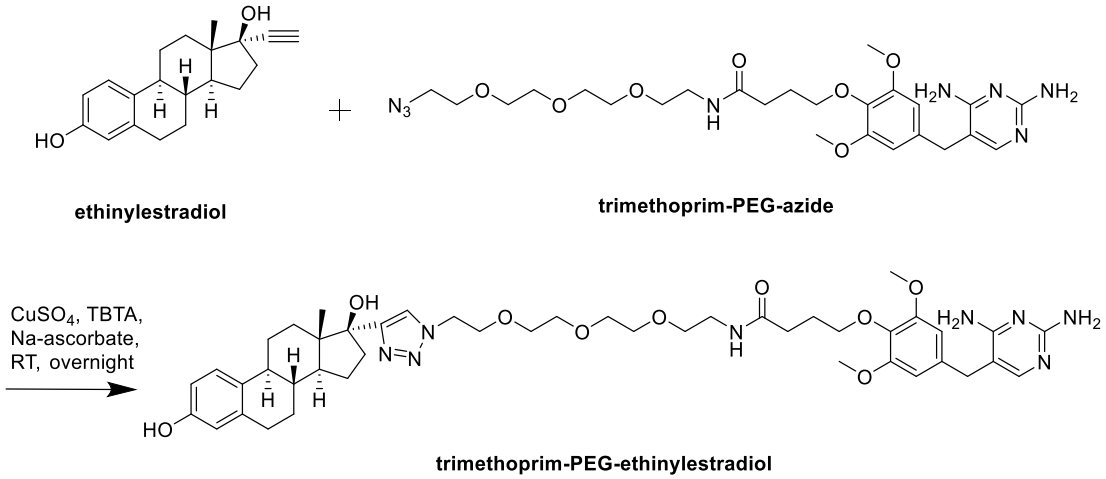

Ethinylestradiol (2.0 mg, 6.7 µmol) and trimethoprim-PEG-azide (THK15) (3.8 mg, 6.7 µmol, 1 eq) were dissolved in 1.35 ml of DMSO. A catalyst mixture of 30 µl of $CuSO_4$ pentahydrate (25 mg/ml in H_2O), 167 µl of 20 mM tris((1-benzyl-4-triazolyl)methyl)amine (TBTA) in DMSO and 67 µl of sodium ascorbate (100 mg/ml) in

H_2O was prepared separately and immediately added to the mixture of ethinylestradiol and THK15. The mixture was stirred at RT under nitrogen atmosphere overnight. The reaction mixture was cleaned up by semi-preparative HPLC. The solvent was evaporated in vacuo to yield 4.6 mg (5.4 µmol, 80%) of trimethoprim-PEG-ethinylestradiol.

3.2.6.3 Y3H screening of ethinylestradiol

Both mammary gland cDNA library and pancreas cDNA library with the amount of about 25-50 µl stock were diluted in 1× TE and then homogeneously spread on large plates (150 mm diameter) containing complete minimal medium minus leucine tryptophan histidine (-LWH) + 2.5 mM 3-amino-1,2,4-triazole (3-AT) + 10 µM trimethoprim-PEG-ethinylestradiol (diluted from a 10 mM stock in DMSO) + 1% (w/v) agarose. After 10 d at 30°C, all colonies larger than 1 mm in diameter were picked and resuspended in 100 µl 1× TE each in 96 well plates. Using a metal 96-prong replicator, the resuspended colonies were transferred onto -LWH plates with 2.5 mM 3-AT first and then onto -LW plates. After 5 d at 30°C, all colonies which did not grow in -LWH plates but grew in -LW plates were picked and resuspended in 100 µl 1× TE in 96 well plates. The resuspended colonies were transferred onto -LWH plates only with 1 mM 3-AT first and then onto -LWH plates with 1 mM 3-AT and 10 µM trimethoprim-PEG-ethinylestradiol using a metal 96-prong replicator. After 3 d at 30°C, all colonies which grew better in plates with trimethoprim-PEG-ethinylestradiol than in plates without the compound were picked and resuspended in 100 µl 1× TE in 96 well plates. 2 µl of the resuspended yeast cells were spotted on a -LW plate to ensure robust growth. After 3 d at 30°C, the colonies were picked with tips and resuspended in 1 ml -LW medium. Yeast cultures were then incubated at 30°C overnight. The cDNA inserts were amplified by colony PCR.

3.2.6.4 Colony PCR

For each colony PCR sample, 5 µl 10× PCR Buffer without Mg, 1.5 µl 50 mM $MgCl_2$, 1 µl 10 mM dNTP Mix, 0.2 µl Taq DNA Polymerase (5 U/µl) and 11.3 µl H_2O were mixed to get the PCR mix. Each colony was picked with the amount of a tip head and dissolved in 30 µl H_2O. The PCR mix was added to the DNA sample in a PCR tube. Then, the tubes were put in the cycler and the proper program was selected to amplify target DNA fragments. Afterwards, the PCR products were analyzed by Agarose gel and those samples with bands on the gel were sent for sequencing (Eurofins Scientific). The cDNA identity was determined by BLAST analysis. The only sequencing result that led to a hit was identified as DNA fragment of PLOD2 (procollagen-lysine 2-oxoglutarate 5-dioxygenase 2, Table 7).

GTTCTCTTCGTCCTCATCATGATGCTTCTACATTTACCATAAACATTGCACTTA
ATAACGTGGGAGAAGACTTTCAGGGAGGTGGTTGCAAATTTCTAAGGTACAAT
TGCTCTATTGAGTCACCACGAAAAGGCTGGAGCTTCATGCATCCTGGGAGAC
TCACACATTTGCATGAAGGACTTCCTGTTAAAAATGGAACAAGATACATTGCA
GTGTCATTTATAGATCCCTAAGTTATTTACTTTTCATTGAATTGAAATTTATTTT
GGATGAATGACTGGCATGAACACGTCTTTGAAGTTGTGGCTGAGAAGATGAG
AGGAATATTTAAATAACATCAACAGAACAACTTCACTTTGGGCCAAACATTTGA
AAAACTTTTTATAAAAAATTGTTTGATATTTCTTAATGTCTGCTCTGAGCCTTAA
AACACAGATTGAAGAAGAAAAGAAAGAAAAAACTTAAATATTTATTTCTATGCT
TTGTTGCCTCTGAGAATAATGACAATTTATGAATTTGTGTTTCAAATTGATAAAA
TATTTAGGTACAAATAACAAGACTAATAATATTTTCTTATTTAAAAAAAGCATGG
GAAGATTTTTATTTATCAAAATATAGAGGAAATGTAGACAAAATGGATATAAAT
GAAAATTACCATGTTGTAAAACCTTGAAAATCAGATTCTAACTGGATTTGTATG
CAACTAAGTATTTTTCTGAACACCTATGCAGGTCTTATTTACAGTAGTTACTAA
GGGAACACACAAAGAATTACACAACGTTTTCCTCAAGAAAATGGTACAAAACA
CAACCGAGGAGCGTATACAGTTGAAAACATTTTTGTTTTGATTGGAAGGCAGA

TTATTTTATATTAGTATTAAAAATCAAACCCTATGTTTCTTTCAGATGAATCTTC
CAAAGTGGATTATATTAAGCAGGTATTAGATTTAGGAAAACCTTTCCATTTCTT
AAAGTATTATCAAGTGTCAAGATCAGCAAGTGTCCTTAAGTCAAACAGGTTTTT
TTTGTTGGTGGTTTTTGCTTTGTTTCCTTTTTTAGAAAGTTCTAGAAAATAGGG
AAAC

Table 7. Sequencing result of PLOD2 hit

3.2.6.5 Amplification of ethinylestradiol hit plasmids in *E. coli*

Plasmid DNAs of potential ethinylestradiol target proteins were isolated with a commercial kit according to the manufacturer's instructions (EZ-10 Spin Column Yeast Plasmid DNA Mini-Preps Kit), and transferred into *E. coli* cells using electroporation. After incubation at 37°C for 1 h, the *E. coli* cells were homogeneously spread on plates (100 mm diameter) containing LB medium + 50 µg/ml ampicillin. After overnight incubation at 37°C, single colonies were picked from each plate and suspended in 5 ml LB medium with 50 µg/ml ampicillin. After overnight culture at 37°C and *100 rpm* in the thermoshaker, *E. coli* cell pellets were recovered by centrifugation. Plasmid DNAs were then isolated with a commercial kit according to the manufacturer's instructions (QIAprep® Spin Miniprep Kit (250), Qiagen). The cDNA inserts were analyzed by sequencing (Eurofins Scientific) and subsequent BLAST analysis. The standard GAL4 AD primer was used for DNA sequencing.

3.2.6.6 Yeast transformation with ethinylestradiol hit plasmids

Re-streaked *Saccharomyces cerevisiae* Y2H Gold strain (Takara Bio) yeast cells were collected with a sterile tip with the amount of a match head and dissolved in 6 ml YPAD medium in a 50 ml tube. After an overnight culture in the thermoshaker at 30°C and *120 rpm*, the yeast cells were pelleted by centrifugation at *13000 rpm* for 45 s at RT. The cell pellet was resuspended in 1 ml sterile water and centrifuged at *11000 rpm* for

45 s at RT. The supernatant was discarded. Afterwards, 240 µl PEG 3350 (50% w/v), 36 µl LiAc (1.0 M), 50 µl single-stranded carrier DNA (2.0 mg/ml) and 34 µl of sterile water plus ethinylestradiol hit plasmid DNA (up to 1 mg), were added to the pellet in the order given, and mixed by vortex mixing briskly until resuspended. The mixture was incubated in the thermoshaker at 40°C for 1 h and then pelleted by centrifugation at *11000 rpm* for 45 s at RT. 100 µl of sterile water was added to the pellet, which was stirred afterwards to break up the cell pellet and vortexed to thoroughly resuspend. The cells were spread onto small -L plate (100 mm diameter) and dried near the flame. The plate was incubated at 30°C for 4 d until there were yeast colonies growing.

3.2.6.7 Yeast cell lysates for ethinylestradiol affinity chromatography

For each transformed yeast strain, a 5 ml of overnight culture in YPAD medium was prepared. After incubation, the YPAD medium was discarded by centrifugation. The pellet was resuspended in -L medium and vortexed for 30 s to disperse cell clumps. Then the cell culture was diluted with -L medium to an OD600 value of about 0.2. The cells were incubated at 30°C, *120 rpm* for the protein expression until the OD600 value reached 0.4-0.6. The culture was poured into pre-chilled 50 ml falcons halfway filled with ice. The tubes were immediately placed in a pre-chilled rotor and centrifuged at *1000 g* for 5 min at 4°C. The cell pellet was washed with 50 ml of ice-cold H_2O. Glass beads of the same volume as the cell pellet were added to the pellet. A 150 µl portion of RIPA buffer (150 mM NaCl, 50 mM Tris-HCl pH 8, 1% Nonidet P-40, 0.5% sodium deoxycholate and 0.1% SDS) with 1 mM PMSF was added to resuspend the pellet. The mixture was vortexed for 1 min and incubated on ice for 1 min afterwards. The vortex/chill cycle was repeated 4 more times. The supernatant was collected after centrifugation at *18 000 rpm* for 10 min at 4°C. The remaining pellet was extracted with another 150 µl of RIPA buffer with 1 mM PMSF and the lysates were pooled. The protein concentration of the lysate was determined by Bradford assay.

3.2.6.8 Synthesis of biotin-PEG-ethinylestradiol

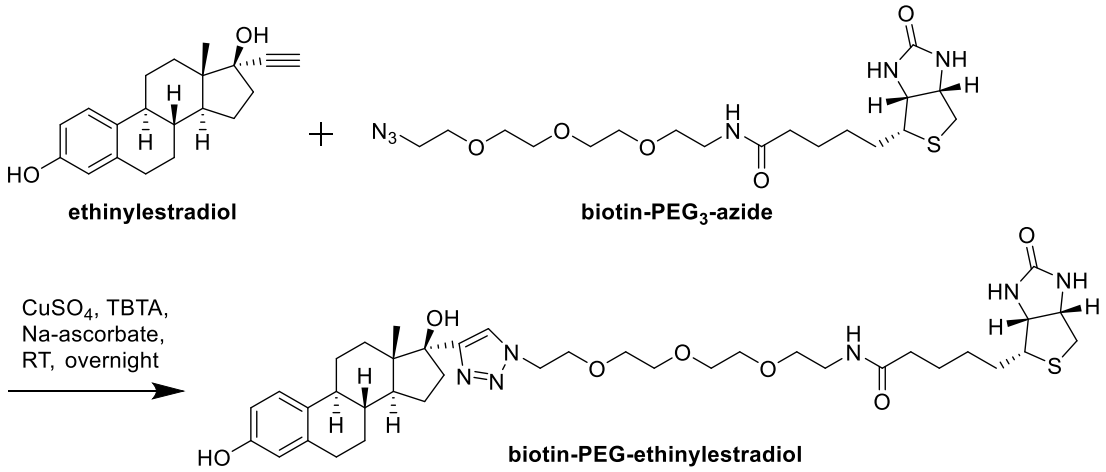

Biotin-PEG_3-azide (2.0 mg, 4.5 µmol) and ethinylestradiol (6.67 mg, 22.5 µmol, 5 eq) were dissolved in 0.5 ml of DMSO. A catalyst mixture of 25 µl of $CuSO_4$ pentahydrate (25 mg/ml in H_2O), 115 µl of 20 mM TBTA in DMSO and 45 µl of sodium ascorbate (100 mg/ml in H_2O) was prepared separately and immediately added to the mixture of biotin-PEG-azide and ethinylestradiol. The mixture was stirred at RT under nitrogen atmosphere overnight. The reaction mixture was cleaned up by semi-preparative HPLC. The solvent was evaporated in vacuo to yield 3 mg (4.1 µmol, 89%) of biotin-PEG-ethinylestradiol.

3.2.6.9 Biotin-tag-based ethinylestradiol pull-down

The pull-down assay was performed as described by Chidley et al. [70]with adaptations. 100 µl of streptavidin beads suspension were washed with washing buffer (10 mM HEPES-NaOH, 50 mM KCl, 1 mM EDTA-2Na, 10% glycerol, pH 7.9) and resuspended in 50 µl of washing buffer. 50 µl of 2 mM biotin-PEG-ethinylestradiol conjugate or biotin-PEG_3-azide as negative control were added to the beads. The mixture was incubated at RT for 30 min. After washing 3 times with 1 ml of washing buffer each, 100 µl of either yeast cell lysate (total 1 mg of protein as determined by Bradford assay) or 200 ng of human recombinant PLOD2 (Abnova™, full-length ORF AAH37169, amino acids 27-758, with GST tag at N-terminal) were added. The mixture

was incubated at 4°C for 1 h. The beads were washed 2 times with 0.5 ml of washing buffer each. The supernatant was discarded by centrifugation at *3000 rpm* for 3 min at 4°C. The samples were then kept at -80°C until Western Blot analysis.

3.2.6.10 Western blot analysis

45 µl of 1× Western blot sample buffer was added to the pull-down samples. The proteins were denatured at 99°C for 5 min and then separated by sodium dodecyl sulfate polyacrylamide gel electrophoresis (SDS-PAGE) in electrophoresis buffer on discontinuous polyacrylamide gels (100 V, 21 min then 200 V, 43 min) and then transferred to 0.2 µm polyvinylidene difluoride (PVDF) membranes by western blotting in 1× tank buffer (100 V, 90 min, 4 °C). The membranes were incubated with blocking buffer (5% bovine serum albumin (BSA) in PBS with 0.1% Tween 20) for 1 h, followed by incubating with primary antibody overnight at 4°C. Either a GAL4 AD primary antibody (abcam) was used for the fragment (GAL4 AD target protein fusion protein), or a PLOD2 antibody (abcam) for the detection of human recombinant PLOD2. The primary antibody was removed, and the membrane was washed 4 times by 1× TBS-T for 5 min each. The membrane was then exposed to secondary antibodies for 1 h, followed by 4 washing steps with TBS-T for 5 min each. Membranes were conjugated with ECL solution with 2.5 mM luminol afterwards, and conjugated proteins were detected by the ChemiDoc™ Touch Imaging System (Bio-Rad, Munich, Germany). The bands were identified by comparison with Page Ruler™ Plus Prestained Protein Ladder. The protein level was normalized to total protein level and quantified by Image Lab™ Software (Bio-Rad).

Separation Gel	6-12 %
Rotiophorese™ Gel 30	40-80%
Tris (pH 8.8)	375 mM
SDS	0.1%
TEMED	0.1%
APS	0.05%
H_2O	

Stacking gel	
Rotiophorese™ Gel 30	17%
Tris (pH 6.8)	125 mM
SDS	0.1%
TEMED	0.2%
APS	0.1%
H_2O	

5× SDS sample buffer	
Tris-HCl pH 6.8	3.125 M
Glycerol	50%
SDS	5%
DTT	2%
Pryonin Y	0.025%
H_2O	

Electrophoresis buffer	
Tris	4.9 mM
Glycine	38 mM
SDS	0.1 %
H_2O	

TBS-T (pH 7.6)	
Tris-HCl	50 mM
NaCl	150mM
Tween 20	0.05%
H_2O	

Tank buffer	
Tris base	48 mM
Glycine	39 mM
MeOH	20 %
H_2O	

Table 8. Buffers and solutions for Western blot analysis

3.2.6.11 PLOD2 activity assay

The activity assay was performed as described by Devkota et al. [75] with minor adaptations. In brief, 15 µl of 0.47 µM PLOD2 in assay buffer (50 mM HEPES pH 7.4, 150 mM NaCl, 0.5% DMSO, 0.01% Triton-X 100) were added to a white 96 well plate. Then, 5 µl of 5× compound stock or DMSO in assay buffer were added. After incubation for 50 min at RT, 5 µl of 5× substrate mix (1 mM $[IKG]_3$ peptide, 0.1 mM α-ketoglutarate, 1 mM ascorbic acid, 0.1 mM $FeCl_2$ (freshly prepared) in assay buffer) were added to the well. The plate was incubated for 3 h at RT. The succinate detection reagents from

Promega's Succinate-Glo™ Assay kit were added according to the manufacturer's instruction. Luminescence was measured on an Orion II Microplate Luminometer.

3.2.6.12 Collagen I staining

A collagen gel with a concentration of 2 mg/ml was prepared. For that, 58.8 µl of collagen was mixed with 30 µl of 10× PBS, 1.4 µl of 1N NaOH and 209.8 µl of H_2O. 2.5% of FITC labelled collagen were added to the collagen solution for visualization. 30 µl of collagen was added to each well of an 8 well ibidi slide and distributed with a pipette tip to coat the whole bottom of the well. The slide was placed in a 10 cm petri dish and a wet paper towel was added to the petri dish to avoid drying out of the collagen. The collagen was incubated at 37°C/5% CO_2 for 30 min to allow polymerization. In the meantime, HeLa cells were prepared at a concentration of 27000 cells/ml. 230 µl of the cell suspension was seeded to each well after the collagen had polymerized. Afterwards, 20 µl of the compound samples was added to each well. The slide was incubated at 37°C/5% CO_2. After 24 h, cellular nuclei were stained using 2.5 mg/ml Hoechst 33342 at 37°C/5% CO_2 for 20 min. Afterwards, the cells were washed with PBS once and 250 µl of medium was added to each well again. The cells were imaged on a Leica TCS SP8 confocal laser scanning microscope. A HC PL APO CS2 63×/1.4 NA oil objective was applied. The pinhole size was set to 1.0 airy units and the pixel size was set to 2048×2048. Following lasers were employed: 405 nm (diode) for excitation of Hoechst 33342, 488 nm (argon) for excitation of FITC labelled collagen. Mean intensities of collagen fibers around cells were evaluated using ImageJ (Version 1.53c) and normalized to a no cell control.

3.2.6.13 PLOD2 expression levels

HeLa cells were seeded in 6 well plates (3×10^5 cells/well) and allowed to attach for 24 h. Cells were stimulated with compounds and DMSO control for 24 h, before cell

medium was removed and cells were washed with ice cold PBS twice. 100 µl of RIPA buffer (150 mM NaCl, 50 mM Tris-HCl pH 8, 1% Nonidet P-40, 0.5% sodium deoxycholate and 0.1% SDS) were added to each well and plates were incubated overnight at -80°C. Cells were scraped with a cell scraper after thawing on ice. Cell lysates were collected and centrifuged at *14 000* rpm for 10 min at 4°C, before protein concentrations were determined by Bradford assay using BSA as standard. Proteins were denatured by heating at 99°C for 5 min in SDS sample buffer and equal amounts of protein were separated by SDS-PAGE on discontinuous polyacrylamide gels (12%). Proteins from the gels were transferred to 0.2 µm PVDF membranes by western blotting. For detection of PLOD2 expression, a PLOD2 primary antibody (abcam) and a Goat anti-Rabbit IgG secondary antibody (dianova) were used. Protein bands were detected by chemiluminescence using a ChemiDoc™ Touch Imaging System (Bio-Rad, Munich, Germany). Protein bands were analyzed by comparison with the Page Ruler™ Plus Prestained Protein Ladder and intensities of protein bands were analyzed using Image Lab™ software (Bio-Rad, Munich, Germany).

3.2.7 Y3H screening of phyllobilins

3.2.7.1 Y3H screening of PleB

3.2.7.1.1 Synthesis of trimethoprim-PEG-PleB

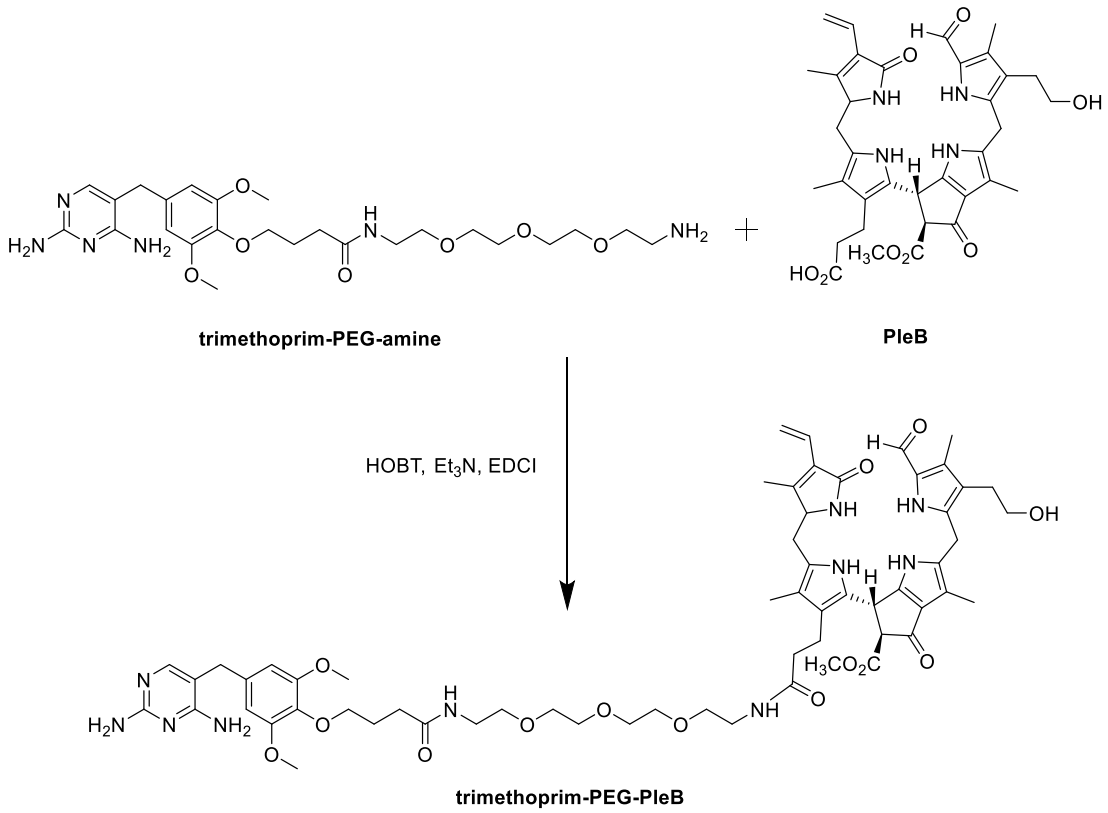

PleB (2.53 mg, 4 µmol) was dissolved in 0.5 ml of DMSO in a 5 ml round bottom flask. HOBT (5.41 mg, 40 µmol, 10 eq) and EDCl (7.67 mg, 40 µmol, 10 eq) were dissolved in 0.2 ml of DMSO and transferred to the flask. The mixture was stirred for 1 h at RT under air in the dark. Et_3N (5.6 µl, 40 µmol, 10 eq) was dissolved in 0.1 ml of DMSO and transferred to the flask. Trimethoprim-PEG-amine (THK42) (4.29 mg, 8 µmol, 2 eq) was dissolved in 0.2 ml of DMSO and added to the flask slowly and the reaction mixture was stirred at RT under air in the dark overnight. The reaction mixture was purified by semi-preparative HPLC, and solvent was evaporated in vacuo to yield 2.54 mg (2.2 µmol, 55%) of trimethoprim-PEG-PleB.

3.2.7.1.2 Y3H screening of PleB

Mammary gland cDNA library, pancreas cDNA library and kidney cDNA library with the amount of about 25-60 µl stock were diluted in 1× TE and then homogeneously spread on large -LWH plates (150 mm diameter) + 2.5 mM 3-AT + 10 µM trimethoprim-PEG-PleB + 1% (w/v) agarose. After 10 d at 30°C, all colonies larger than 1 mm in diameter were picked and resuspended in 100 µl 1× TE each in 96 well plates. Using a metal 96-prong replicator, the resuspended colonies were transferred onto -LWH plates with 2.5 mM 3-AT first and then onto -LW plates. After 5 d at 30°C, all colonies, which did not grow in -LWH plates but grew in -LW plates, were picked and resuspended in 100 µl 1× TE in 96 well plates. The resuspended colonies were transferred onto -LWH plates only with 1 mM 3-AT first and then onto -LWH plates with 1 mM 3-AT and 10 µM trimethoprim-PEG-PleB using a metal 96-prong replicator. After 3 d at 30°C, all colonies which grew better in plates with trimethoprim-PEG-PleB than in plates without the compound were picked and resuspended in 100 µl 1× TE in 96 well plates. 2 µl of the resuspended yeast cells were spotted on a -LW plate to ensure robust growth. After 3 d at 30°C, the colonies were picked with tips and resuspended in 1 ml -LW medium. Yeast cultures were then incubated at 30°C overnight. The cDNA inserts were amplified by colony PCR and analyzed by sequencing (Eurofins Scientific). The cDNA identity was determined by BLAST analysis.

3.2.7.2 Y3H screening of PxB

3.2.7.2.1 Synthesis of trimethoprim-PEG-PxB

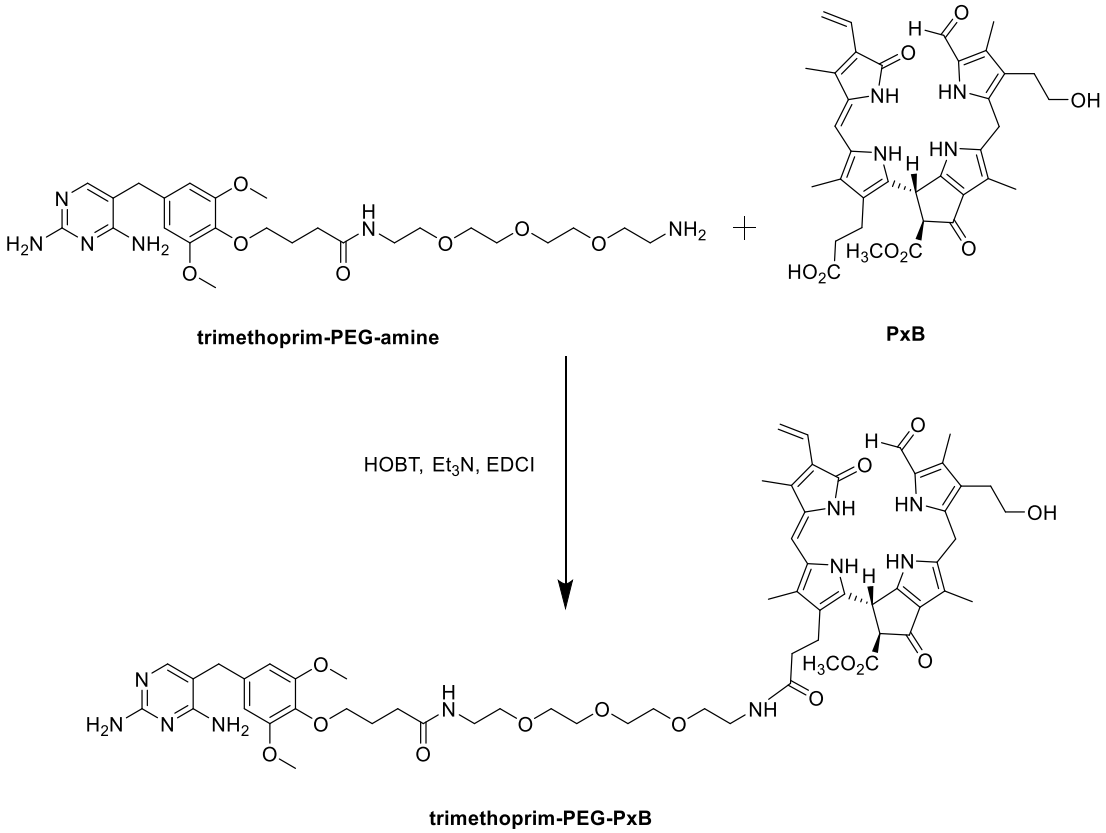

PxB (3.59 mg, 5.7 µmol) was dissolved in 0.5 ml of DMSO in a 5 ml round bottom flask. HOBT (7.66 mg, 57 µmol, 10 eq) and EDCI (10.93 mg, 57 µmol, 10 eq) were dissolved in 0.2 ml of DMSO and transferred to the flask. The mixture was stirred for 1 h at RT under air in the dark. Et_3N (8 µl, 57 µmol, 10 eq) was dissolved in 0.1 ml of DMSO and transferred to the flask. Trimethoprim-PEG-amine (THK42) (6.11 mg, 11.4 µmol, 2 eq) was dissolved in 0.2 ml of DMSO and added to the flask slowly and the reaction mixture was stirred at RT under air in the dark overnight. The reaction mixture was purified by semi-preparative HPLC, and solvent was evaporated in vacuo to yield 4.07 mg (3.5 µmol, 61%) of trimethoprim-PEG-PxB.

3.2.7.2.2 Y3H screening of PxB

Mammary gland cDNA library, pancreas cDNA library and kidney cDNA library with the amount of about 25-60 µl stock were diluted in 1× TE and then homogeneously spread on large -LWH plates (150 mm diameter) + 2.5 mM 3-AT + 10 µM trimethoprim-PEG-PxB + 1% (w/v) agarose. After 10 d at 30°C, all colonies larger than 1 mm in diameter were picked and resuspended in 100 µl 1× TE each in 96 well plates. Using a metal 96-prong replicator, the resuspended colonies were transferred onto -LWH plates with 2.5 mM 3-AT first and then onto -LW plates. After 5 d at 30°C, all colonies which did not grow in -LWH plates but grew in -LW plates were picked and resuspended in 100 µl 1× TE in 96 well plates. The resuspended colonies were transferred onto -LWH plates only with 1 mM 3-AT first and then onto -LWH plates with 1 mM 3-AT and 10 µM trimethoprim-PEG-PxB using a metal 96-prong replicator. After 3 d at 30°C, all colonies which grew better in plates with trimethoprim-PEG-PxB than in plates without the compound were picked and resuspended in 100 µl 1× TE in 96 well plates. 2 µl of the resuspended yeast cells were spotted on a -LW plate to ensure robust growth. After 3 d at 30°C, the colonies were picked with tips and resuspended in 1 ml -LW medium. Yeast cultures were then incubated at 30°C overnight. The cDNA inserts were amplified by colony PCR and analyzed by sequencing (Eurofins Scientific). The cDNA identity was determined by BLAST analysis. NPC intracellular cholesterol transporter 2 (NPC2, Table 9) and promyelocytic leukemia protein (PML, Table 10) were identified as hits by the sequencing results.

CGTCCCAGTTCCCTTTCCCATTCCTGAGCCTGATGGTTGTAAGAGTGGAATTA
ACTGCCCTATCCAAAAAGACAAGACCTATAGCTACCTGAATAAACTACCAGTG
AAAAGCGAATATCCCTCTATAAAACTGGTGGTGGAGTGGCAACTTCAGGATGA
CAAAAACCAAAGTCTCTTCTGCTGGGAAATCCCAGTACAGATCGTTTCTCATC
TCTAAGTGCCTCATTGAGTTCGGTGCATCTGGCCAATGAGTCTGCTGAGACTC
TTGACAGCACCTCCAGCTCTGCTGCTTCAACAACAGTGACTTGCTCTCCAATG
GTATCCAGTGATTCGTTGAAGAGGAGGTGCTCTGTAGCAGAAACTGAGCTCC
GGGTGGCTGGTTCTCAGTGGTTGTCTCATGTCTCTTTTTCTGTCTTAGGTGGT
TTCATTAAATGCAGCACTTGGTTAGCAGATGTTTAATTTTTTTTTTAACAACATT
AACTTGTGGCCTCTTTCTACACCTGGAAATTTACTCTTGAATAAATAAAAACTC
GTTTGTCTTGTCTTCTGCA

Table 9. Sequencing result of NPC2 hit

CGTTGACCTGCCCGAGGAGGCAGAGAGAGTGAAGGCCCAGGTTCAGGCCCT
GGGGCTGGCTGAAGCCCAGCCTATGGCTGTGGTACAGTCAGTGCCCGGGGC
ACACCCCGTGCCAGTGTACGCCTTCTCCATCAAAGGCCCTTCCTATGGAGAG
GATGTCTCCAATACAACGACAGCCCAGAAGAGGAAGTGCAGCCAGACCCAGT
GCCCCAGGAAGGTCATCAAGATGGAGTCTGAGGAGGGGAAGGAGGCAAGGT
TGGCTCGGAGCTCCCCGGAGCAGCCCAGGCCCAGCACCTCCAAGGCAGTCT
CACCACCCCACCTGGATGGACCGCCTAGCCCCAGGAGCCCCGTCATAGGAA
GTGAGGTCTTCCTGCCCAACAGCAACCACGTGGCCAGTGGCGCCGGGGAGG
CAGAGGAACGCGTTGTGGTGATCAGCAGCTCGGAAGACTCAGATGCCGAAAA
CTCGGTGAGTGGCCCAGAAGTTCAGCCCAGGACTCCTGCCTCCCCCCATTTC
AGGTCCCAGGGGGCACAGCCACAGCAGGTGACTCTCAGACTTGCCTTGCGC
CTGGGGAATTTTCCAGTGAGGCATTGAGTCCCAAGCTGTGCTGAGGACAGTC
TCCAAATGACAGCTGCATGCCTGGACCACCCCAGCCCTCCCACTACACCAGG
GCCAGGAGCTCTTCTGAAATGCTGATAGCATGTGTCCAGAGCCCTGTCTCTTT

TCTGGAATGTCCAAGACCTTTGTCTGGAGCTTCCTTATGCATTTTCTGTCCTCT
AAGTCCTCAGTGAGGAGGGCTGGACAAGAATCCATTCCTTGGTTTATTACAGC
CAGTGGGGGCCAGTGAAGGGGTGTCAGGCCACAGGGCAGCTATATAGGGGC
CAAACAAGTGAGGTTTGACTCCATCCATGTAGAAAGATATATAAATCCATTCCA
CAGTGAAACAGGTGGCCTCGTGGGTAGTGACCCTTCTGTCCCTAGAGGTTTA
TTACTAGAGGCTGGACTATCACCTGTCCAGGGGAAAAGGGGATCTGAATAGA
GTGAAAGGTTGGACTGGGTGGCCCCTGAGGTCT

Table 10. Sequencing result of PML hit

3.2.7.2.3 Amplification of PxB hit plasmids in *E. coli*

Plasmid DNAs of potential PxB target proteins were transferred into *E. coli* cells using electroporation. After incubation at 37°C for 1 h, the *E. coli* cells were homogeneously spread on plates (100 mm diameter) containing LB medium + 50 µg/ml ampicillin. After overnight incubation at 37°C, single colonies were picked from each plate and suspended in 5 ml LB medium with 50 µg/ml ampicillin. After overnight culture at 37°C and *100 rpm* in the thermoshaker, *E. coli* cell pellets were recovered by centrifugation. Plasmid DNAs were then isolated with a commercial kit according to the manufacturer's instructions (QIAprep® Spin Miniprep Kit (250), Qiagen). The cDNA inserts were analyzed by sequencing (Eurofins Scientific) and subsequent BLAST analysis. The standard GAL4 AD primer was used for DNA sequencing.

3.2.7.2.4 Yeast transformation with PxB hit plasmids

Re-streaked *Saccharomyces cerevisiae* Y2H Gold strain (Takara Bio) yeast cells were collected with a sterile tip with the amount of a match head and dissolved in 6 ml YPAD medium in a 50 ml tube. After an overnight culture in the thermoshaker at 30°C and *120 rpm*, the yeast cells were pelleted by centrifugation at *13000 rpm* for 45 s at RT. The cell pellet was resuspended in 1 ml sterile water and centrifuged at *11000 rpm* for

45 s at RT. The supernatant was discarded. Afterwards, 240 µl PEG 3350 (50% w/v), 36 µl LiAc (1.0 M), 50 µl single-stranded carrier DNA (2.0 mg/ml) and 34 µl of sterile water plus PxB hit plasmid DNA (up to 1 mg), were added to the pellet in the order given, and mixed by vortex mixing briskly until resuspended. The mixture was incubated in the thermoshaker at 40°C for 1 h and then pelleted by centrifugation at *11000 rpm* for 45 s at RT. 100 µl of sterile water was added to the pellet, which was stirred afterwards to break up the cell pellet and vortexed to thoroughly resuspend. The cells were spread onto -L plate (100 mm diameter) and dried near the flame. The plate was incubated at 30°C for 4 d until there were yeast colonies growing.

3.2.7.2.5 Yeast cell lysates for PxB affinity chromatography

For each transformed yeast strain, 5 ml of an overnight culture in YPAD medium was prepared. After incubation, the YPAD medium was discarded by centrifugation. The pellet was resuspended in -L medium and vortexed for 30 s to disperse cell clumps. Then the cell culture was diluted with -L medium to an OD600 value of about 0.2. The cells were incubated at 30°C *120 rpm* for the protein expression until the OD600 value reached 0.4-0.6. The culture was poured into pre-chilled 50 ml falcons halfway filled with ice. The tubes were immediately placed in a pre-chilled rotor and centrifuged at *1000 g* for 5 min at 4°C. The cell pellet was washed with 50 ml of ice-cold H_2O. Glass beads of the same volume as the cell pellet were added to the pellet. A 150 µl portion of RIPA buffer (150 mM NaCl, 50 mM Tris-HCl pH 8, 1% Nonidet P-40, 0.5% sodium deoxycholate and 0.1% SDS) with 1 mM PMSF was added to resuspend the pellet. The mixture was vortexed for 1 min and incubated on ice for 1 min afterwards. The vortex/chill cycle was repeated 4 more times. The supernatant was collected after centrifugation at *18 000 rpm* for 10 min at 4°C. The remaining pellet was extracted with another 150 µl of RIPA buffer with 1 mM PMSF and the lysates were pooled. The protein concentration of the lysate was determined by Bradford assay.

3.2.7.2.6 Synthesis of biotin-PEG-PxB

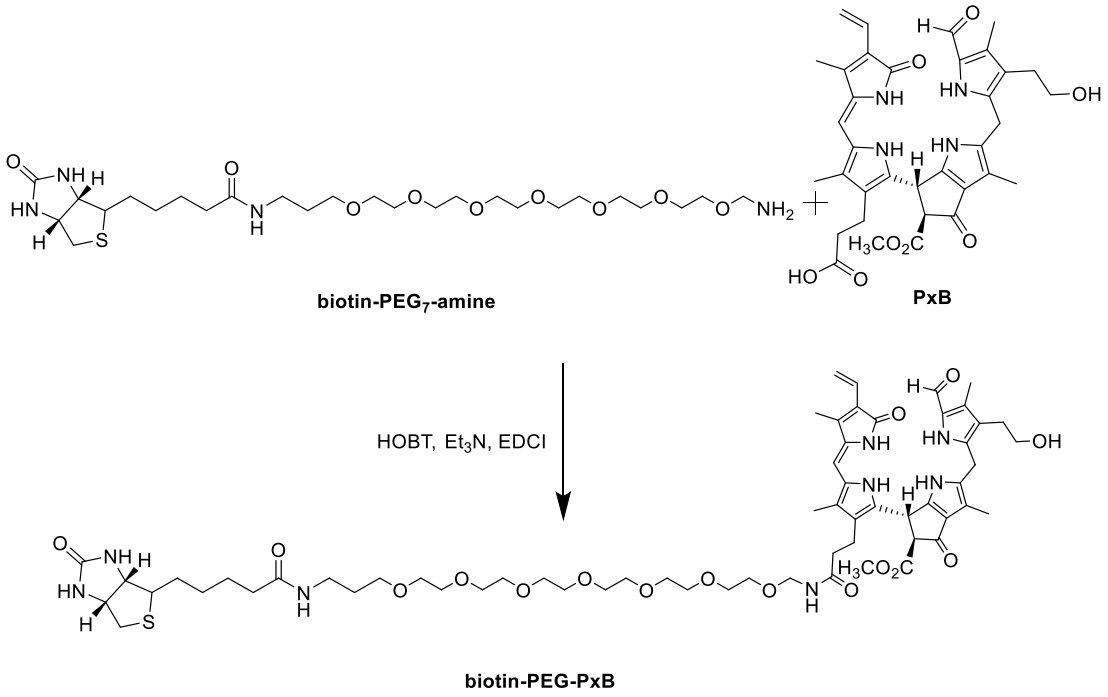

PxB (3.21 mg, 5 µmol) was dissolved in 1 ml of DMSO in a 5 ml round bottom flask. HOBT (6.76 mg, 50 µmol, 10 eq) and EDCl (9.56 mg, 50 µmol, 10 eq) were dissolved in 0.2 ml of DMSO and transferred to the flask. The mixture was stirred for 1 h at RT under air in the dark. Et_3N (6.97 µl, 50 µmol, 10 eq) was dissolved in 0.1 ml of DMSO and transferred to the flask. Biotin-PEG_7-amine (5.95 mg, 10 µmol, 2 eq) was dissolved in 0.5 ml of DMSO and added to the flask slowly and the reaction mixture was stirred at RT under air in the dark overnight. The reaction mixture was purified by semi-preparative HPLC, and solvent was evaporated in vacuo to yield 3.03 mg (2.5 µmol, 50%) of biotin-PEG-PxB.

3.2.7.2.7 Biotin-tag-based PxB pull-down

100 µl of streptavidin beads suspension were washed with washing buffer (10 mM HEPES-NaOH, 50 mM KCl, 1 mM EDTA-2Na, 10% glycerol, pH 7.9) and resuspended in 75 µl of washing buffer. 25 µl of 2 mM biotin-PEG-PxB conjugate or biotin-PEG_7-amine as negative control were added to the beads. The mixture was incubated at RT for 30 min. After washing 3 times with 1 ml of washing buffer each, 100 µl of yeast cell

lysate (total 1 mg of protein as determined by Bradford assay) were added. The mixture was incubated at 4°C for 1 h. The beads were washed 2 times with 0.5 ml of washing buffer each. The supernatant was discarded by centrifugation at *3000 rpm* for 3 min at 4°C. 45 µl of 1× Western blot sample buffer was added. The samples were boiled at 99°C for 5 min. The eluates were separated by SDS-PAGE on discontinuous polyacrylamide gels (12%). Proteins from the gels were transferred to 0.2 µm PVDF membranes by western blotting. For detection, a GAL4 AD primary antibody (abcam) was used for the fragment (GAL4 AD target protein fusion protein). Protein bands were detected by chemiluminescence using a ChemiDoc™ Touch Imaging System (Bio-Rad, Munich, Germany). Protein bands were analyzed by comparison with the Page Ruler™ Plus Prestained Protein Ladder and intensities of protein bands were analyzed using Image Lab™ software (Bio-Rad, Munich, Germany).

3.2.8 MS-based affinity chromatography for phyllobilins

3.2.8.1 Synthesis of biotin-PEG-PleB and biotin-PEG-PxB

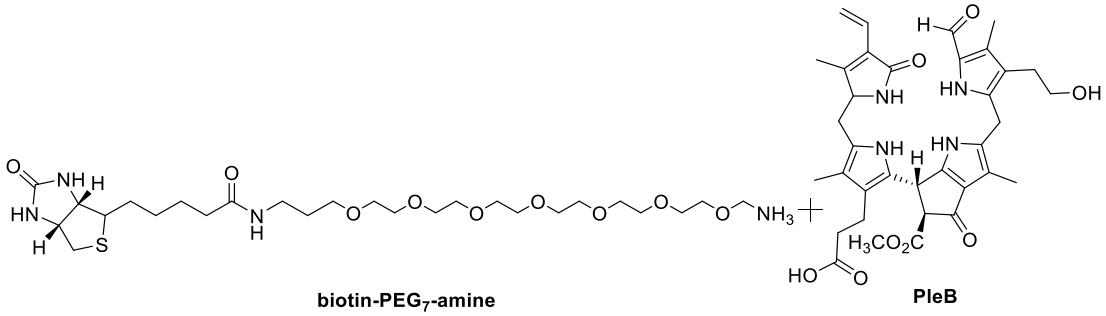

biotin-PEG$_7$-amine **PleB**

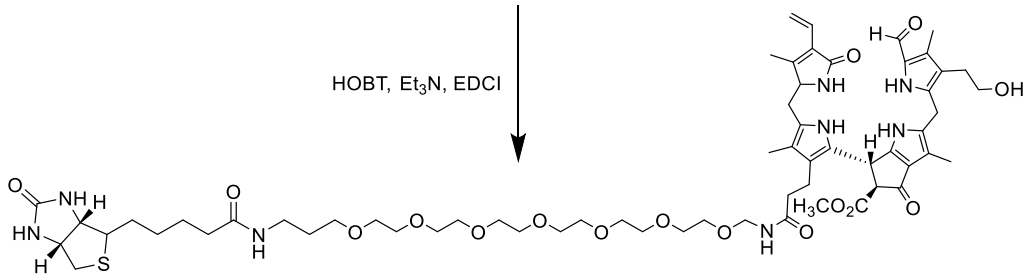

biotin-PEG-PleB

PleB (4 mg, 6.2 µmol) was dissolved in 1 ml of DMSO in a 5 ml round bottom flask. HOBT (8.38 mg, 62 µmol, 10 eq) and EDCI (11.88 mg, 62 µmol, 10 eq) were dissolved

in 0.5 ml of DMSO and transferred to the flask. The mixture was stirred for 1 h at RT under air in the dark. Et_3N (8.64 µl, 62 µmol, 10 eq) was dissolved in 0.1 ml of DMSO and transferred to the flask. Biotin-PEG_7-amine (7.37 mg, 12.4 µmol, 2 eq) was dissolved in 0.5 ml of DMSO and added to the flask slowly and the reaction mixture was stirred at RT under air in the dark overnight. The reaction mixture was purified by semi-preparative HPLC, and solvent was evaporated in vacuo to yield 1.98 mg (1.6 µmol, 26%) of biotin-PEG-PleB.

The synthesis of biotin-PEG-PxB was performed as described previously.

3.2.8.2 Synthesis of biotin-PEG-acetate

Acetic acid (4.4 µl, 7.6 µmol, 10 eq) was dissolved in 1 ml of DMSO in a 5 ml round bottom flask. HOBT (1.03 mg, 7.6 µmol, 10 eq) and EDCl (1.46 mg, 7.6 µmol, 10 eq) were dissolved in 0.3 ml of DMSO and transferred to the flask. The mixture was stirred for 1 h at RT under air in the dark. Et_3N (1.06 µl, 7.6 µmol, 10 eq) was dissolved in 0.2 ml of DMSO and transferred to the flask. Biotin-PEG_7-amine (0.46 mg, 0.76 µmol) was dissolved in 0.5 ml of DMSO and added to the flask slowly and the reaction mixture was stirred at RT under air in the dark overnight. The reaction mixture was purified by semi-preparative HPLC, and solvent was evaporated in vacuo to yield 0.098 mg (0.15 µmol, 20%) of biotin-PEG-acetate.

3.2.8.3 Affinity chromatography

25 µl of streptavidin beads suspension were washed with washing buffer (10 mM HEPES-NaOH, 50 mM KCl, 1 mM EDTA-2Na, 10% glycerol, pH 7.9) and resuspended in 100 µl of washing buffer. 5 µl of 2 mM biotin-PEG-PleB/PxB conjugate or biotin-PEG-acetate as negative control were added to the beads. The mixture was incubated at RT for 30 min. After washing 3 times with 1 ml of washing buffer each, yeast cell lysate (total 100 µg of protein as determined by Bradford assay) was added. The

mixture was incubated at 4°C for 1 h. The beads were washed 2 times with 1 ml of washing buffer each. The supernatant was discarded by centrifugation at *3000 rpm* for 3 min at 4°C. 45 µl of 1× Western blot sample buffer was added. The samples were boiled at 99°C for 5 min.

3.2.8.4 Mass spectrometry analysis

Samples from affinity chromatography were transferred onto pre-casted polyacrylamide gels which were run until gel pockets were empty. Protein containing areas were excised, destained and subsequently reduced with 45 mM Dithioerythritol (DTE) (30 min, 55°C) and alkylated with 100 mM iodoacetamide in the dark (2× for 15 min each, RT). Gel slices were washed twice for 15 min with 50 mM NH_4HCO_3 and an overnight in-gel digestion was performed using 70 ng sequencing grade modified trypsin. Supernatants were collected and dried using a vacuum centrifuge. The resulting peptides were dissolved in 0.1% formic acid in water and injected to a trap column (Acclaim® PepMap 100, 100 µm × 2 cm, nanoViper C18, 5 µm, 100 Å, Thermo Scientific) and separated at a flow rate of 250 nl/min using EasySpray columns (PepMap RSLC C18, 75 µm ID, 2 µm, Thermo Fisher Scientific) and 0.1% formic acid in water as solvent A. The chromatography method consisted of two consecutive gradients from 3% to 25% solvent B (0.1% formic acid in ACN) in 30 min and from 25% to 40% B in 5 min. For data dependent acquisition cycles of one full scan (350 to 1600 m/z) at a resolution of 60k and up to 12 data-dependent MS/MS scans at a resolution of 15k were used. Spectra were searched using MaxQuant (V1.6.1) and the Human subset of the Uniprot database. Statistical evaluation was done using Perseus (V1.5.3.2) by uploading the protein intensities to generate volcano plots with a $\log_2$ fold change of sample and control intensities against the $-\log_{10}$ p value.

3.2.9 Characterization of synthesized compounds

3.2.9.1 Characterization of trimethoprim-PEG-purvalanol B

R_t (retention time) = 15.7 min. UV/Vis online spectrum from HPLC run (nm, rel ε): 220 (1.00), 266 (0.68), 322 (0.81) nm.

HR-ESI-MS: $m/z_{calculated}$ ($C_{45}H_{63}ClN_{12}O_9$) = 951.46077 $[M + H]^+$; m/z_{found} = 951.45773 (Δ = -3.2 ppm).

^{1}H NMR (500 MHz, methanol-d_4) δ 8.31 (s, 1H), 7.91 (s, 1H), 7.75 (s, 1H), 7.45 (m, 1H), 7.33 (s, 1H), 7.31 (s, 1H), 6.51 (s, 1H), 5.17 (s, 1H), 4.72 – 4.66 (m, 3H), 4.58 (s, 4H), 4.00 (m, 2H), 3.80 – 3.41 (m, 20H), 2.04 (s, 2H), 1.95 (s, 6H), 1.61 – 1.56 (m, 6H), 1.04 (t, *J* = 6.8 Hz, 6H).

3.2.9.2 Characterization of trimethoprim-PEG-ethinylestradiol

R_t = 18.4 min. UV/Vis online spectrum from HPLC run (nm, rel ε): 210 (1.00), 286 (0.24) nm.

HR-ESI-MS: $m/z_{calculated}$ ($C_{45}H_{62}N_8O_9$) = 859.47180 $[M + H]^+$; m/z_{found} = 859.46965 (Δ = -2.5 ppm).

^{1}H NMR (500 MHz, methanol-d_4) δ 7.87 (s, 1H), 7.29 (s, 1H), 6.98 (d, *J* = 8.4 Hz, 1H), 6.53 (s, 2H), 6.49 (dd, *J* = 8.4, 2.6 Hz, 1H), 6.46 (d, *J* = 2.7 Hz, 1H), 4.56 (s, 2H), 3.91 (t, *J* = 6.1 Hz, 3H), 3.78 (s, 6H), 3.58 (d, *J* = 2.6 Hz, 2H), 3.54 (s, 3H), 3.49 (t, *J* = 5.4 Hz, 2H), 2.80 – 2.70 (m, 2H), 2.66 (s, 1H), 2.44 (t, *J* = 7.4 Hz, 2H), 2.03 (s, 1H), 1.95 (dt, *J* = 13.5, 6.5 Hz, 3H), 1.84 (s, 1H), 1.64 – 1.52 (m, 3H), 1.46 – 1.37 (m, 2H), 1.29 (d, *J* = 5.1 Hz, 1H), 1.05 (s, 3H). ^{13}C NMR (500 MHz, methanol-d_4) δ 171.64, 166,31, 165.38, 155.96, 154.96, 138.87, 136.91, 135.18, 132.46, 127.15, 116.06, 113.70, 107.04, 73.36, 71.59, 71.46, 71.25, 70.58, 56.64, 44.98, 41.09, 40.41, 34.33, 33.63, 30.72, 30.67, 28.79, 27.55, 27.36, 14.88.

3.2.9.3 Characterization of biotin-PEG-ethinylestradiol

R_t = 12.7 min. UV/Vis online spectrum from HPLC run (nm, rel ε): 206 (1.00), 280 (0.09) nm.

HR-ESI-MS: $m/z_{calculated}$ ($C_{38}H_{56}N_6O_7S$) = 741.40094 $[M + H]^+$; m/z_{found} = 741.40130 (Δ = 0.5 ppm).

^{1}H NMR (500 MHz, methanol-d_4) δ 7.86 (s, 1H), 6.99 (d, *J* = 8.4 Hz, 1H), 6.50 (dd, *J* = 8.5, 2.7 Hz, 1H), 6.46 (d, *J* = 2.7 Hz, 1H), 4.47 (ddd, *J* = 7.9, 5.0, 0.9 Hz, 1H), 4.28 (dd, *J* = 7.9, 4.4 Hz, 1H), 3.91 (dd, *J* = 5.5, 4.6 Hz, 2H), 3.63 – 3.56 (m, 7H), 3.53 – 3.47 (m, 3H), 3.39 (d, *J* = 3.2 Hz, 2H), 3.22 – 3.15 (m, 2H), 2.89 (d, *J* = 5.0 Hz, 1H), 2.76 (s, 1H), 2.71 – 2.65 (m, 1H), 2.20 (t, *J* = 7.4 Hz, 2H), 2.16 (s, 2H), 1.73 – 1.24 (m, 16H), 1.05 (s, 3H). ^{13}C NMR (500 MHz, methanol-d_4) δ 176.14, 166.11, 155.95, 138.84, 132.43, 124.89, 116.06, 113.71, 83.18, 71.63, 71.58, 71.48, 71.24, 70.59, 70.56, 63.36, 61.62, 56.99, 51.35, 45.01, 41.11, 41.04, 40.35, 38.42, 36.74, 34.37, 30.74, 30.67, 29.77, 29.50, 28.79, 27.57, 26.85, 24.65, 14.91.

3.2.9.4 Characterization of trimethoprim-PEG-PleB

R_t = 13.4 min. UV/Vis online spectrum from HPLC run (nm, rel ε): 210 (1.00), 240 (0.59), 306 (0.33) nm.

HR-ESI-MS: $m/z_{calculated}$ ($C_{60}H_{78}N_{10}O_{14}$) = 1163.57772 $[M + H]^+$; m/z_{found} = 1163.57256 (Δ = -4.4 ppm).

^{1}H NMR (500 MHz, methanol-d_4) δ 9.38 (s, 1H), 7.41 (s, 1H), 6.56 (s, 2H), 6.45 (s, 1H), 6.12 (d, J = 17.7 Hz, 2H), 5.37 (d, J = 11.6 Hz, 2H), 3.95 – 3.92 (m, 4H), 3.80 (s, 6H), 3.77 (s, 3H), 3.66 (s, 3H), 3.59 (d, J = 3.1 Hz, 7H), 3.53 (dd, J = 10.4, 4.8 Hz, 7H), 3.45 (s, 3H), 3.25 (s, 2H), 2.65 (dd, J = 15.0, 7.1 Hz, 4H), 2.45 (d, J = 7.6 Hz, 2H), 2.30 (s, 3H), 2.27 (s, 3H), 2.05 (s, 3H), 1.92 (s, 3H).

3.2.9.5 Characterization of trimethoprim-PEG-PxB

R_t = 12.9 min and 13.9 min. UV/Vis online spectrum from HPLC run (nm, rel ε): 206 (1.00), 240 (0.44), 306 (0.32), 422 (0.49) nm.

HR-ESI-MS: $m/z_{calculated}$ ($C_{60}H_{76}N_{10}O_{14}$) = 1161.56207 $[M + H]^+$; m/z_{found} = 1161.55705 (Δ = -4.3 ppm).

^{1}H NMR (500 MHz, methanol-d_4) δ 9.39 (s, 1H), 7.53 (s, 1H), 6.34 (s, 1H), 6.19 (d, *J* = 2.4 Hz, 1H), 6.16 (s, 3H), 5.41 (dd, *J* = 11.8, 2.4 Hz, 2H), 3.90 (d, *J* = 6.1 Hz, 5H), 3.78 – 3.76 (m, 9H), 3.58 – 3.55 (m, 5H), 3.52 – 3.51 (m, 9H), 3.22 (s, 6H), 2.65 (d, *J* = 7.7 Hz, 4H), 2.43 (d, *J* = 7.5 Hz, 3H), 2.29 (s, 3H), 1.98 (s, 3H), 1.95 – 1.92 (m, 4H), 1.70 (s, 3H).

3.2.9.6 Characterization of biotin-PEG-PxB

R_t = 13.0 min and 13.9 min. UV/Vis online spectrum from HPLC run (nm, rel ε): 208 (1.00), 246 (0.51), 312 (0.66), 424 (1.00) nm.

HR-ESI-MS: $m/z_{calculated}$ ($C_{61}H_{86}N_8O_{16}S$) = 1219.59607 $[M + H]^+$; m/z_{found} = 1219.59612 (Δ = 0.1 ppm).

^{1}H NMR (500 MHz, methanol-d_4) δ 9.41 (s, 1H), 6.52 – 6.46 (m, 1H), 6.36 (s, 1H), 5.42 (dd, *J* = 11.8, 2.3 Hz, 1H), 5.35 (s, 1H), 5.04 (s, 3H), 4.50 (dd, *J* = 7.9, 4.9 Hz, 6H), 4.32 (td, *J* = 7.5, 6.8, 4.3 Hz, 6H), 3.96 (d, *J* = 9.6 Hz, 8H), 3.79 (d, *J* = 3.5 Hz, 11H), 3.24 – 3.18 (m, 6H), 2.93 (ddd, *J* = 12.6, 5.0, 1.6 Hz, 5H), 2.73 (d, *J* = 4.8 Hz, 4H), 2.67 (d, *J* = 1.2 Hz, 1H), 2.31 (s, 3H), 2.15 (s, 8H), 2.02 (s, 3H), 1.74 (d, *J* = 9.2 Hz, 6H), 0.92 (t, *J* = 6.8 Hz, 2H). ^{13}C NMR (500 MHz, methanol-d_4) δ 191.18, 176.10, 175.25, 173.21, 171.59, 166.10, 143.53, 140.40, 137.77, 134.62, 129.53, 127.42, 126.12, 125.56, 124.56, 112.45, 107.32, 102.17, 62.83, 61.59, 57.44, 56.97, 53.07, 41.04, 40.31, 37.99, 37.54, 37.24, 36.70, 30.74, 29.74, 29.47, 28.08, 26.81, 23.52, 21.27, 16.84, 14.42, 12.29, 9.73.

3.2.9.7 Characterization of biotin-PEG-PleB

R_t = 10.4 min. UV/Vis online spectrum from HPLC run (nm, rel ε): 212 (1.00), 242 (0.69), 312 (0.60) nm.

HR-ESI-MS: $m/z_{calculated}$ ($C_{61}H_{88}N_8O_{16}S$) = 1221.61172 $[M + H]^+$; m/z_{found} = 1221.61517 (Δ = 2.8 ppm).

3.2.10 Statistical analysis

All figures are indicated as mean ± SD (standard deviation) of at least 3 independent experiments unless stated otherwise. The significant symbol indicated as following: *, p-value<0.05, **, p-value <0.01, ***, p-value<0.005, and ****, p-value<0.0001. Statistical differences for the two groups were calculated using either a two-tailed Student's t-test or a one-tailed Student's t-test. For comparison, for more than 2 groups, one- or two-way Analysis of Variance (ANOVA) was applied and followed by a stated post-hoc test. Sketch and calculation were performed with Prism 8.

RESULTS

4 Results

4.1 Characterization of phyllobilins from Plane tree

HR-ESI-MS analysis of purified compounds from Plane tree leaves revealed a molecular formula of $C_{35}H_{40}O_8N_4$ for *Po*-PleB (Supplementary Figure 1)**,** and $C_{35}H_{38}O_8N_4$ for *Po*-PxB (Supplementary Figure 2), indicating them to have an identical molecular composition as *Cj*-PleB and *Cj*-PxB from Katsura tree leaves. From the HPLC co-elution experiment (Figure 8), the two PleB signals showed similar but not identical retention times. Since the mass spectra of the two compounds showed identical molecular formula, we concluded that the *Po*-PleB is the C16-epimer of the *Cj*-PleB. For the two PxBs, however, the chromatograms showed identical peaks and chromatographic characteristics, indicating *Po*-PxB to be the identical compound as *Cj*-PxB, which will just be referred as PxB in the following content.

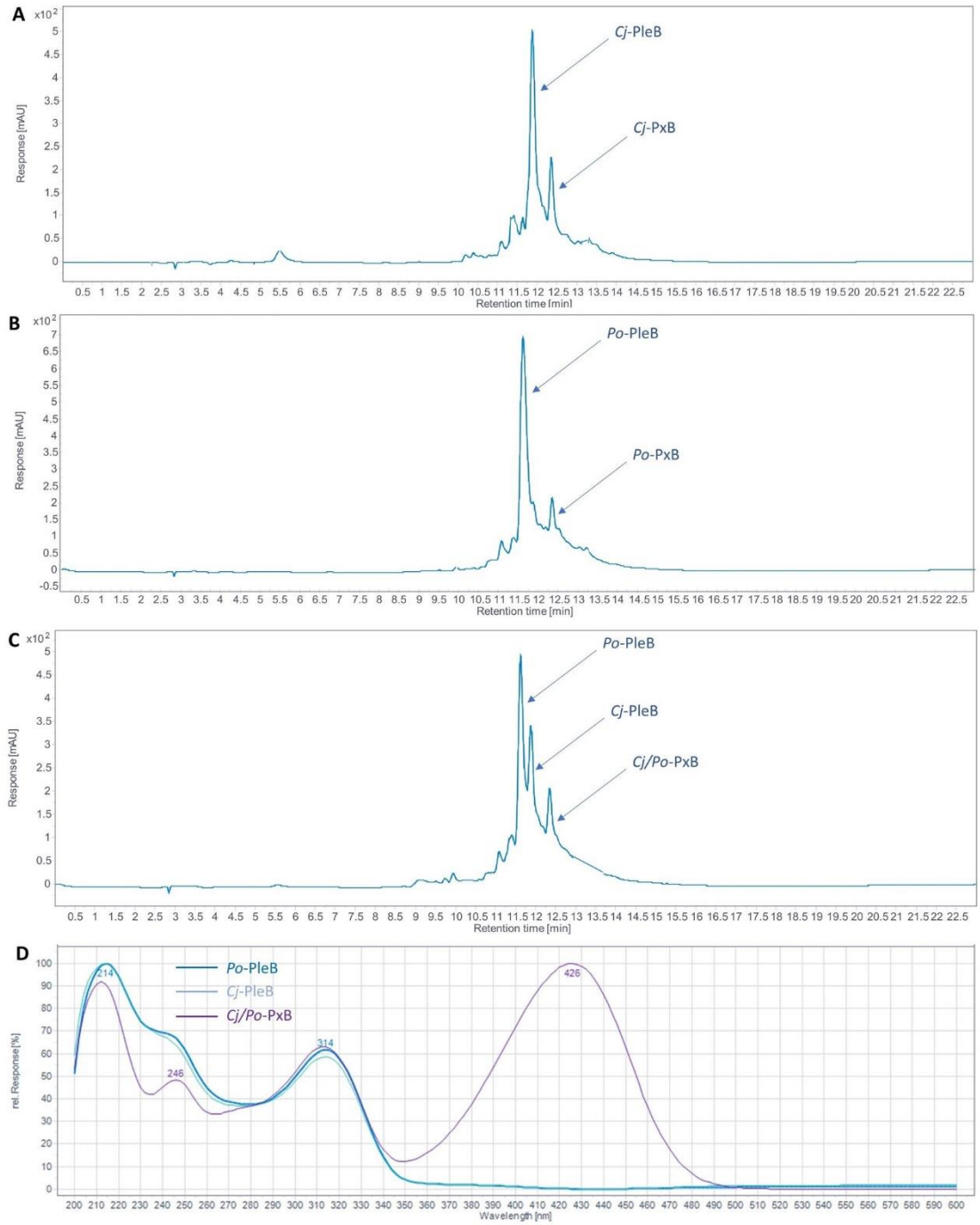

Figure 8. HPLC analysis of Plane tree phyllobilins.

A. Co-injection of *Cj*-PleB and *Cj*-PxB. B. Co-injection of *Po*-PleB and *Po*-PxB. C. Co-injection of *Cj*-PleB, *Cj*-PxB, *Po*-PleB and *Po*-PxB indicates *Po*-PleB to be the C16-epimer of the *Cj*-PleB, while *Po*-PxB to be identical to *Cj*-PxB. D. UV/Vis online spectra of *Po*-PleB, *Cj*-PleB and *Cj/Po*-PxB. Signals were detected at 320 nm.

4.2 Anti-proliferative activity of phyllobilins on T24 cells

After we extracted *Cj*-PleB and *Cj*-PxB from Katsura tree leaves, we first esterified *Cj*-PleB with different alcohols to get PleB esters (See Supplementary Figure 3 and 4). Then we continued to oxidize PleB esters to PxB esters by solid-phase oxidation (See Supplementary Figure 5 and 6). With the previously mentioned modified extraction method, we also isolated *Po*-PleB from Plane tree leaves. The different phyllobilin structures were then tested for their anti-proliferative activities on T24 cells.

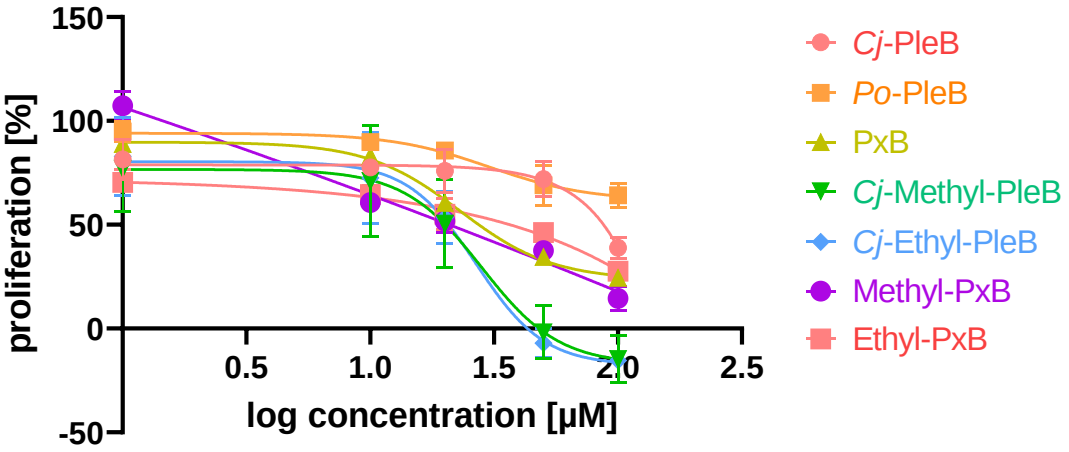

Figure 9. Anti-proliferative activity of phyllobilins and derivatives.

Both *Cj*-PleB and *Po*-PleB didn't show clear anti-proliferative effect on T24 cells in high concentrations up to 100 µM. Surprisingly, esterification of *Cj*-PleB increased anti-proliferative activity dramatically, resulting in an IC50 value of 28.11 µM for *Cj*-Methyl-PleB and 26.70 µM for *Cj*-Ethyl-PleB. The isolated PxB demonstrated an anti-proliferative activity with an IC50 of 23.05 µM. However, the esterification of PxB didn't increase the activity as it did for PleB, leading to a similar effect on T24 cells as the original PxB.

4.3 Establishment of yeast three-hybrid system

Having confirmed that phyllobilins possess diverse biological activities, the question about the mechanisms behind those activities arose. One of the main approaches to elucidate mode of actions and mechanisms of biological effects is to identify protein

binding partners for compounds of interest. Therefore, we established a yeast three-hybrid (Y3H) system.

4.3.1 Setup of yeast three-hybrid system

The dihydrofolate synthase-trimethoprim (DHFR-Trim) interaction, which has already been validated before [76], was used in our system as the anchor-linker pair (Figure 10).

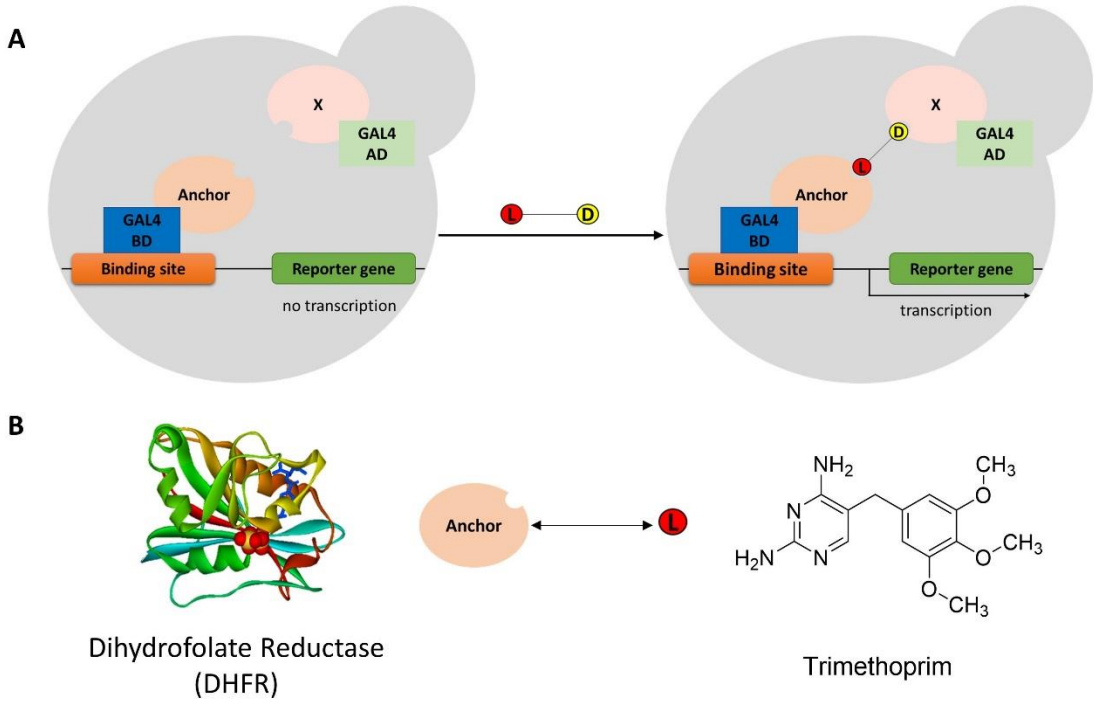

Figure 10. Setup of Y3H system (DHFR-Trim pair).

A. In the Y3H system, a small molecule-linker hybrid is added to the Y2H setup. This small molecule (D) is coupled to a linker (L) that allows for binding to an anchor protein coupled with the DNA binding domain of a split transcription factor (BD). In this system, the small molecule is screened against a library of potential binding partners (X) fused to the activation domain of a split transcription factor (AD). Transcription of a reporter gene and thus survival of the yeast cell on selective plates only occurs upon interaction of the small molecule (D) with a protein (X). B. Our Y3H setup is based on a dihydrofolate reductase (DHFR) anchor that binds tightly to the linker trimethoprim.

On the other side of the setup, we chose the interaction of purvalanol B (PurB) and the cyclin dependent kinase 5 (CDK5) as positive control (Figure 11), which has also been validated in another Y3H setup [68].

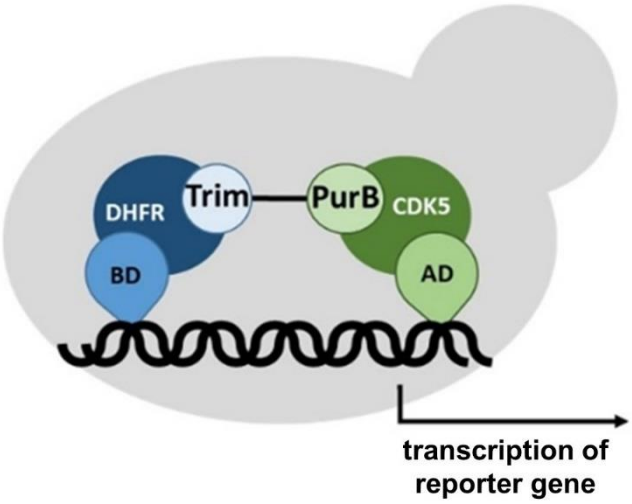

Figure 11. Setup of Y3H system (PurB-CDK5 pair).

For proof of principle, the known interaction of cyclin dependent kinase 5 (CDK5) with the CDK5 inhibitor purvalanol B (PurB) was tested in the system.

Therefore, a trimethoprim derivatized purvalanol B was needed to form the ligand of the setup. Because of the carboxyl group of purvalanol B, we used the newly designed trimethoprim-PEG-amine (THK42) to couple with purvalanol B to connect those two functional compounds via a PEG linker (Section 3.2.5.2).

As for the construction of vectors, the *dhfr* (*E. coli*) gene and the *cdk5* (human) gene was successfully cloned into the Y2H bait and prey vector from the Matchmaker Gold Y2H system (Takara Bio), respectively, by Eva M. Staschik (Prof. Dr. Angelika M. Vollmar, Department of Pharmacy, LMU Munich). Afterwards, both of them were transformed into the modified yeast reporter strain ABC9Δ, which we obtained from the Agency for Science, Technology and Research (A*STAR) institute in Singapore. This strain has 9 efflux pump deletions, and a higher permeability for small molecules, which is a superior advantage for yeast based screenings, since the uptake of the

compound of interest to the yeast cells has been a major challenge of the yeast based system [77].

4.3.2 Spot test with trimethoprim-PEG-purvalanol B probe

A spot test was then performed by Dr. Simone Moser (Prof. Dr. Angelika M. Vollmar, Department of Pharmacy, LMU Munich). The yeast containing both bait vector and prey vector was then spotted on unselective plates (-LW), on selective plates (-LWH) without the trimethoprim-PEG-purvalanol B probe, and also on selective plates (-LWH) with the trimethoprim-PEG-purvalanol B probe. The spot test showed that the yeast grew well on selective plates only in the presence of the probe (Figure 12. Spot test with trimethoprim-PEG-purvalanol B probe.

12).

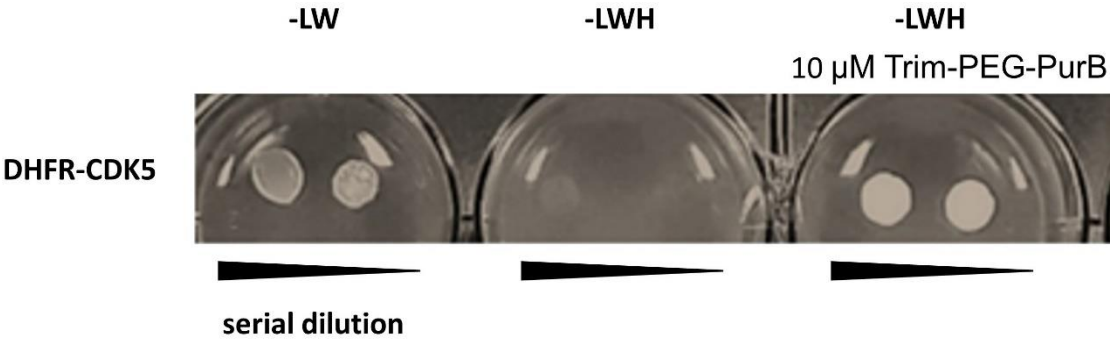

Figure 12. Spot test with trimethoprim-PEG-purvalanol B probe.

The yeast reporter strain expressing CDK5 fused to the DNA activation domain, and DHFR fused to the DNA binding domain was grown on medium selecting for the two plasmids (-LW) and plates selecting for the interaction (-LWH) in the presence and absence of the trimethoprim-PEG-purvalanol B (Trim-PEG-PurB) probe.

4.4 Y3H system validation with ethinylestradiol as model drug

Since we knew that our Y3H system can indeed be applied to detect small molecule-protein interactions, next we wanted to validate this setup for the identification of protein binding partners of small molecules from a pool of proteins. Therefore, we

chose ethinylestradiol (EE) as model drug, with the rationale that it features an ethynyl moiety that allows for a simple modification of the molecule. A clickable trimethoprim probe with a PEG linker and an azide moiety was synthesized by Thomas Klaßmüller (Prof. Dr. Franz Bracher, Department of Pharmacy, LMU Munich). In brief, the 4''-hydroxy analogue (TMP-OH) of trimethoprim was connected with a butyrate spacer [78], which in turn was amidated with 11-azido-3,6,9-trioxaundecan-1-amine. The resulting compound trimethoprim-PEG-azide was coupled to ethinylestradiol via a copper-catalyzed alkyne-azide 'click' reaction generating a triazole unit at C17 of ethinylestradiol to obtain the final trimethoprim-PEG-ethinylestradiol probe.

To construct the protein pool for screening, we used conventional cDNA libraries for Y2H screens, which were commercially available, and we used an electroporation protocol [74] to transform a mammary gland and pancreas cDNA library to the ABC9Δ strain containing the DHFR bait plasmid, respectively, which was performed by Dr. Simone Moser, Jana Peliskova and Rita Socher (Prof. Dr. Angelika M. Vollmar, Department of Pharmacy, LMU Munich). The viability of the transformed yeast strains was determined by cfu plating and was found to be larger than 10^9 cfu/ml for both libraries.

4.4.1 Y3H screening of ethinylestradiol

After synthesizing the trimethoprim derivatized ethinylestradiol, the Y3H screen was then performed with the probe similar to previously described procedures [70, 79]. In brief, different stocks of yeast libraries were spread onto selective -LWH plates containing 2.5 mM 3-AT and 10 µM trimethoprim-PEG-ethinylestradiol. 3-AT is a known inhibitor of the *his3* reporter gene, and addition of 3-AT was found to be able to lower false positive rates.

One 150 mm diameter plate was used per screen and library, and more than 5×10^7 yeast cells were used per plate to ensure that it was 10 times larger than the library

coverage, which was indicated as 3 × 10^6 by the manufacturer. The plates were incubated at 30°C for 10 d, followed by picking well grown colonies onto -LWH and -LW plates first to eliminate false positives; after this time, colonies that only grew on -LW plates were picked and applied to a growth dependence test by spotting them on selective plates with and without the drug conjugate, which allows for the elimination of further possible false positives. In the end, only colonies which grew on plates containing the ethinylestradiol probe, but showed no growth on plates without it, were classified as hits and analyzed further (Figure 13B). 18 hits were obtained from the mammary gland library, while the pancreas library screen yielded 12 colonies which were classified as hits.

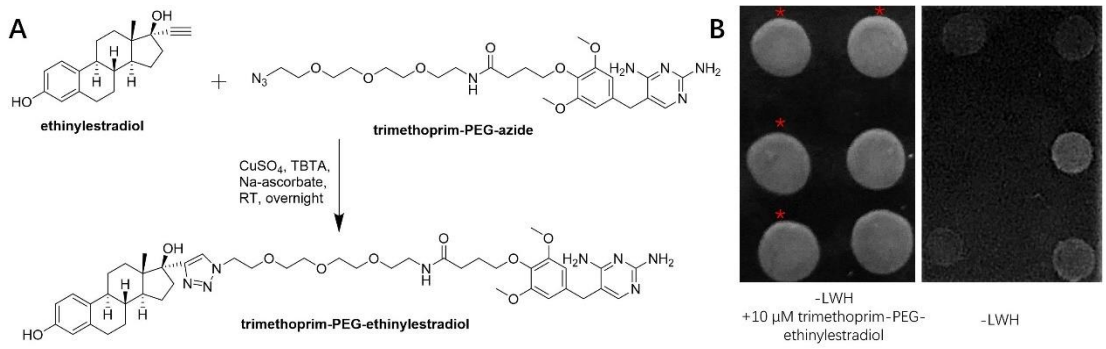

Figure 13. The Y3H system was used to screen potential binding proteins of ethinylestradiol.

A. The coupling of trimethoprim-PEG-amine and ethinylestradiol led to the linker probe trimethoprim-PEG-ethinylestradiol, which could anchor with DHFR and allow for the setup of Y3H system. B. By picking and applying colonies to a growth dependence test in the presence and absence of the probe, we could eliminate most of the false positives. Only colonies that showed growth on the plates containing the linker probe but no growth on the plate without the probe, were classified as 'hits' (marked with a red asterisk*).

4.4.2 PLOD2 was clarified as a potential target protein of ethinylestradiol

After picking colonies as potential hits, colony PCR of all hits was performed as described previously (Supplementary Figure 8). Amplified cDNA inserts were sent for

sequencing and further false positives were excluded by analyses of all cDNA inserts sequencing results, either because the obtained sequence was out of frame with GAL4 AD, or due to the DNA fragment not being part of a coding sequence. In the end, hits from the screening of the pancreas library all turned out to be false positives, while the mammary gland library screen yielded one hit. This hit was identified twice and encoded for the last 81 amino acids of procollagen-lysine 2-oxoglutarate 5-dioxygenase 2 (PLOD2, alternative name lysyl hydroxylase 2 (LH2)) (Table 7).

4.4.3 Validation of PLOD2 as an interaction partner of ethinylestradiol

4.4.3.1 Biotin-tag-based pull-down assay with PLOD2 fragment overexpressed yeast cell lysate

To further validate that PLOD2 is a real hit and interaction partner of ethinylestradiol, we first performed a biotin-tag-based pull-down assay. The biotin-PEG-ethinylestradiol conjugate was synthesized as described previously in section 3.2.6.8. The derivatization allowed ethinylestradiol to be immobilized on streptavidin beads, which were then incubated with whole cell lysates of yeast overexpressing the identified PLOD2 fragment as GAL4 AD fusion. A biotin azide derivative with the same linker as the ethinylestradiol probe was also immobilized on the streptavidin beads as a negative control. After washing, bound proteins were eluted with SDS and heat, and analyzed by Western blot using a GAL4 antibody for the detection of the GAL4 AD fusion protein from the Y3H vector.

As expected, no band was detected in the eluate from the beads modified with biotin-PEG-azide as negative control. In the biotin-PEG-ethinylestradiol group, however, a faint band was observed, indicating the enrichment of the PLOD2 fragment identified in our Y3H screen on ethinylestradiol modified beads (Figure 14A). The Western blot revealed similar effects after 3 repetitions (Figure 14B and Supplementary Figure 9).

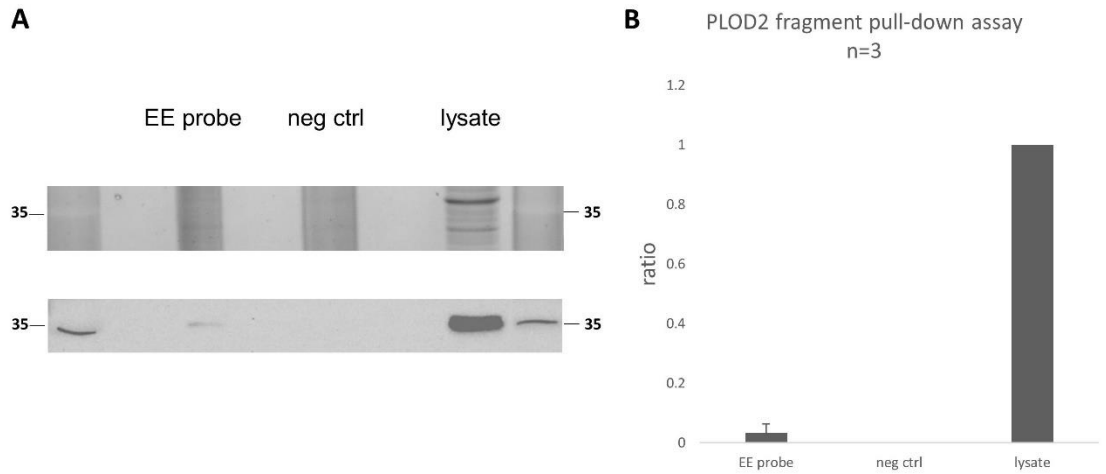

Figure 14. Validation of the interaction between ethinylestradiol and PLOD2 fragment identified in Y3H screen.

A. Affinity chromatography. The biotin-PEG-ethinylestradiol probe was immobilized on streptavidin beads. Next, yeast cell lysate overexpressing PLOD2 fragment (total 1 mg of protein as determined by Bradford assay) were added. After incubation and washing, bound proteins were eluted and analyzed by SDS-PAGE. A Western blot using a GAL4 AD antibody revealed an enrichment for the eluate from the ethinylestradiol modified solid phase compared to beads modified with pegylated biotin as negative control. Top panel: SDS-PAGE loading control. Lower panel: exemplary photo of a Western blot (Western blots of all three replicates can be found in the Supplementary Figure 9). B. The intensities of Western blot bands were evaluated using ChemiDoc and showed that identified PLOD2 fragment GAL4 AD fusion protein was enriched on ethinylestradiol modified beads while no enrichment was observed in negative control.

4.4.3.2 Biotin-tag-based pull-down assay with human recombinant PLOD2 protein

Having confirmed the interaction between ethinylestradiol and the 81 amino acids fragment of PLOD2 identified in the Y3H screen, we performed the same experiment using human recombinant PLOD2. A PLOD2 antibody (abcam) was used for staining to detect the whole PLOD2 protein, showing that also the whole protein can be

enriched with the ethinylestradiol probe in a pull-down setup, yielding a more intense band compared to the fragment (Figure 15 and Supplementary Figure 10).

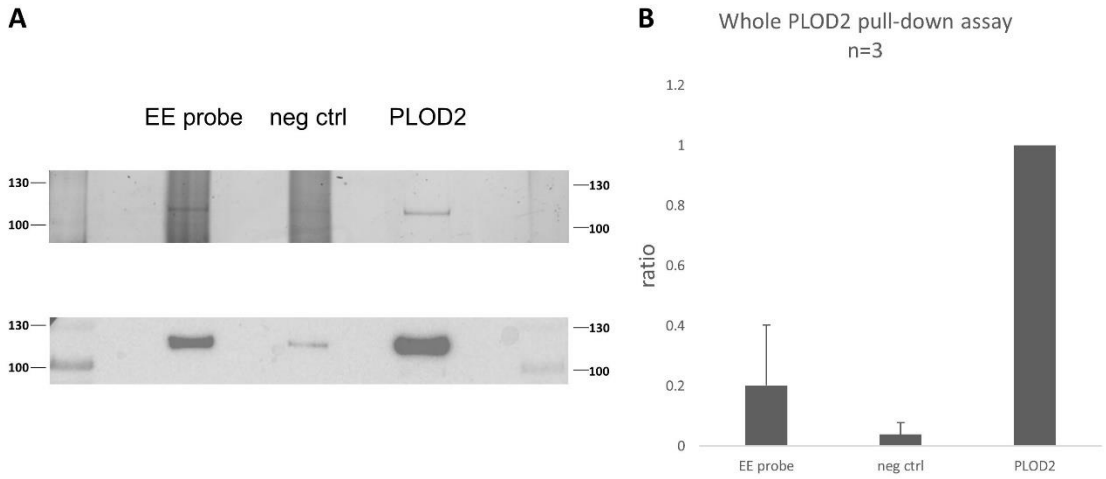

Figure 15. Validation of the ethinylestradiol-PLOD2 interaction pair using commercially available human recombinant PLOD2 (whole protein).

A. The intense PLOD2 protein band detected by a PLOD2 antibody in the ethinylestradiol probe group indicated that there is an interaction between ethinylestradiol and human recombinant PLOD2. B. Stronger intensity of Western blot bands revealed higher affinity of ethinylestradiol with PLOD2 protein compared with PLOD2 GAL4 AD fusion protein identified in our Y3H screen.

4.4.3.3 PLOD2 activity assay

In order to further investigate the interaction between ethinylestradiol and PLOD2, we also conducted a PLOD2 activity assay. PLOD2 is involved in collagen cross-linking by hydroxylating lysyl residues in telopeptides of fibrillary collagens. Succinate is created during this reaction, which in turn can be detected in a luminescence based *in vitro* assay and allows for monitoring of PLOD2 activity. Using the assay developed by Devkota et al. [75], the influence of ethinylestradiol on PLOD2 activity was determined. Indeed, using human recombinant PLOD2, a decrease in the formation of succinate was observed upon treatment with ethinylestradiol (Figure 16).

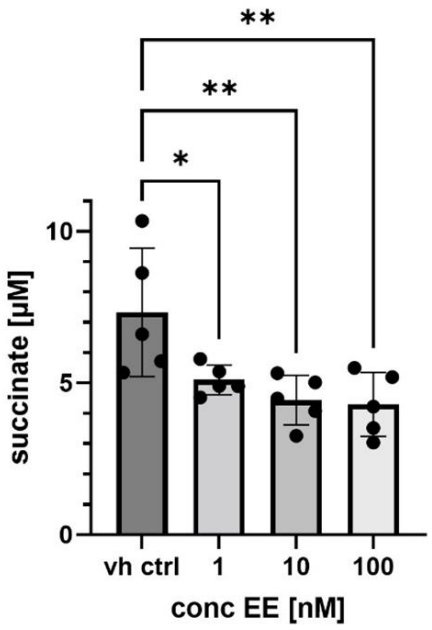

Figure 16. PLOD2 activity assay.

A bioluminescence-based activity assay was performed that measures the succinate formed by PLOD2 [75]. A clear down-regulation of PLOD2 activity was observed upon treatment of ethinylestradiol comparing to the vehicle control (vh ctrl). n = 5, mean values are shown. Error bars represent standard deviations. * $p < 0.05$, ** $p < 0.01$.

4.4.3.4 Collagen I staining

PLOD2 catalyzes the hydroxylation of lysine residues in the telopeptides of fibrillar collagens, which leads to the formation of stable collagen cross-links. A recent study also showed that PLOD2 can be secreted by tumor cells and modify collagen in the extracellular space [80]. To further investigate the effect of ethinylestradiol on PLOD2, we conducted a collagen I staining to see whether ethinylestradiol treatment could alter extracellular collagen fibers. As a known inhibitor of PLOD2 expression, minoxidil [81] was also included as a positive control. From the confocal microscope images (Figure 17A), we could see that without treatment, cells actively remodeled the collagen fibers creating a cage-like structure around themselves. The addition of ethinylestradiol and the control substance minoxidil, however, significantly impaired matrix remodeling. At a higher concentration of ethinylestradiol or minoxidil, the cells appeared to interact

less with the underlying collagen, so that a cage around the cells could no longer be observed.

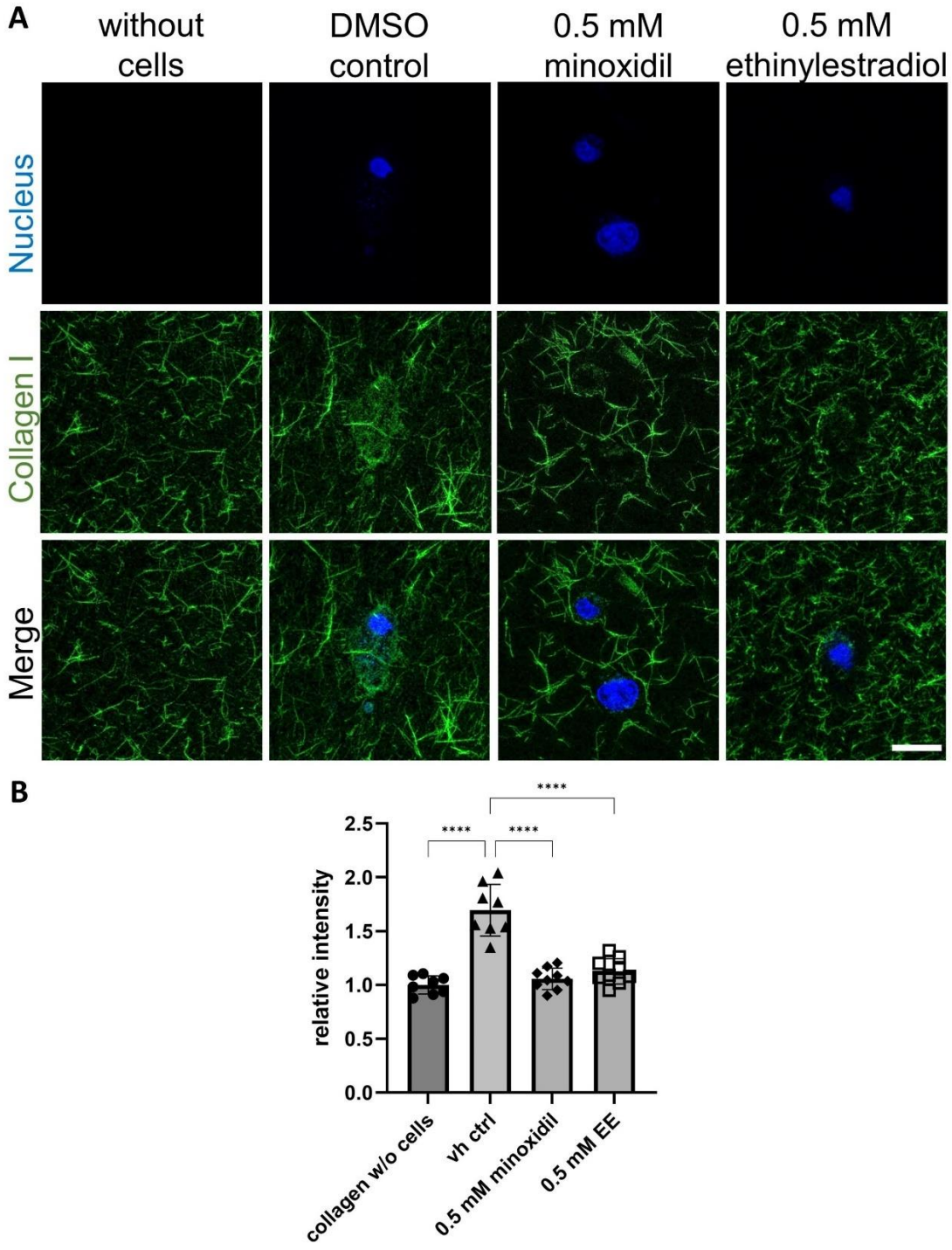

Figure 17. Ethinylestradiol inhibits collagen remodeling.

HeLa cells were seeded onto FITC labeled collagen I (2 mg/ml) and treated with either ethinylestradiol, minoxidil (an inhibitor of PLOD2 expression [81]) as positive control, or a DMSO vehicle control. A. Images taken 24 h after cell seeding were shown with the nuclei in

blue (live cell Hoechst staining) and the collagen fibers in green (scale bar 25 µm). B. Evaluation of collagen fluorescence intensity showed that treatment with ethinylestradiol or the positive control minoxidil led to reduced density of collagen fibers in close proximity of the cells, indicating a potential effect of ethinylestradiol on PLOD2 in comparison to a vehicle control (vh ctrl, **** $p < 0.0001$).

4.4.3.5 PLOD2 expression level

Having confirmed that ethinylestradiol could inhibit the activity of PLOD2 protein, next we probed if ethinylestradiol also had an effect on the expression level of PLOD2 in T24 cells. The three replicates for the PLOD2 expression experiment showed that an impairment of PLOD2 expression was observed upon addition of ethinylestradiol in comparison to DMSO control and also to the known PLOD2 inhibitor minoxidil (Figure 18 and Supplementary Figure 11).

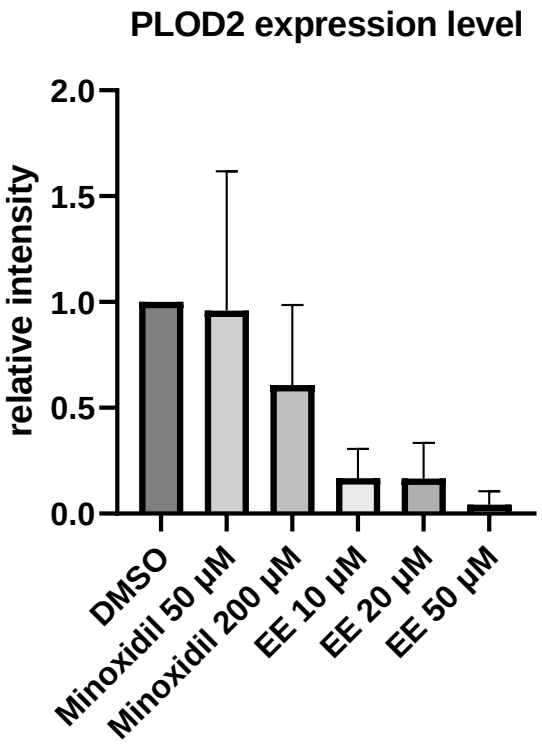

Figure 18. Evaluation of PLOD2 expression levels.

Intensities of Western blot bands were evaluated using ChemiDoc and were shown relative to the band of DMSO control. A dose-dependent down-regulation of ethinylestradiol on the

expression level of PLOD2 was observed. Lower concentration of ethinylestradiol even showed stronger inhibition to PLOD2 expression compared to higher concentration of minoxidil, which is a known inhibitor of PLOD2.

4.5 Y3H screening of phyllobilins

Since we know that phyllobilins not only possess large structural diversity with modifications at the different side chains, but also show incredible potential regarding different biological activities, it is necessary to find binding proteins for phyllobilins using complementary target identification methods. With the well-established yeast three-hybrid system, we first started the target protein screening for the phyllobilins with the most common structures, PleB and PxB from *Cercidiphyllum japonicum*.

4.5.1 Y3H screening of PleB

After synthesizing the trimethoprim derivatized PleB, we performed the Y3H screen with the PleB probe using similar methods we used for the ethinylestradiol screen. In order to increase the potential of finding target proteins, a kidney cDNA library was also transformed into the ABC9Δ yeast strain. For the screening of phyllobilins, this newly transformed library was used, as were a mammary gland cDNA library and a pancreas cDNA library. However, no real hit was identified in the Y3H screen of PleB.

4.5.2 Y3H screening of PxB

Trimethoprim derivatized PxB was synthesized and applied in our Y3H setup in order to find binding partners for PxB. After the similar Y3H process as described previously, NPC intracellular cholesterol transporter 2 (NPC2) was identified as potential target partner of PxB from the kidney library (Table 9), while promyelocytic leukemia protein (PML) was identified as another potential binding partner of PxB from the mammary gland library (Table10). The downstream confirmation was carried out similar to the procedure described for the ethinylestradiol screen. In brief, the cDNAs containing

NPC2 and PML expressing DNA fragments were transferred into *E. coli* cells first, and then amplified in living *E. coli* cells. The amplified plasmid DNAs were then extracted from *E. coli* cells and transferred back to Y2H Gold yeast strain. At last, yeast cells were spread onto -L plates and incubated until the growth of yeast cells overexpressing the identified NPC2 and PML protein fragments.

4.5.2.1 Validation of NPC2 as an interaction partner of PxB

In order to validate NPC2 as an interaction partner of PxB, we performed a biotin-tag-based pull-down assay. The biotin-PEG-PxB probe was synthesized first and immobilized on streptavidin beads. The modified beads were then incubated with whole cell lysates of yeast overexpressing the identified NPC2 fragment as GAL4 AD fusion. Afterwards the beads were washed and bound proteins were analyzed by Western blot using a GAL4 antibody again for the detection of the potential NPC2 GAL4 AD fusion protein. The Western blot revealed a clear enrichment of NPC2 GAL4 AD fusion protein on the PxB modified streptavidin beads compared with the biotin-PEG-amine modified negative control, indicating the interaction between PxB and this identified NPC2 fragment by our Y3H setup (Figure 19).

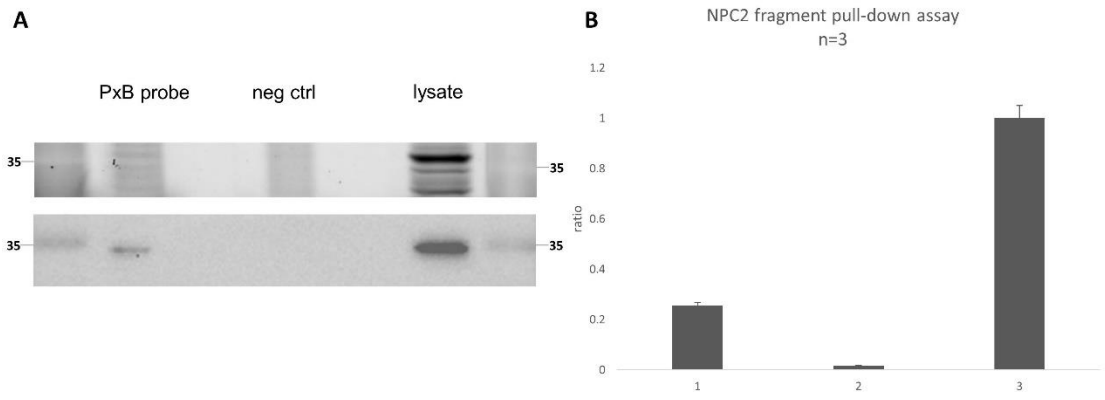

Figure 19. Validation of the interaction between PxB and NPC2 fragment identified in Y3H screen.

A. Affinity chromatography. The Western blot using a GAL4 AD antibody revealed an enrichment for the eluate from the PxB modified solid phase compared to beads modified with

pegylated biotin as negative control. Top panel: SDS-PAGE loading control. Lower panel: exemplary photo of a Western blot (Western blots of all three replicates can be found in the Supplementary Figure 12). B. The intensities of Western blot bands show that identified NPC2 fragment GAL4 AD fusion protein was enriched on PxB modified beads while no enrichment was observed for the negative control.

4.5.2.2 Validation of PML as an interaction partner of PxB

Similarly, we also performed biotin-tag-based pull-down assay to validate PML as another interaction partner of PxB. Same as NPC2, the PML fragment GAL4 AD fusion protein was also enriched by biotin-PEG-PxB, immobilized by streptavidin beads and detected by Western blot.

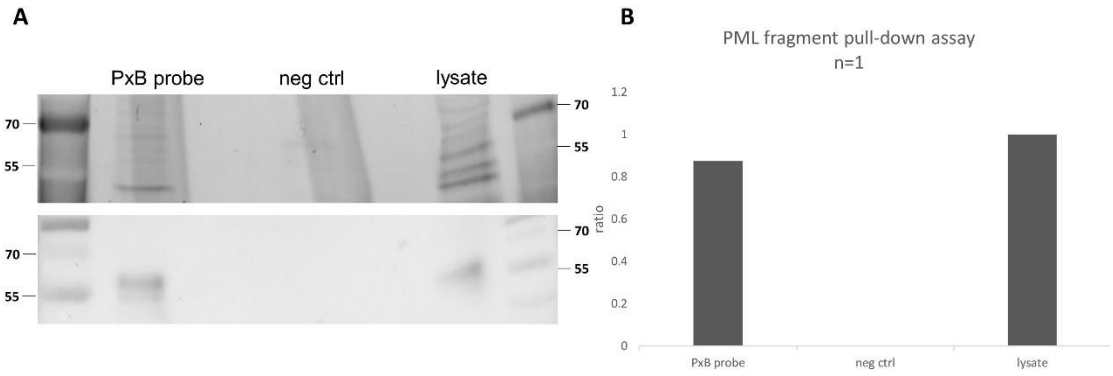

Figure 20. Validation of the interaction between PxB and PML fragment identified in Y3H screen.

A. Affinity chromatography. The Western blot using a GAL4 AD antibody revealed an enrichment for the eluate from the PxB modified solid phase compared to beads modified with pegylated biotin as negative control. Top panel: SDS-PAGE loading control. Lower panel: exemplary photo of a Western blot. B. The intensities of Western blot bands show that identified PML fragment GAL4 AD fusion protein was enriched on PxB modified beads while no enrichment was observed for the negative control.

4.6 MS-based affinity chromatography for phyllobilins

Biotinylated PleB and PxB were immobilized on streptavidin beads and incubated with T24 cell lysates. Biotin-PEG-acetate (Supplementary Figure 7) was used as a negative control and T24 cell lysates were used to identify total proteins. Unbound proteins were removed with a washing step, and bound proteins were analyzed by LC-MS/MS (performed by Dr. Thomas Fröhlich, Gene Center - Laboratory for Functional Genome Analysis, LMU Munich) after elution with 0.1% formic acid in water and 0.1% formic acid in ACN. More than 2500 proteins were identified in the cell lysates and 470 proteins were identified in the experiment groups (Figure 21).

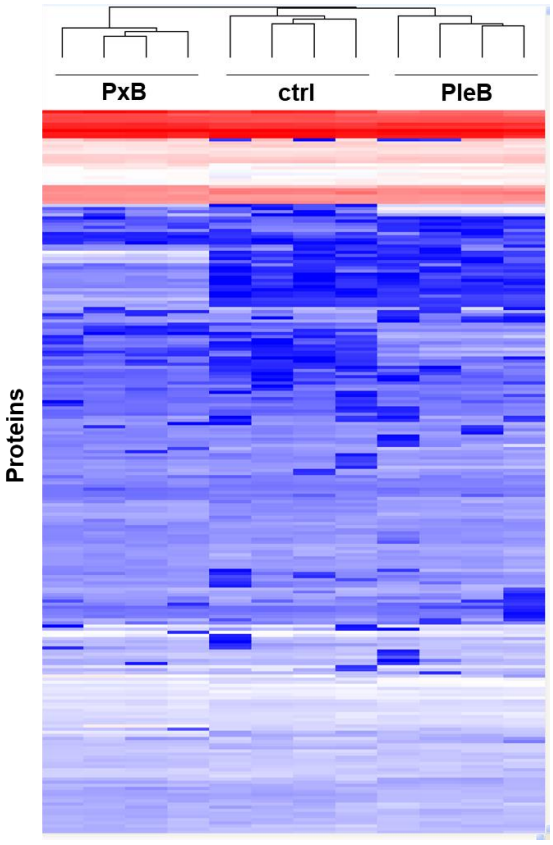

Figure 21. Heatmap of proteins bound to small molecules.

LC-MS/MS based proteomics identified and quantified more than 2500 proteins. Proteomic profiles of 470 proteins identified in the phyllobilins groups and negative control group were shown in a schematic heatmap with color-coded normalized abundances. Higher intensity of the color indicates higher abundance of the corresponding protein.

4.6.1 Potential target proteins of phyllobilins

Among all of the identified proteins, those which intensities decreased significantly in the control group compared to the phyllobilins experiment groups are the most likely targets. Thus, we analyzed the data not only by calculating $\log_2$ fold change values of the protein intensity between experiment and control groups, but also calculating p values and elucidating the $-\log_{10}$ p values in volcano plot figures to demonstrate whether the differences between sample and control values are significant.

Potential target proteins of PleB with a total amount of 73 proteins were demonstrated in a volcano plot (Figure 22). 11 proteins show a $\log_2$ fold change substantially >2, among which KHSRP and PABPC1 show the most significant $\log_2$ fold change while demonstrating significant $-\log_{10}$ p values as well.

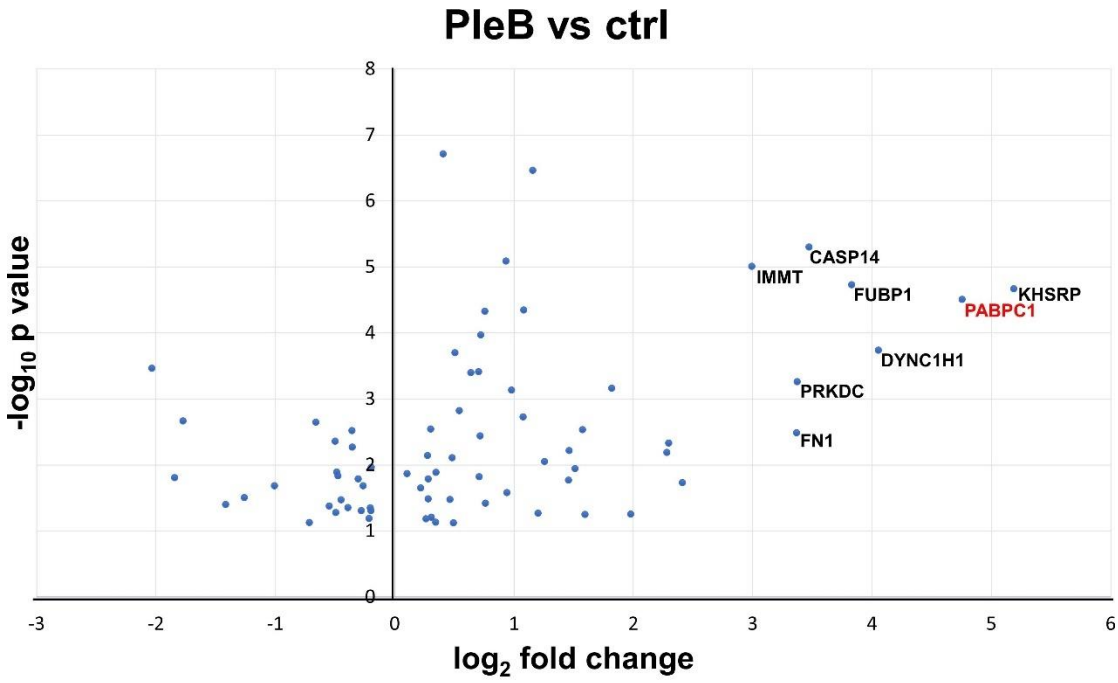

Figure 22. Volcano plot of potential protein targets of PleB.

Volcano plot of the ratio of eluate protein intensities in sample (PleB probe) and control experiments. The *x*-axis shows the $\log_2$ fold changes, whereas the *y*-axis shows the $-\log_{10}$ p values for a t-test of whether the sample and control experiments differ significantly. The plot shows 73 total proteins.

For PxB, a total amount of 91 potential target proteins were demonstrated in a volcano plot (Figure 23). More than PleB group, 18 proteins demonstrated a significant log_2 fold change >2, with RPS27, PPP1R13L and MCCC2 showing a log_2 fold change higher than 5.

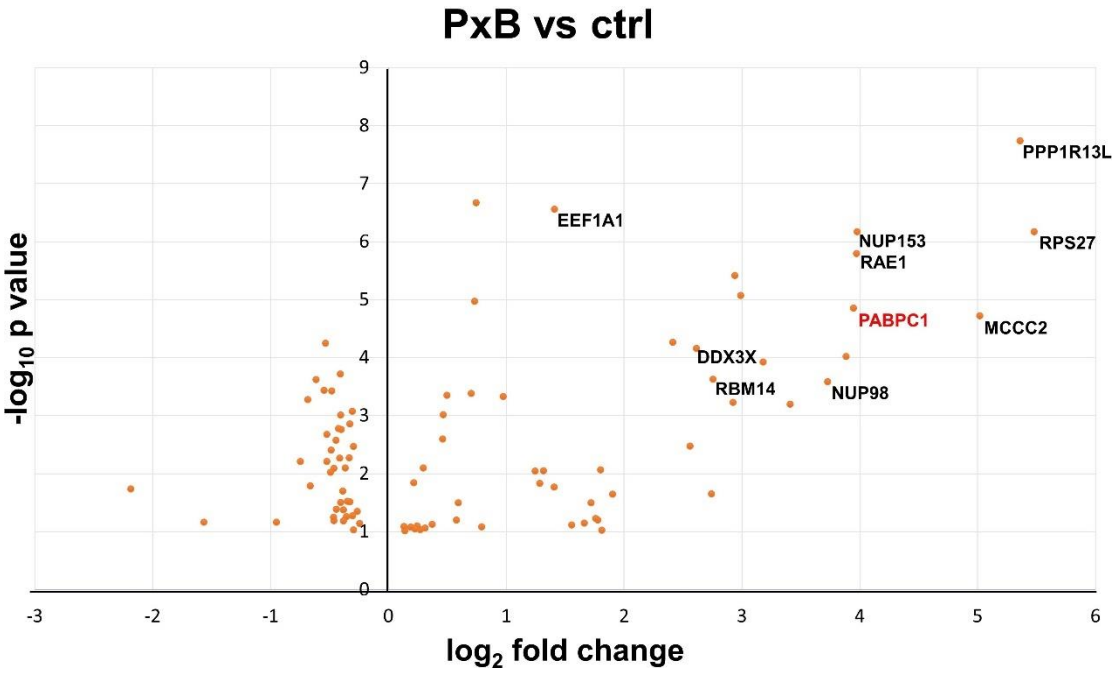

Figure 23. Volcano plot of potential protein targets of PxB.

Volcano plot of the ratio of eluate protein intensities in sample (PxB probe) and control experiments. The plot shows 91 total proteins.

Among all those potential protein targets of phyllobilins, of particular interest is the PABPC1 (Polyadenylate-binding protein 1), which showed a significant enrichment in both, PleB and PxB groups, making it the most promising target to investigate further. PABPC1 binds the poly(A) tail of mRNA, and regulates processes of mRNA metabolism such as mRNA stabilization and degradation. Overexpression of PABPC1 inhibited cell proliferation, migration, and invasion, while promoted apoptosis in glioblastoma cells [82]. It regulates proliferation and transformation of gastric cancer cells *in vitro* and *in vivo* [83].

4.6.2 Potential interaction partners of phyllobilins

To highlight the mechanism of action of phyllobilins and try to discover potential interaction partner, proteins with higher log_2 fold changes and $-log_{10}$ p values were mapped onto protein-protein interaction networks using STRING [84] (Figure 24). Interestingly, in the largest clusters of both PleB and PxB potential target proteins, almost all of the submitted proteins had RNA binding function (blue nodes in STRING network graphic), including the most promising target PABPC1.

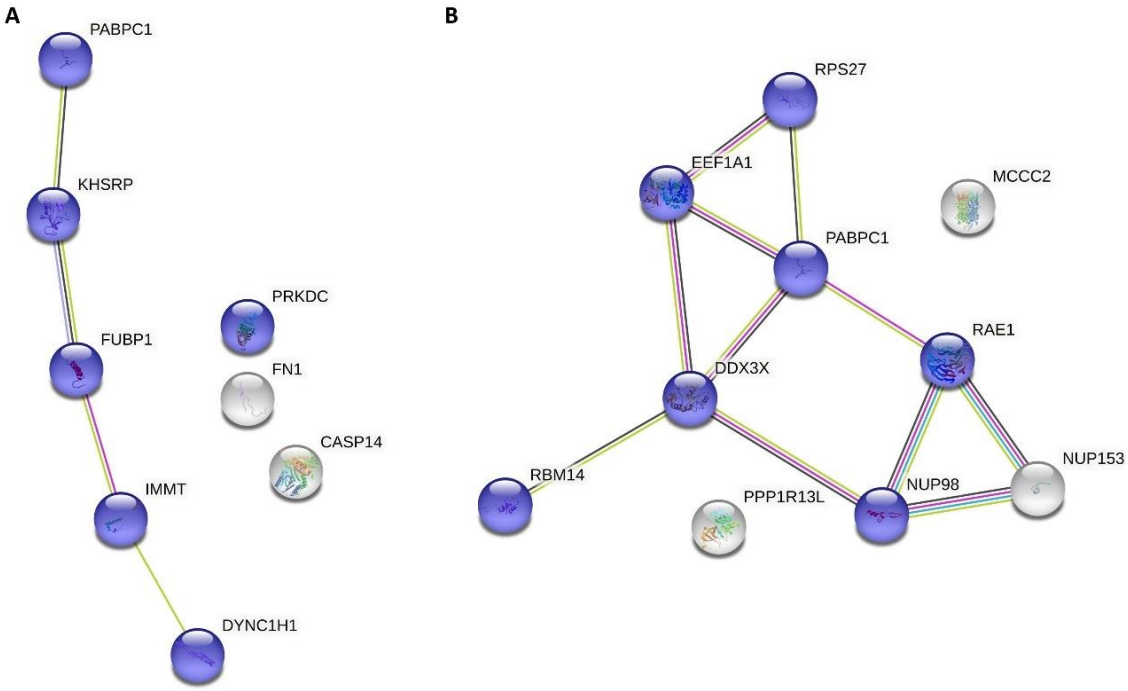

Figure 24. Protein-protein interaction networks obtained with STRING.

Proteins with higher potential as binding partners of phyllobilins were sorted together. As expected for non-random clusters with more than 3 proteins, a large majority of proteins had a same molecular function or are involved in a same pathway. In the largest cluster of phyllobilins target binding proteins, the same function was RNA binding.

Having identified those proteins with MS-based affinity chromatography, the next step is to validate them as real target proteins of phyllobilins. Here, a Y3H spot test will serve as complementary method for target confirmation. In brief, genes of interest will be amplified from genomic DNA using PCR and cloned into the Y3H vector. This allows

for performing a Y3H spot test using the phyllobilin probes employed for the Y3H screening.

DISCUSSION

5 Discussion

5.1 Diverse biological activities of phyllobilins

As the degradation products of Chl breakdown, phyllobilins were long considered as waste products of this detoxification processes performed by plants. Therefore, research on phyllobilins was mainly focused on elucidation of the wide structural diversity. However, phyllobilins show striking similarities with the same tetrapyrrolic structure core to the catabolites of heme, the bilins, which have been shown by several studies to possess interesting pharmacologically relevant activities[48], indicating phyllobilins are also an interesting class of compounds for pharmaceutical approaches that is worth further study. The structural diversity, which is mainly related to modifications of phyllobilins depending on the plant species, makes it even more interesting to elucidate pharmacological activities as well as pharmacodynamics and pharmacokinetics, which are related to structure, and could differ dramatically.

With the modified hot water extraction method, we isolated PleBs and PxB from Katsura and Plane tree leaves and tested their anti-proliferative effects on T24 cells. Surprisingly, PxB showed good activity with an IC50 of 23.05 µM, whereas this clear effect was not indicated by treatment with PleBs.

For natural products, chemical modification has always been an effective way to enhance bioactivities. Among all four different main modification positions of phyllobilins (Figure 5), of particular interest for chemical modification is the esterification of the propionic acid group at C12. Natural esterification of this side chain was also discovered in different degradation stages: PluBs in banana peels [38], PleBs in leaves of wych elm [28]and *Vitis vinifera* [36], and also on the PxB level in *Epipremnum aureum* [85], which was found very recently. Because of its high abundance, *Cj*-PleB with a free propionic acid functionality was used as the starting material for chemical modification, and esters of the propionic acid side chain with increasing length of the alkyl chain were synthesized. Interestingly, upon modifying

inactive PleB by esterification, an anti-proliferative activity was observed to be increasing with the chain length of the alkyl esters, indicating that the polarity might impact cytotoxic potential for these modified PleBs, which could be partially explained by cellular uptake being increased with the length of the alkyl side chain. These results also pointed towards a promising direction to obtain more pharmacologically active phyllobilin derivatives by simple chemical modification, using phyllobilins with different structures as starting material.

However, the esterification of PxB did not contribute to increasing the anti-proliferative activity. The reason might be that with the already lower polarity of PxB compared with PleBs, adding a longer side chain could further decrease the polarity and therefore lead to solubility issues.

Apart from the anti-cancer activity of phyllobilins and their chemically modified derivatives, other studies have revealed that phyllobilins possess diverse biological activities, including anti-oxidative activity [29], anti-inflammatory activity [30], and apoptosis inducing activity. First analysis of herbivore-infested and fungal-infected basil leaves have revealed a significant increase of phyllobilins in the areas of pest infestation, pointing to possible plant defense or signaling mechanisms [52], and leaving room for further investigations of physiologically relevant roles of phyllobilins.

Clearly, the so-far discovered effects of phyllobilins contradict the previous notion of these natural products being only waste products of a detoxification process, and set the starting point for discovering further possible bioactivities. Furthermore, they emphasize the importance of elucidating the impact of this long-overlooked class of natural products on the health and organism of mammals as well as on the plant itself. To achieve that, it is very important to find potential target proteins for phyllobilins and elucidate the mechanisms of their interaction.

5.2 Establishment of Y3H system using two known interaction pairs

Inevitably, the identification of novel protein targets of a small molecule drug represents a key step for its further development. As long as an interaction partner is known, not only downstream mode of action studies could be continued, relative medicinal biochemistry approaches could also be facilitated. In order to fish for binding proteins of phyllobilins, we set up a Y3H platform. In spite of its simplicity, the Y3H system has not been used as broadly as other approaches to find targets of small molecules. As one of the major drawbacks of yeast-based screen system, the drug of interest must be taken up by yeast cells in sufficient amount. To achieve that, we used the *Saccharomyces cerevisiae* ABC9Δ strain as a reporter strain which features 9 efflux pump deletions [77]. Besides, a well validated drug-protein interaction pair of trimethoprim and DHFR [76] was inserted to the system, since the strong inhibition of trimethoprim on DHFR makes this pair suitable for a Y3H setup. Furthermore, to validate that our system can indeed detect drug-protein interactions, we also used a trimethoprim-purvalanol B chemical inducer of dimerization, and CDK5 as prey protein, completing the setup with those two known interaction pairs. After incubation, the yeast grew only on selective plates containing the purvalanol B probe, indicating the system to be working properly.

5.3 PLOD2 as a binding protein of ethinylestradiol was identified using the Y3H system and validated by complementary methods

The Y3H setup was first used to screen for potential target proteins for a model drug ethinylestradiol. Two commercially available cDNA libraries, a mammary gland cDNA library and a pancreas cDNA library, were introduced into the reporter strain containing the DHFR bait plasmid, respectively. Using the trimethoprim derivatized ethinylestradiol as the Y3H system ligand, the screen was performed to yield several colonies that passed the growth dependence test. After sequencing, although none of

the inserts turned out to be real positive hits from the pancreas library screening, from the mammary gland library screening, two colonies among those classified as hits carried a library plasmid with an insert encoding for the last 81 amino acid sequence in the coding sequence of PLOD2. PLOD2 protein consists of 737 amino acids. The 81 amino acid sequence identified in our screen covers a region towards the C-terminus of the protein, and contains the metal binding domain as well as the active site of PLOD2.

To first validate PLOD2 as a binding partner of ethinylestradiol, we performed a complementary affinity chromatography approach. From the Western blot results, the identified PLOD2 fragment could be pulled down by immobilized ethinylestradiol from yeast cell lysates overexpressing the fragment (Figure 14 and Supplementary Figure 9). Afterwards, since the identified cDNA insert did not cover the entire coding sequence, we also wanted to confirm the interaction between ethinylestradiol and PLOD2 using human recombinant PLOD2. Therefore, we repeated the pull-down experiment using the commercially available whole PLOD2 and a PLOD2 antibody for Western blot analysis. Compared to the negative control (pegylated biotin), a clear enrichment was observed when PLOD2 was washed over beads with immobilized ethinylestradiol (Figure 15 and Supplementary Figure 10), which confirmed the validity of the interaction identified in the Y3H screen.

It is not clear whether the identified PLOD2 fragment is properly folded. Nevertheless, we assume that at least it is folded correctly to a degree so that the binding of ethinylestradiol and this fragment could actually happen. This is also indicated by the pull-down experiments, in which a stronger band was observed while using the whole human recombinant PLOD2 protein compared to the fragment identified in the screen.

To further validate the interaction between ethinylestradiol and PLOD2, we assessed the effect of ethinylestradiol on PLOD2 activity. PLOD2 has received growing attention recently, since it has been found to aid tumor metastasis by increasing the stiffness of

the collagen matrix by catalyzing the formation of hydroxyl-lysine residues in collagens [80, 86]. In this process, succinate is formed. By performing a bioluminescence based PLOD2 activity assay that is based on Promega's Succinate-Glo™ Assay [75], the formation of succinate can be monitored. Using the whole PLOD2 protein, this assay revealed that addition of ethinylestradiol led to a decreased formation of succinate, suggesting an inhibition of PLOD2 activity by ethinylestradiol (Figure 16). A recent study showed that PLOD2 is secreted by tumor cells and modifies collagen in the extracellular space [80]. From a collagen staining assay, the decrease of collagen intensity around the cells indicated that the extracellular collagen crosslinking was impaired upon treatment with ethinylestradiol (Figure 17).

In the end, we also assessed PLOD2 expression levels using a PLOD2 antibody and found that both, minoxidil and ethinylestradiol, led to a decrease of PLOD2 expression levels (Figure 18).

Although a previously unknown binding partner of ethinylestradiol was confirmed, estrogen receptor α (ERα), the classical target of ethinylestradiol, has not been identified in the Y3H screen. One possible reason is that the size of the receptor might be too big and has been excluded in the library construction process, which is limited to cDNA of a smaller size range. Even if the receptor or parts of it are included in the library, increasing the number of plates used for screening might also lead to the identification of ERα in the screen.

Nevertheless, the Y3H screen allowed for the identification of a hitherto unknown protein binding partner of the widely used contraceptive ethinylestradiol. The implications of the interaction between PLOD2 and ethinylestradiol as identified in a biological context, especially in cancer biology, is the subject of future studies.

5.4 NPC2 and PML as binding proteins of PxB were identified using the Y3H system and validated by complementary methods

PleB and PxB were also derivatized with trimethoprim and subjected to the Y3H system to screen for potential binding proteins. A kidney cDNA library was screened in addition to the mammary gland cDNA library and pancreas cDNA library. Unfortunately, from all the PleB screens, no real hit was identified.

From the kidney library screening plates of PxB, however, one hit was identified 9 times, coding for the last 72 amino acid sequence in the coding sequence of NPC intracellular cholesterol transporter 2 (NPC2), which consists of 151 amino acids.

Therefore, a complementary affinity chromatography approach was performed to validate the interaction between NPC2 and PxB. The identified NPC2 fragment was clearly enriched on PxB modified streptavidin beads, indicating the NPC2 as a legit binding partner of PxB (Figure 19 and Supplementary Figure 12).

NPC2 plays an important role in the transportation of cholesterol, as well as other lipids, in the lysosomal compartment and works with NPC1, which is responsible for accepting cholesterol from NPC2 and egressing cholesterol out of the lysosomal compartment [87]. NPC2 binds cholesterol with submicromolar affinity.

Whether PxB has an active effect or inhibitory effect on NPC2 is still unclear, and should be the focus of future study. If we could confirm that treatment of PxB leads to the inhibition of NPC2 and subsequent down-regulation of the sequestration of unesterified cholesterol, as well as other lipids, it would render NPC2 as a promising PxB target to investigate.

Furthermore, from the PxB mammary gland library screening, two colonies were also clarified as hits carrying a library plasmid with an insert fragment, coding for 151 amino acid sequence in the coding sequence of the promyelocytic leukemia protein (PML). PML protein consists of 882 amino acids. The 151 amino acids sequence identified in

our screen covers a region from amino acid 412 to 571, and contains nuclear localization signal motif of PML.

PML is a tumor suppressor protein functioning via its association with PML-nuclear bodies in a wide range of important cellular processes. It regulates transcriptional regulation, apoptosis, senescence, DNA damage response, and viral defense mechanisms [88].

The interaction between PxB and PML fragment was also confirmed by affinity chromatography (Figure 20).

5.5 MS-based affinity chromatography for target identification of phyllobilins

Biotinylated PleB and PxB were applied to affinity chromatography by incubating with T24 cell lysates to fish for potential binding proteins. Those bound proteins with higher log2 fold changes and -log10 p values were analyzed using the online tool STRING (www.string-db.org). Surprisingly, most of them have RNA binding function. RNA binding proteins have been confirmed to be involved in many posttranscriptional mechanisms, including RNA splicing, polyadenylation, transport, translation, localization and all other aspects of RNA life [89, 90].

Among those potential targets, PABPC1 draws the highest attention due to its high abundance in both the PleB and PxB groups. A previous study has reported PABPC1 as an oncogene [91]. The mRNA and protein expression of PABPC1 was found to be increased in cancer cells and upregulation of PABPC1 was found to promote cancer cell growth [92]. It regulates mRNAs by binding to the poly(A) tails and promote mRNA translation [93]. Whether PABPC1 is indeed a binding partner of phyllobilins, how they interact, and what this interaction implies, is the subject of future studies.

Apart from PABPC1, there were also several interesting target proteins identified by affinity chromatography. Another RNA binding protein in the PxB cluster, EEF1A1 (Eukaryotic translation elongation factor 1-alpha 1), was shown to be a druggable

target for the inhibition of SARS-CoV-2 replication since it is required for the translation of viral proteins and viral replication during human coronavirus SARS-CoV-2 infection [94]. Out of the RNA binding cluster, PPP1R13L, which is the protein with the highest significance in PxB group, encodes for RelA-associated inhibitor. It was shown to be an efficient inhibitor of HIV-1 gene expression by directly blocking the DNA-binding of NF-kappa-B [95].

Further validation of those potential binding proteins of phyllobilins needs to be done by using complementary target identification approaches including the yeast three-hybrid system we established previously.

5.6 Complementary approaches for target identification for phyllobilins

Here in this work, we used affinity chromatography and a yeast three-hybrid system as two complementary target identification approaches to find potential binding partner for phyllobilins.

On the one hand, potential targets of PxB we identified from the yeast three-hybrid system (NPC2 and PML), were further validated using biotin-based affinity chromatography. We succeeded in confirming their interactions and revealed them as promising target proteins for phyllobilins for further studies. However, they were not identified in the MS-based affinity chromatography. PML was only identified in the T24 cell lysates with low intensity but wasn't detected in the PxB group. The reason could be that the expression of PML in T24 cells was not high enough to be fished out by modified PxB probe. A previous study has shown that overexpression of PML might promote efficient growth inhibition of human bladder cancer cells by inducing a G1 cell cycle arrest and apoptosis [96], which might be the reason why PML was not present in high abundance in T24 cell lysates. Neither could the other target of PxB identified in the Y3H screen, NPC2, be identified by affinity chromatography.

On the other hand, those potential target proteins we identified from MS-based affinity chromatography can be further validated using our established yeast three-hybrid system. Although none of them was identified in our previous phyllobilins yeast three-hybrid screen, increasing the number of plates used for screening might yield different results.

Drug target identification is inevitably the major bottlenecks in the drug discovery procedure. Therefore, the combination of complementary target identification approaches is a strategy to significantly increase the chances of understanding the effects of a certain drug. By applying affinity chromatography and the yeast three-hybrid system, we identified new potential binding partners for phyllobilins.

REFERENCES

6 References

1. Hendry GA, Houghton JD, Brown SB: **Tansley Review No. 11. The degradation of chlorophyll-A biological enigma**. *New phytologist* 1987:255-302.
2. Kräutler B, Jaun B, Matile P, Bortlik K, Schellenberg M: **On the enigma of chlorophyll degradation: the constitution of a secoporphinoid catabolite**. *Angewandte Chemie International Edition in English* 1991, **30**(10):1315-1318.
3. Hörtensteiner S, Kräutler B: **Chlorophyll breakdown in higher plants**. *Biochimica et Biophysica Acta (BBA)-Bioenergetics* 2011, **1807**(8):977-988.
4. Matile P: **Biochemistry of Indian summer: physiology of autumnal leaf coloration**. *Experimental gerontology* 2000, **35**(2):145-158.
5. Kräutler B, Matile P: **Solving the riddle of chlorophyll breakdown**. *Accounts of Chemical Research* 1999, **32**(1):35-43.
6. Kräutler B, Hörtensteiner S: **Chlorophyll breakdown: chemistry, biochemistry, and biology**. In: *Handbook of Porphyrin Science (Volume 28) With Applications to Chemistry, Physics, Materials Science, Engineering, Biology and Medicine—Volume 28: Chlorophyll, Photosynthesis and Bio-inspired Energy.* edn.: World Scientific; 2014: 117-185.
7. Matile P, Hörtensteiner S, Thomas H, Kräutler B: **Chlorophyll breakdown in senescent leaves**. *Plant physiology* 1996, **112**(4):1403.
8. Falk H: **The chemistry of linear oligopyrroles and bile pigments**, vol. 1: Springer Science & Business Media; 1989.
9. Müller T, Moser S, Ongania KH, Pruzinska A, Hörtensteiner S, Kräutler B: **A divergent path of chlorophyll breakdown in the model plant Arabidopsis thaliana**. *ChemBioChem* 2006, **7**(1):40-42.
10. Folly P, Engel N: **Chlorophyll b to chlorophyll a conversion precedes chlorophyll degradation in Hordeum vulgare L**. *Journal of Biological Chemistry* 1999, **274**(31):21811-21816.
11. Oster U, Tanaka R, Tanaka A, Rüdiger W: **Cloning and functional expression of the gene encoding the key enzyme for chlorophyll b biosynthesis (CAO) from Arabidopsis thaliana**. *The Plant Journal* 2000, **21**(3):305-310.
12. Tanaka R, Tanaka A: **Tetrapyrrole biosynthesis in higher plants**. *Annu Rev Plant Biol* 2007, **58**:321-346.
13. Tanaka R, Tanaka A: **Chlorophyll cycle regulates the construction and destruction of the light-harvesting complexes**. *Biochimica et Biophysica Acta (BBA)-Bioenergetics* 2011, **1807**(8):968-976.
14. Hörtensteiner S, Vicentini F, Matile P: **Chlorophyll breakdown in senescent cotyledons of rape, Brassica napus L.: enzymatic cleavage of phaeophorbide a in vitro**. *New Phytologist* 1995, **129**(2):237-246.
15. Hörtensteiner S, Wüthrich KL, Matile P, Ongania K-H, Kräutler B: **The Key Step in Chlorophyll Breakdown in Higher Plants: CLEAVAGE OF PHEOPHORBIDE aMACROCYCLE BY A MONOOXYGENASE**. *Journal of Biological Chemistry* 1998, **273**(25):15335-15339.
16. Kräutler B: **Phyllobilins–the abundant bilin-type tetrapyrrolic catabolites of the green plant pigment chlorophyll**. *Chemical Society Reviews* 2014, **43**(17):6227-6238.

17. Mühlecker W, Ongania KH, Kräutler B, Matile P, Hörtensteiner S: **Tracking down chlorophyll breakdown in plants: elucidation of the constitution of a "fluorescent" chlorophyll catabolite**. *Angewandte Chemie International Edition in English* 1997, **36**(4):401-404.
18. Pruzinska A, Anders I, Aubry S, Schenk N, Tapernoux-Luthi E, Müller T, Kräutler B, Hörtensteiner S: **In vivo participation of red chlorophyll catabolite reductase in chlorophyll breakdown**. *The Plant Cell* 2007, **19**(1):369-387.
19. Wüthrich KL, Bovet L, Hunziker PE, Donnison IS, Hörtensteiner S: **Molecular cloning, functional expression and characterisation of RCC reductase involved in chlorophyll catabolism**. *The Plant Journal* 2000, **21**(2):189-198.
20. Christ B, Süssenbacher I, Moser S, Bichsel N, Egert A, Müller T, Kräutler B, Hörtensteiner S: **Cytochrome P450 CYP89A9 is involved in the formation of major chlorophyll catabolites during leaf senescence in Arabidopsis**. *The Plant Cell* 2013, **25**(5):1868-1880.
21. Oberhuber M, Berghold J, Kräutler B: **Chlorophyll breakdown by a biomimetic route**. *Angewandte Chemie International Edition* 2008, **47**(16):3057-3061.
22. Oberhuber M, Berghold J, Breuker K, Hörtensteiner S, Kräutler B: **Breakdown of chlorophyll: a nonenzymatic reaction accounts for the formation of the colorless "nonfluorescent" chlorophyll catabolites**. *Proceedings of the National Academy of Sciences* 2003, **100**(12):6910-6915.
23. Hörtensteiner S, Hauenstein M, Kräutler B: **Chlorophyll breakdown—regulation, biochemistry and phyllobilins as its products**. In: *Advances in Botanical Research. Volume 90*, edn.: Elsevier; 2019: 213-271.
24. Hauenstein M, Christ B, Das A, Aubry S, Hörtensteiner S: **A role for TIC55 as a hydroxylase of phyllobilins, the products of chlorophyll breakdown during plant senescence**. *The Plant Cell* 2016, **28**(10):2510-2527.
25. Moser S, Ulrich M, Müller T, Kräutler B: **A yellow chlorophyll catabolite is a pigment of the fall colours**. *Photochemical & Photobiological Sciences* 2008, **7**(12):1577-1581.
26. Scherl M, Müller T, Kräutler B: **Chlorophyll catabolites in senescent leaves of the lime tree (Tilia cordata)**. *Chemistry & Biodiversity* 2012, **9**(11):2605-2617.
27. Wakana D, Kato H, Momose T, Sasaki N, Ozeki Y, Goda Y: **NMR-based characterization of a novel yellow chlorophyll catabolite, Ed-YCC, isolated from Egeria densa**. *Tetrahedron Letters* 2014, **55**(18):2982-2985.
28. Scherl M, Müller T, Kreutz CR, Huber RG, Zass E, Liedl KR, Kräutler B: **Chlorophyll catabolites in fall leaves of the wych elm tree present a novel glycosylation motif**. *Chemistry–A European Journal* 2016, **22**(28):9498-9503.
29. Karg CA, Wang P, Vollmar AM, Moser S: **Re-opening the stage for Echinacea research-Characterization of phylloxanthobilins as a novel anti-oxidative compound class in Echinacea purpurea**. *Phytomedicine* 2019, **60**:152969.
30. Karg CA, Doppler C, Schilling C, Jakobs F, Dal Colle MC, Frey N, Bernhard D, Vollmar AM, Moser S: **A yellow chlorophyll catabolite in leaves of Urtica dioica L.: An overlooked phytochemical that contributes to health benefits of stinging nettle**. *Food Chemistry* 2021, **359**:129906.

31. Ulrich M, Moser S, Müller T, Kräutler B: **How the colourless 'nonfluorescent'chlorophyll catabolites rust**. *Chemistry–A European Journal* 2011, **17**(8):2330-2334.
32. Li C, Ulrich M, Liu X, Wurst K, Müller T, Kräutler B: **Blue transition metal complexes of a natural bilin-type chlorophyll catabolite**. *Chemical Science* 2014, **5**(9):3388-3395.
33. Süssenbacher I, Christ B, Hörtensteiner S, Kräutler B: **Hydroxymethylated phyllobilins: a puzzling new feature of the dioxobilin branch of chlorophyll breakdown**. *Chemistry–A European Journal* 2014, **20**(1):87-92.
34. Christ B, Hauenstein M, Hörtensteiner S: **A liquid chromatography–mass spectrometry platform for the analysis of phyllobilins, the major degradation products of chlorophyll in Arabidopsis thaliana**. *The Plant Journal* 2016, **88**(3):505-518.
35. Li C, Kräutler B: **A pink colored dioxobilin-type phyllobilin from breakdown of chlorophyll**. *Monatshefte für Chemie-Chemical Monthly* 2019, **150**(5):813-820.
36. Erhart T, Mittelberger C, Liu X, Podewitz M, Li C, Scherzer G, Stoll G, Valls J, Robatscher P, Liedl KR: **Novel types of hypermodified fluorescent phyllobilins from breakdown of chlorophyll in senescent leaves of grapevine (Vitis vinifera)**. *Chemistry–A European Journal* 2018, **24**(65):17268-17279.
37. Karg CA, Schilling CM, Allmendinger L, Moser S: **Isolation, characterization, and antioxidative activity of a dioxobilin-type phylloxanthobilin from savoy cabbage**. In: *PORPHYRIN SCIENCE BY WOMEN: In 3 Volumes*. edn.: World Scientific; 2019: 1257-1264.
38. Moser S, Müller T, Ebert MO, Jockusch S, Turro NJ, Kräutler B: **Blue luminescence of ripening bananas**. *Angewandte Chemie International Edition* 2008, **47**(46):8954-8957.
39. Banala S, Moser S, Müller T, Kreutz C, Holzinger A, Lütz C, Kräutler B: **Hypermodified fluorescent chlorophyll catabolites: source of blue luminescence in senescent leaves**. *Angewandte Chemie International Edition* 2010, **49**(30):5174-5177.
40. Kräutler B, Banala S, Moser S, Vergeiner C, Müller T, Lütz C, Holzinger A: **A novel blue fluorescent chlorophyll catabolite accumulates in senescent leaves of the peace lily and indicates a split path of chlorophyll breakdown**. *FEBS letters* 2010, **584**(19):4215-4221.
41. Pruzinská A, Tanner G, Aubry S, Anders I, Moser S, Müller T, Ongania K-H, Kräutler B, Youn J-Y, Liljegren SJ: **Chlorophyll breakdown in senescent Arabidopsis leaves. Characterization of chlorophyll catabolites and of chlorophyll catabolic enzymes involved in the degreening reaction**. *Plant Physiology* 2005, **139**(1):52-63.
42. Erhart T, Mittelberger C, Vergeiner C, Scherzer G, Holzner B, Robatscher P, Oberhuber M, Kräutler B: **Chlorophyll catabolites in senescent leaves of the plum tree (Prunus domestica)**. *Chemistry & biodiversity* 2016, **13**(11):1441-1453.
43. Berghold J, Breuker K, Oberhuber M, Hörtensteiner S, Kräutler B: **Chlorophyll breakdown in spinach: on the structure of five nonfluorescent chlorophyll catabolites**. *Photosynthesis research* 2002, **74**(2):109-119.

44. Stocker R, Yamamoto Y, McDonagh AF, Glazer AN, Ames BN: **Bilirubin is an antioxidant of possible physiological importance**. *Science* 1987, **235**(4792):1043-1046.
45. Kumar S, Bandyopadhyay U: **Free heme toxicity and its detoxification systems in human**. *Toxicology letters* 2005, **157**(3):175-188.
46. Zheng J, Nagda D, Lajud S, Kumar S, Mouchli A, Bezpalko O, O'Malley B, Li D: **Biliverdin's regulation of reactive oxygen species signalling leads to potent inhibition of proliferative and angiogenic pathways in head and neck cancer**. *British journal of cancer* 2014, **110**(8):2116-2122.
47. Zahir F, Rabbani G, Khan RH, Rizvi SJ, Jamal MS, Abuzenadah AM: **The pharmacological features of bilirubin: the question of the century**. *Cellular and molecular biology letters* 2015, **20**(3):418-447.
48. Gazzin S, Vitek L, Watchko J, Shapiro SM, Tiribelli C: **A novel perspective on the biology of bilirubin in health and disease**. *Trends in molecular medicine* 2016, **22**(9):758-768.
49. Müller T, Ulrich M, Ongania KH, Kräutler B: **Colorless tetrapyrrolic chlorophyll catabolites found in ripening fruit are effective antioxidants**. *Angewandte Chemie International Edition* 2007, **46**(45):8699-8702.
50. Barañano DE, Rao M, Ferris CD, Snyder SH: **Biliverdin reductase: a major physiologic cytoprotectant**. *Proceedings of the national academy of sciences* 2002, **99**(25):16093-16098.
51. Pellati F, Benvenuti S, Magro L, Melegari M, Soragni F: **Analysis of phenolic compounds and radical scavenging activity of Echinacea spp**. *Journal of Pharmaceutical and Biomedical Analysis* 2004, **35**(2):289-301.
52. Moser S, Erhart T, Neuhauser S, Kräutler B: **Phyllobilins from senescence-associated chlorophyll breakdown in the leaves of Basil (Ocimum basilicum) show increased abundance upon herbivore attack**. *Journal of agricultural and food chemistry* 2020, **68**(27):7132-7142.
53. Inglese J, Johnson RL, Simeonov A, Xia M, Zheng W, Austin CP, Auld DS: **High-throughput screening assays for the identification of chemical probes**. *Nature chemical biology* 2007, **3**(8):466-479.
54. Axelrod M, Ou Z, Brett L, Zhang L, Lopez E, Tamayo A, Gordon V, Ford R, Williams M, Pham L: **Combinatorial drug screening identifies synergistic co-targeting of Bruton's tyrosine kinase and the proteasome in mantle cell lymphoma**. *Leukemia* 2014, **28**(2):407-410.
55. Bunnage ME, Gilbert AM, Jones LH, Hett EC: **Know your target, know your molecule**. *Nature chemical biology* 2015, **11**(6):368-372.
56. Futamura Y, Muroi M, Osada H: **Target identification of small molecules based on chemical biology approaches**. *Molecular bioSystems* 2013, **9**(5):897-914.
57. Han T, Nijhawan D: **Exome Sequencing of Drug-Resistant Clones for Target Identification**. In: *Systems Chemical Biology.* edn.: Springer; 2019: 175-187.
58. Rix U, Superti-Furga G: **Target profiling of small molecules by chemical proteomics**. *Nature chemical biology* 2009, **5**(9):616-624.
59. Lomenick B, Olsen RW, Huang J: **Identification of direct protein targets of small molecules**. *ACS chemical biology* 2011, **6**(1):34-46.

60. Kim YK, Lee JS, Bi X, Ha HH, Ng SH, Ahn Yh, Lee JJ, Wagner BK, Clemons PA, Chang YT: **The binding of fluorophores to proteins depends on the cellular environment**. *Angewandte Chemie* 2011, **123**(12):2813-2815.
61. Su Y, Ge J, Zhu B, Zheng Y-G, Zhu Q, Yao SQ: **Target identification of biologically active small molecules via in situ methods**. *Current opinion in chemical biology* 2013, **17**(5):768-775.
62. Sato S-I, Kwon Y, Kamisuki S, Srivastava N, Mao Q, Kawazoe Y, Uesugi M: **Polyproline-rod approach to isolating protein targets of bioactive small molecules: isolation of a new target of indomethacin**. *Journal of the American Chemical Society* 2007, **129**(4):873-880.
63. Sleno L, Emili A: **Proteomic methods for drug target discovery**. *Current opinion in chemical biology* 2008, **12**(1):46-54.
64. Chernobrovkin A, Marin-Vicente C, Visa N, Zubarev RA: **Functional Identification of Target by Expression Proteomics (FITExP) reveals protein targets and highlights mechanisms of action of small molecule drugs**. *Scientific reports* 2015, **5**(1):1-9.
65. Fields S, Song O: **A novel genetic system to detect protein-protein interactions**. *Nature* 1989, **340**(6230):245-246.
66. Brückner A, Polge C, Lentze N, Auerbach D, Schlattner U: **Yeast two-hybrid, a powerful tool for systems biology**. *International journal of molecular sciences* 2009, **10**(6):2763-2788.
67. Licitra EJ, Liu JO: **A three-hybrid system for detecting small ligand–protein receptor interactions**. 1996, **93**(23):12817-12821.
68. Becker F, Murthi K, Smith C, Come J, Costa-Roldán N, Kaufmann C, Hanke U, Degenhart C, Baumann S, Wallner W *et al*: **A Three-Hybrid Approach to Scanning the Proteome for Targets of Small Molecule Kinase Inhibitors**. *Chemistry & Biology* 2004, **11**(2):211-223.
69. Henthorn DC, Jaxa-Chamiec AA, Meldrum E: **A GAL4-based yeast three-hybrid system for the identification of small molecule–target protein interactions**. *Biochemical Pharmacology* 2002, **63**(9):1619-1628.
70. Chidley C, Haruki H, Pedersen MG, Muller E, Johnsson K: **A yeast-based screen reveals that sulfasalazine inhibits tetrahydrobiopterin biosynthesis**. *Nature chemical biology* 2011, **7**(6):375-383.
71. Li C, Wurst K, Berghold J, Podewitz M, Liedl KR, Kräutler B: **Pyro-Phyllobilins: Elusive Chlorophyll Catabolites Lacking a Critical Carboxylate Function of the Natural Chlorophylls**. *Chemistry–A European Journal* 2018, **24**(12):2987-2998.
72. Gietz RD, Schiestl RH: **Quick and easy yeast transformation using the LiAc/SS carrier DNA/PEG method**. *Nature Protocols* 2007, **2**(1):35-37.
73. Gietz RD, Schiestl RH: **High-efficiency yeast transformation using the LiAc/SS carrier DNA/PEG method**. *Nature Protocols* 2007, **2**(1):31-34.
74. Benatuil L, Perez JM, Belk J, Hsieh CM: **An improved yeast transformation method for the generation of very large human antibody libraries**. *Protein engineering, design & selection : PEDS* 2010, **23**(4):155-159.
75. Devkota AK, Veloria JR, Guo HF, Kurie JM, Cho EJ, Dalby KN: **Development of a High-Throughput Lysyl Hydroxylase (LH) Assay and Identification of Small-Molecule Inhibitors against LH2**. *SLAS Discov* 2019, **24**(4):484-491.

76. Gallagher SS, Miller LW, Cornish VW: **An orthogonal dexamethasone-trimethoprim yeast three-hybrid system**. *Analytical biochemistry* 2007, **363**(1):160.
77. Wong JH, Alfatah M, Sin MF, Sim HM, Verma CS, Lane DP, Arumugam P: **A yeast two-hybrid system for the screening and characterization of small-molecule inhibitors of protein–protein interactions identifies a novel putative Mdm2-binding site in p53**. *BMC biology* 2017, **15**(1):1-17.
78. Li H, Ma S, Zhang X, Li C, Dong B, Mujtaba MG, Wei Y, Liang X, Yu X, Wen K *et al*: **Generic Hapten Synthesis, Broad-Specificity Monoclonal Antibodies Preparation, and Ultrasensitive ELISA for Five Antibacterial Synergists in Chicken and Milk**. *Journal of Agricultural and Food Chemistry* 2018, **66**(42):11170-11179.
79. Moser S, Johnsson K: **Yeast Three-Hybrid Screening for Identifying Anti-Tuberculosis Drug Targets**. *Chembiochem* 2013, **14**(17):2239-2242.
80. Chen Y, Guo H, Terajima M, Banerjee P, Liu X, Yu J, Momin AA, Katayama H, Hanash SM, Burns AR: **Lysyl hydroxylase 2 is secreted by tumor cells and can modify collagen in the extracellular space**. *Journal of Biological Chemistry* 2016, **291**(50):25799-25808.
81. Xu F, Zhang J, Hu G, Liu L, Liang W: **Hypoxia and TGF-β1 induced PLOD2 expression improve the migration and invasion of cervical cancer cells by promoting epithelial-to-mesenchymal transition (EMT) and focal adhesion formation**. *Cancer Cell International* 2017, **17**(1):54.
82. Su R, Ma J, Zheng J, Liu X, Liu Y, Ruan X, Shen S, Yang C, Wang D, Cai H: **PABPC1-induced stabilization of BDNF-AS inhibits malignant progression of glioblastoma cells through STAU1-mediated decay**. *Cell death & disease* 2020, **11**(2):1-17.
83. Zhu J, Ding H, Wang X, Lu Q: **PABPC1 exerts carcinogenesis in gastric carcinoma by targeting miR-34c**. *International journal of clinical and experimental pathology* 2015, **8**(4):3794.
84. Franceschini A, Szklarczyk D, Frankild S, Kuhn M, Simonovic M, Roth A, Lin J, Minguez P, Bork P, Von Mering C: **STRING v9. 1: protein-protein interaction networks, with increased coverage and integration**. *Nucleic acids research* 2012, **41**(D1):D808-D815.
85. Roiser MH, Müller T, Kräutler B: **Colorless chlorophyll catabolites in senescent florets of broccoli (Brassica oleracea var. italica)**. *Journal of agricultural and food chemistry* 2015, **63**(5):1385-1392.
86. Chen Y, Terajima M, Yang Y, Sun L, Ahn Y-H, Pankova D, Puperi DS, Watanabe T, Kim MP, Blackmon SH: **Lysyl hydroxylase 2 induces a collagen cross-link switch in tumor stroma**. *The Journal of clinical investigation* 2015, **125**(3):1147-1162.
87. Vance JE: **Transfer of cholesterol by the NPC team**. *Cell Metabolism* 2010, **12**(2):105-106.
88. Bernardi R, Pandolfi PP: **Structure, dynamics and functions of promyelocytic leukaemia nuclear bodies**. *Nature reviews Molecular cell biology* 2007, **8**(12):1006-1016.
89. Gerstberger S, Hafner M, Tuschl T: **A census of human RNA-binding proteins**. *Nature Reviews Genetics* 2014, **15**(12):829-845.

90. Köster T, Staiger D: **RNA-binding protein immunoprecipitation from whole-cell extracts**. In: *Arabidopsis Protocols.* edn.: Springer; 2014: 679-695.
91. Zhang H, Sheng C, Yin Y, Wen S, Yang G, Cheng Z, Zhu Q: **PABPC1 interacts with AGO2 and is responsible for the microRNA mediated gene silencing in high grade hepatocellular carcinoma**. *Cancer letters* 2015, **367**(1):49-57.
92. Chen D, Chen T, Guo Y, Wang C, Dong L, Lu C: **Suppressive effect of platycodin D on bladder cancer through microRNA-129-5p-mediated PABPC1/PI3K/AKT axis inactivation**. *Brazilian Journal of Medical and Biological Research* 2021, **54**:10222-10000.
93. Stupfler B, Birck C, Séraphin B, Mauxion F: **BTG2 bridges PABPC1 RNA-binding domains and CAF1 deadenylase to control cell proliferation**. *Nature communications* 2016, **7**(1):1-11.
94. White KM, Rosales R, Yildiz S, Kehrer T, Miorin L, Moreno E, Jangra S, Uccellini MB, Rathnasinghe R, Coughlan L: **Plitidepsin has potent preclinical efficacy against SARS-CoV-2 by targeting the host protein eEF1A**. *Science* 2021, **371**(6532):926-931.
95. Takada N, Sanda T, Okamoto H, Yang J-P, Asamitsu K, Sarol L, Kimura G, Uranishi H, Tetsuka T, Okamoto T: **RelA-associated inhibitor blocks transcription of human immunodeficiency virus type 1 by inhibiting NF-κB and Sp1 actions**. *Journal of virology* 2002, **76**(16):8019-8030.
96. He D, Nan X, Chang K-S, Wang Y, Chung LW: **Overexpression of the promyelocytic leukemia gene suppresses growth of human bladder cancer cells by inducing G1 cell cycle arrest and apoptosis**. *Chinese medical journal* 2003, **116**(09):1394-1398.

APPENDIX

7 Appendix

7.1 Supplementary Figures

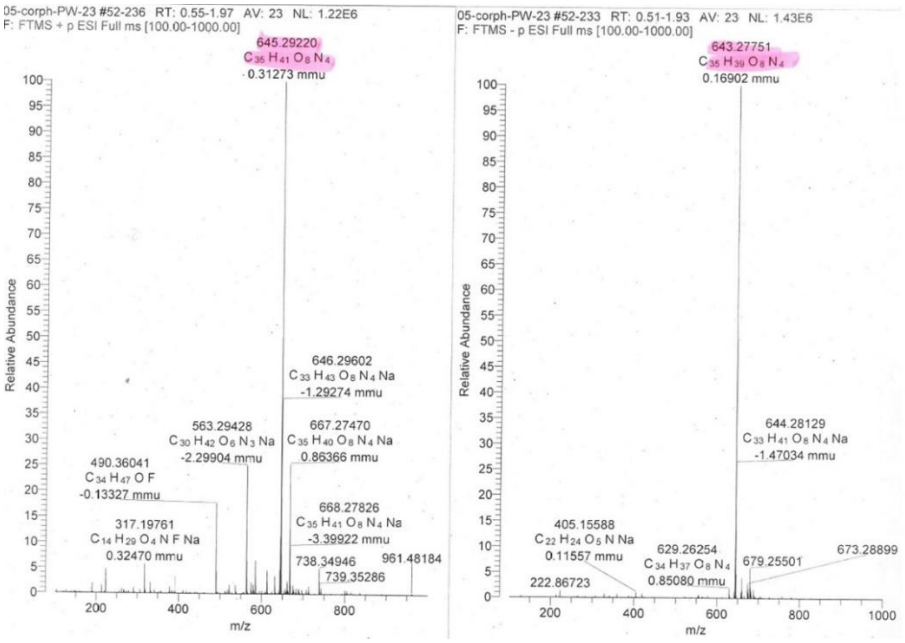

Supplementary Figure 1. HR-ESI-MS spectrum of *Po*-PleB.

HR-ESI-MS: $m/z_{calculated}$ ($C_{35}H_{40}N_4O_8$) = 645.29244 $[M + H]^+$; m/z_{found} = 645.29220 (Δ = -0.4 ppm).

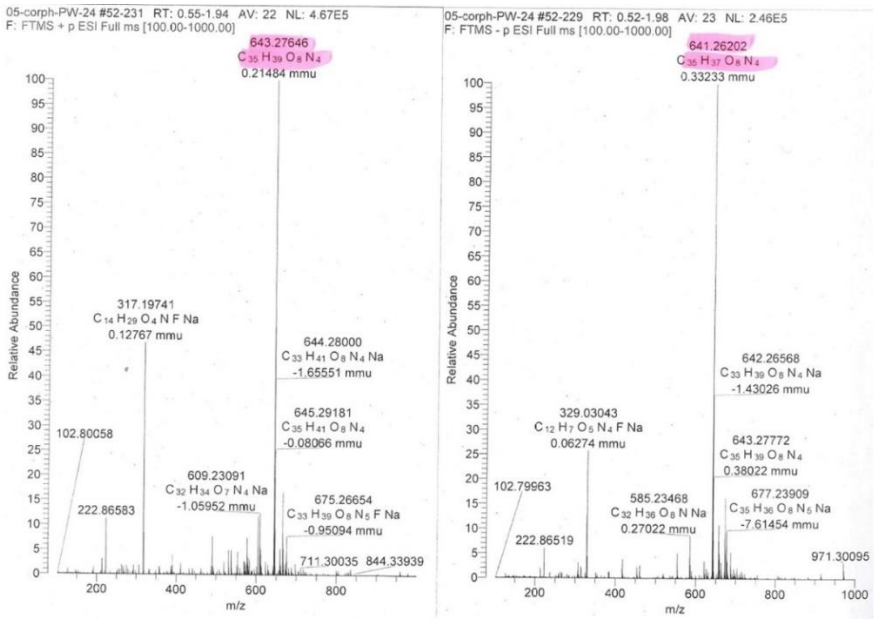

Supplementary Figure 2. HR-ESI-MS spectrum of *Po*-PxB.

HR-ESI-MS: $m/z_{calculated}$ ($C_{35}H_{38}N_4O_8$) = 643.27679 $[M + H]^+$; m/z_{found} = 643.27646 (Δ = -0.5 ppm).

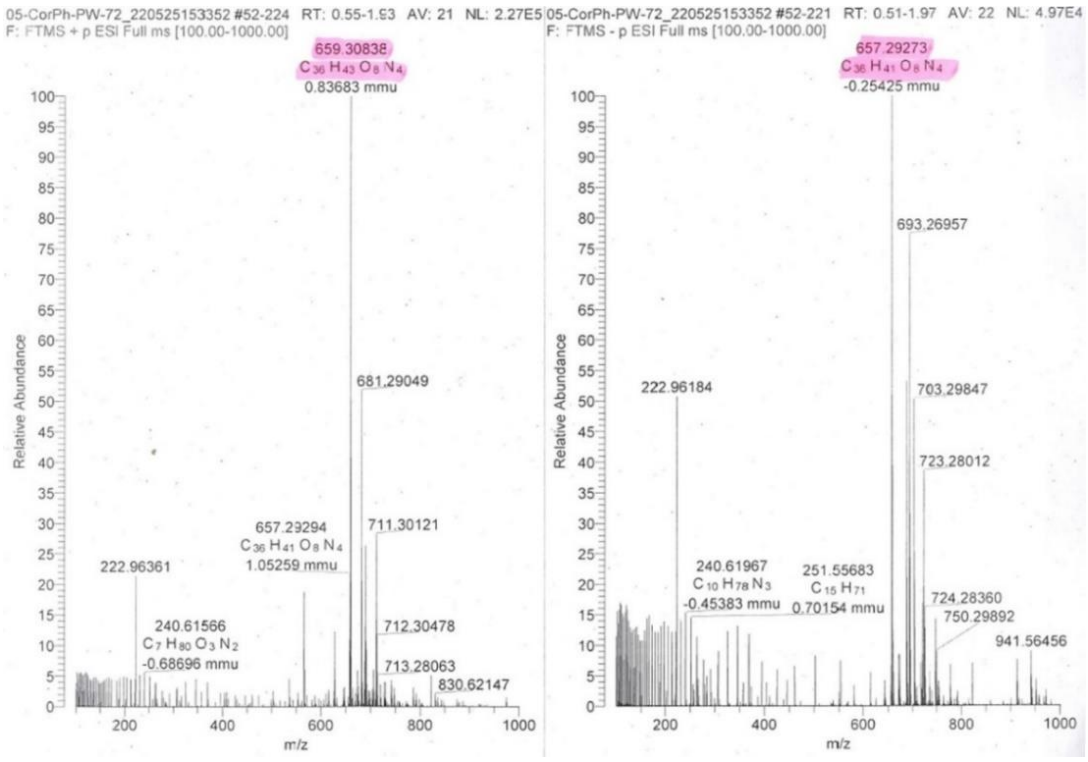

Supplementary Figure 3. HR-ESI-MS spectrum of methyl-PleB.

HR-ESI-MS: $m/z_{calculated}$ ($C_{36}H_{42}N_4O_8$) = 659.30809 $[M + H]^+$; m/z_{found} = 659.30838 (Δ = 0.4 ppm).

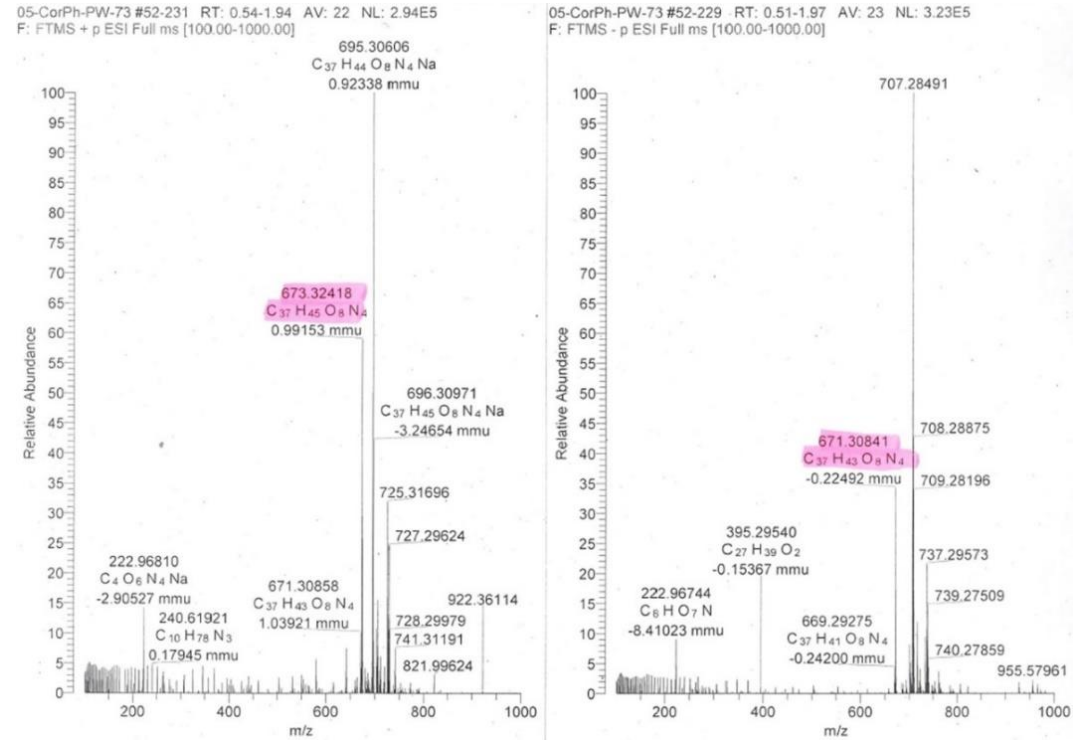

Supplementary Figure 4. HR-ESI-MS spectrum of ethyl-PleB.

HR-ESI-MS: $m/z_{calculated}$ ($C_{37}H_{44}N_4O_8$) = 673.32374 $[M + H]^+$; m/z_{found} = 673.32418 (Δ = 0.6 ppm).

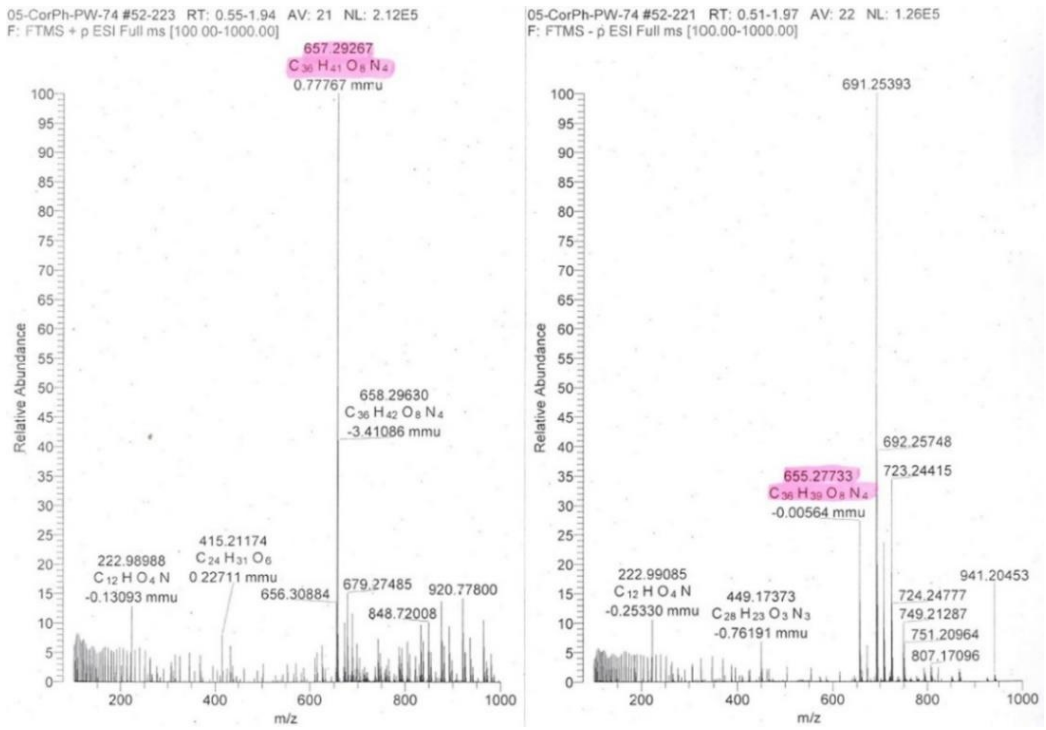

Supplementary Figure 5. HR-ESI-MS spectrum of methyl-PxB.

HR-ESI-MS: $m/z_{calculated}$ ($C_{36}H_{40}N_4O_8$) = 657.29244 $[M + H]^+$; m/z_{found} = 657.29267 (Δ = 0.3 ppm).

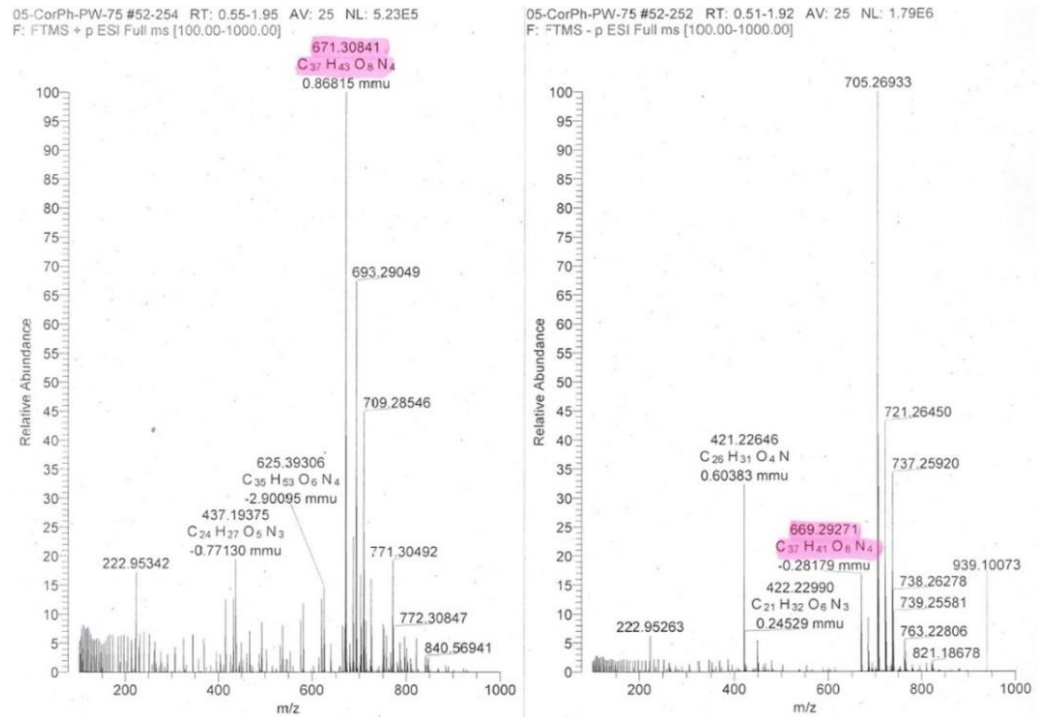

Supplementary Figure 6. HR-ESI-MS spectrum of ethyl-PxB.

HR-ESI-MS: $m/z_{calculated}$ ($C_{37}H_{42}N_4O_8$) = 671.30809 $[M + H]^+$; m/z_{found} = 671.30841 (Δ = 0.5 ppm).

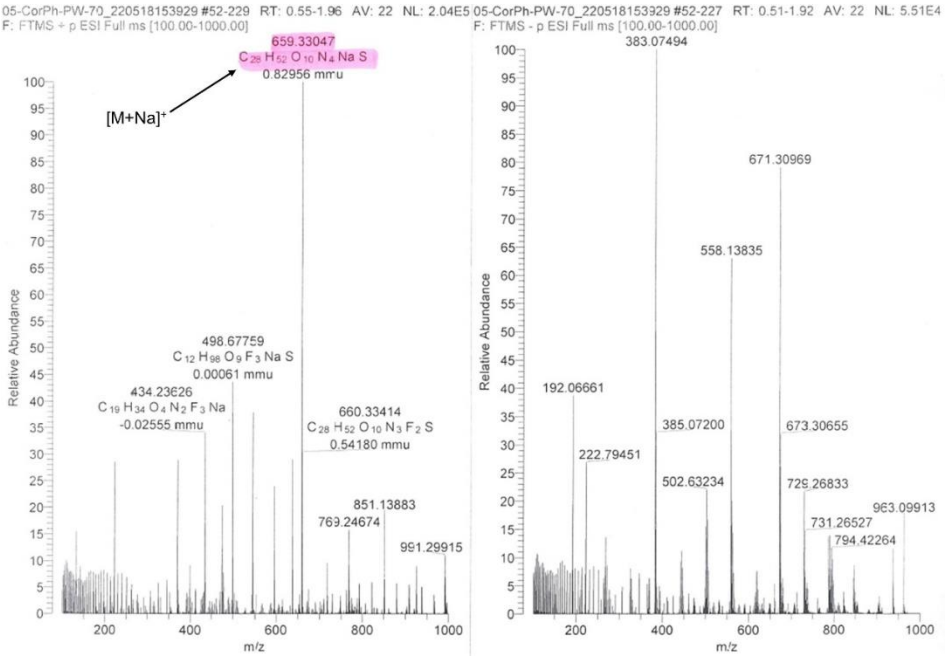

Supplementary Figure 7. HR-ESI-MS spectrum of biotin-PEG-acetate.

HR-ESI-MS: $m/z_{calculated}$ ($C_{28}H_{52}N_4O_{10}S$) = 659.33018 $[M + Na]^+$; m/z_{found} = 659.33047 (Δ = 0.4 ppm).

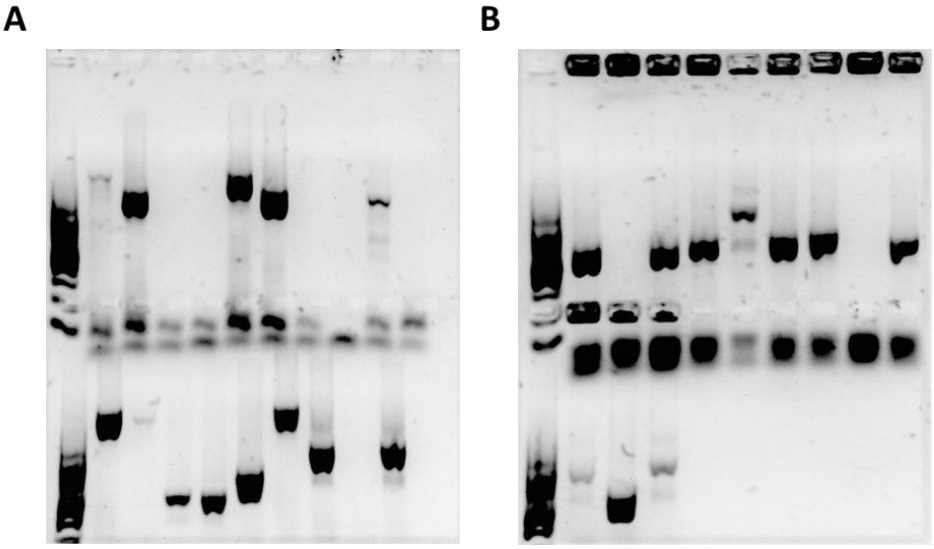

Supplementary Figure 8. Exemplary gels from a colony PCR for colonies classified as ethinylestradiol hits.

A. Colonies from the mammary gland library screening. B. Colonies from the pancreas library screening. For colonies for which no band was obtained, plasmids were isolated and the PCR was repeated.

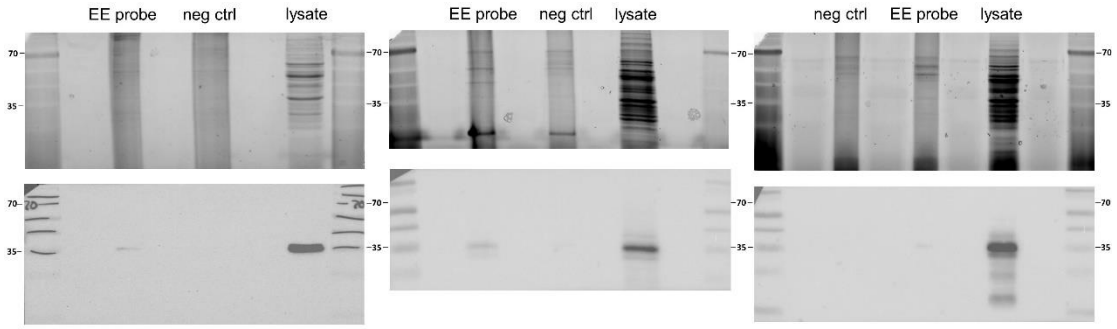

Supplementary Figure 9. Western blot of ethinylestradiol pull-down with PLOD2 fragment containing cell lysate.

The three replicates for the pull-down experiment using a lysate of yeast cells overexpressing the PLOD2 fragment identified in the Y3H screen as GAL4 AD fusion are shown. Top panel: loading control. Bottom panel: Western blot using GAL4 AD antibody.

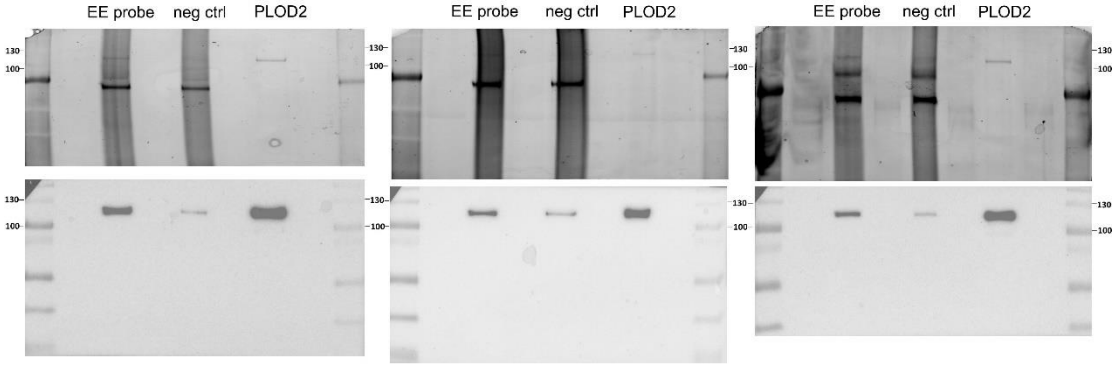

Supplementary Figure 10. Western blot of ethinylestradiol pull-down with PLOD2 protein.

The three replicates for the pull-down experiment using human recombinant PLOD2 are shown. Top panel: loading control. Bottom panel: Western blot using PLOD2 antibody.

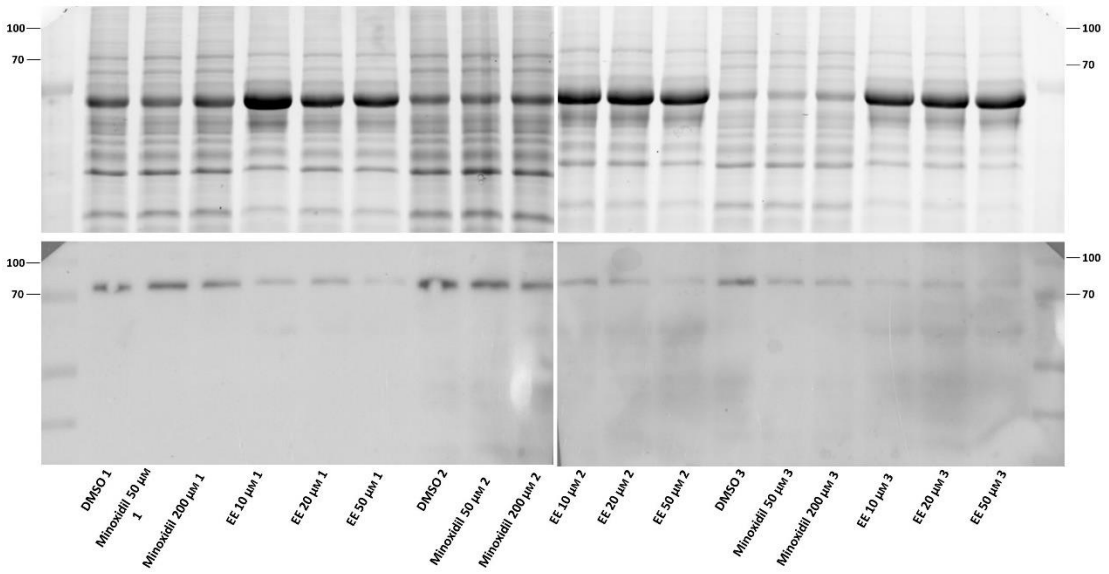

Supplementary Figure 11. Western blot of PLOD2 expression experiment.

The three replicates for the PLOD2 expression experiment are shown. Top panel: loading control. Bottom panel: Western blot using a PLOD2 antibody for detection.

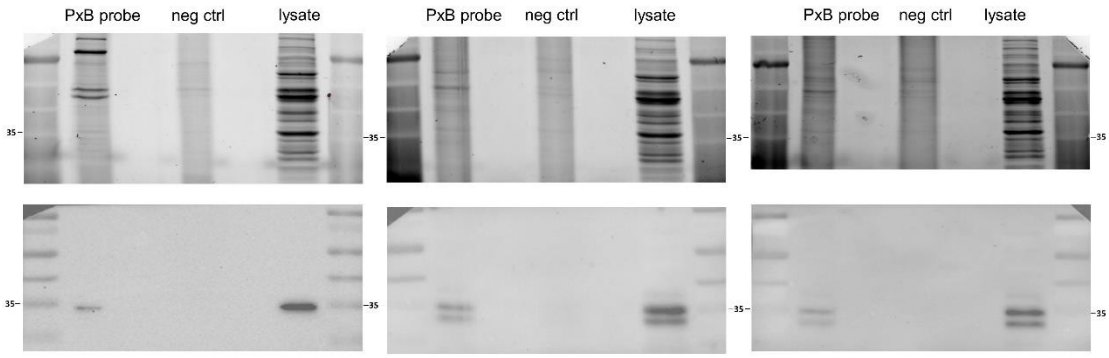

Supplementary Figure 12. Western blot of PxB pull-down with NPC2 fragment containing cell lysate.

The three replicates for the pull-down experiment using a lysate of yeast cells overexpressing the NPC2 fragment identified in the Y3H screen as GAL4 AD fusion are shown. Top panel: loading control. Bottom panel: Western blot using GAL4 AD antibody.

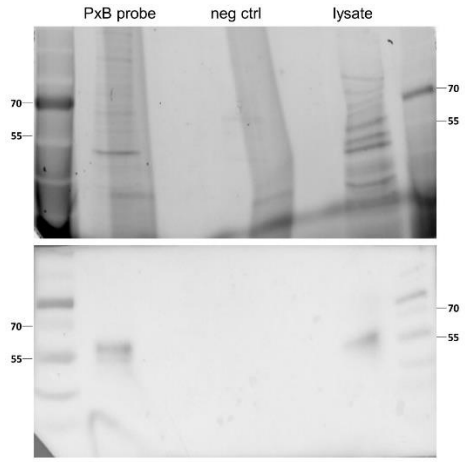

Supplementary Figure 13. Western blot of PxB pull-down with PML fragment containing cell lysate.

The Western blot images for the pull-down experiment using a lysate of yeast cells overexpressing the PML fragment identified in the Y3H screen as GAL4 AD fusion are shown. Top panel: loading control. Bottom panel: Western blot using GAL4 AD antibody.

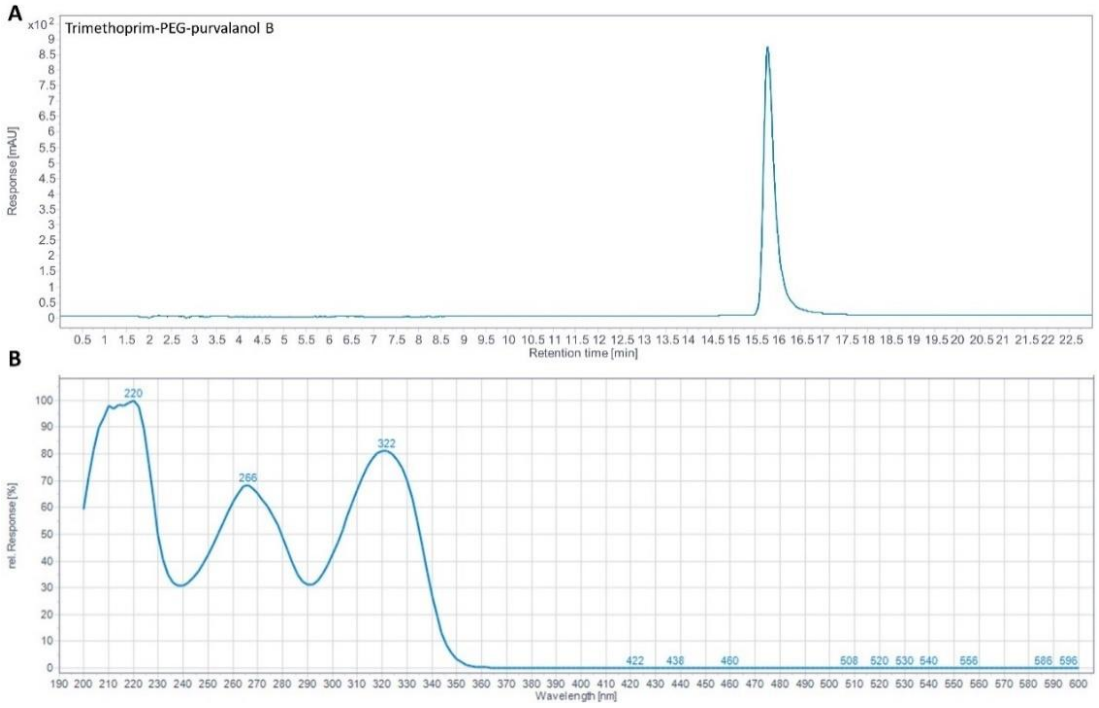

Supplementary Figure 14. Analytical HPL chromatogram and UV spectrum of trimethoprim-PEG-purvalanol B.

A. HPLC analysis of trimethoprim-PEG-purvalanol B at 220 nm indicated the retention time at 15.7 min. B. UV/Vis online spectra of trimethoprim-PEG-purvalanol B.

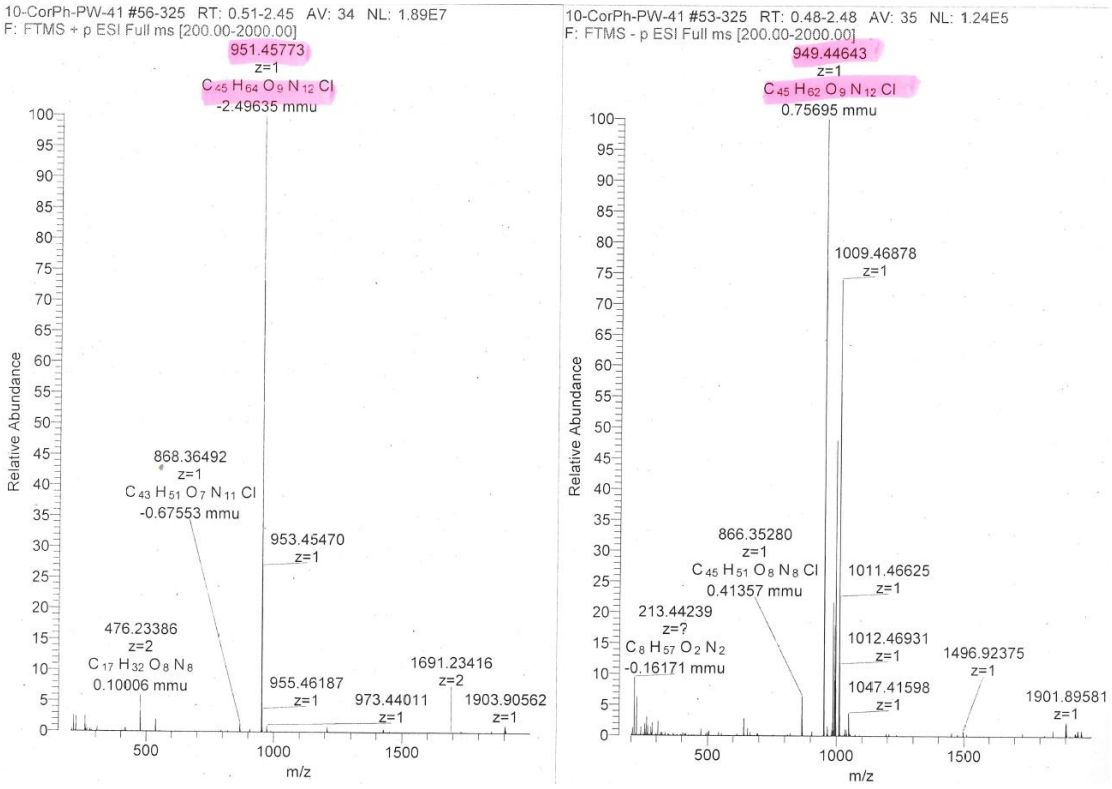

Supplementary Figure 15. HR-ESI-MS spectrum of trimethoprim-PEG-purvalanol B.

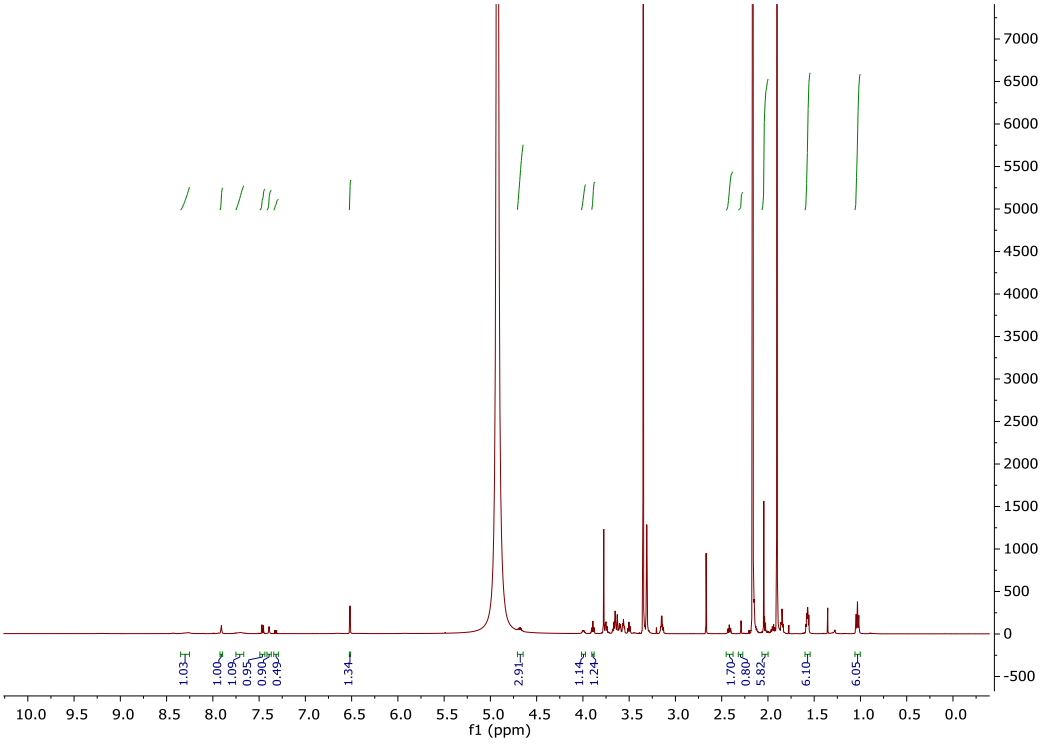

Supplementary Figure 16. NMR spectrum of trimethoprim-PEG-purvalanol B.

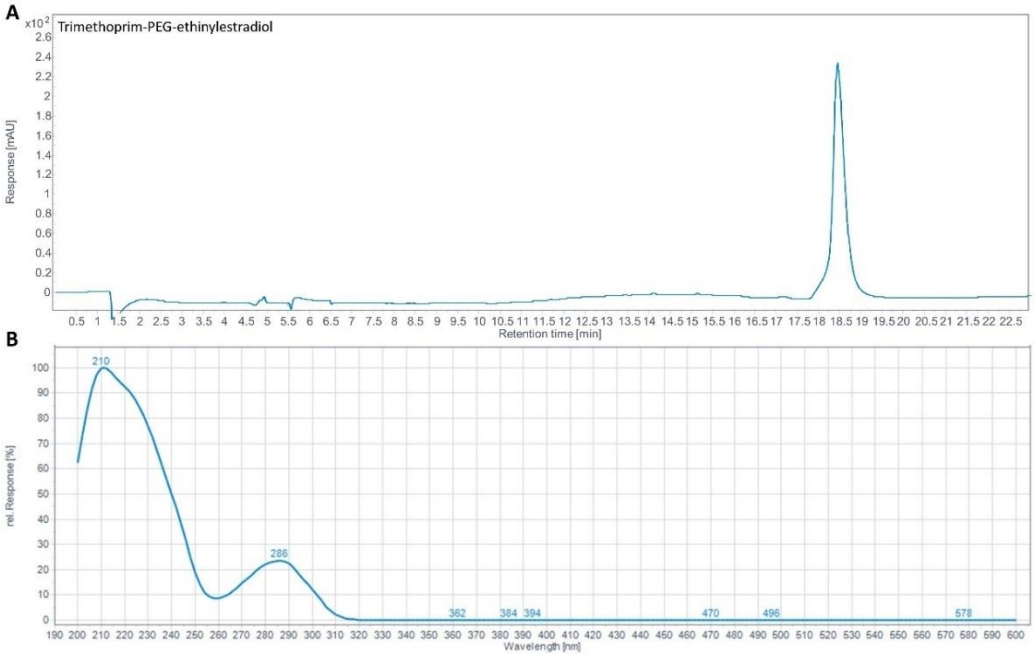

Supplementary Figure 17. Analytical HPL chromatogram and UV spectrum of trimethoprim-PEG-ethinylestradiol.

A. HPLC analysis of trimethoprim-PEG-ethinylestradiol at 220 nm indicated the retention time of its main peak at 18.4 min. B. UV/Vis online spectra of trimethoprim-PEG-ethinylestradiol.

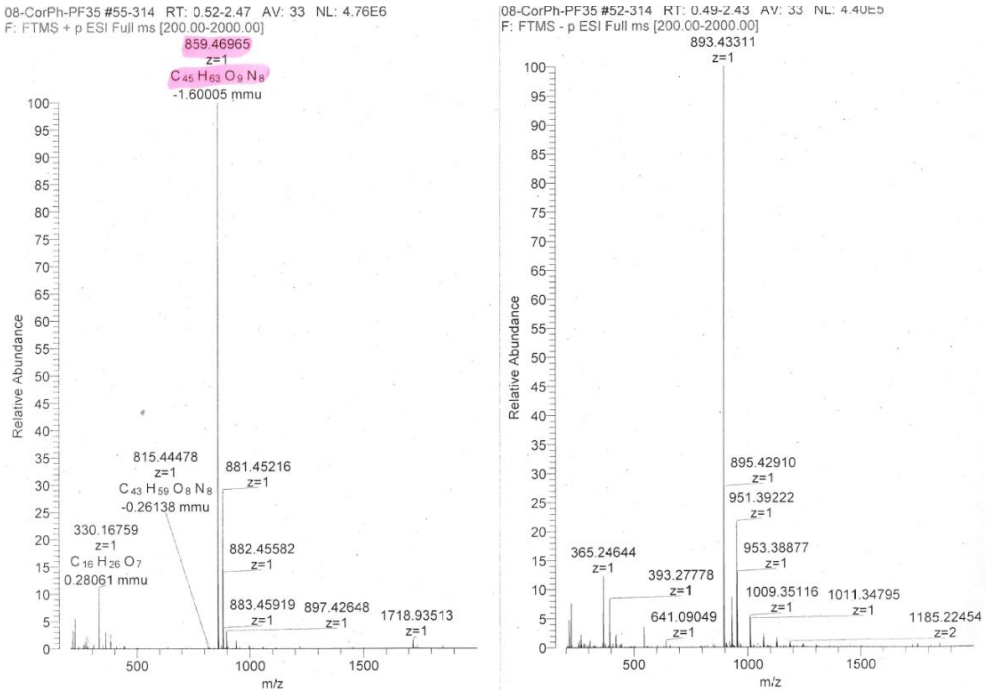

Supplementary Figure 18. HR-ESI-MS spectrum of trimethoprim-PEG-ethinylestradiol.

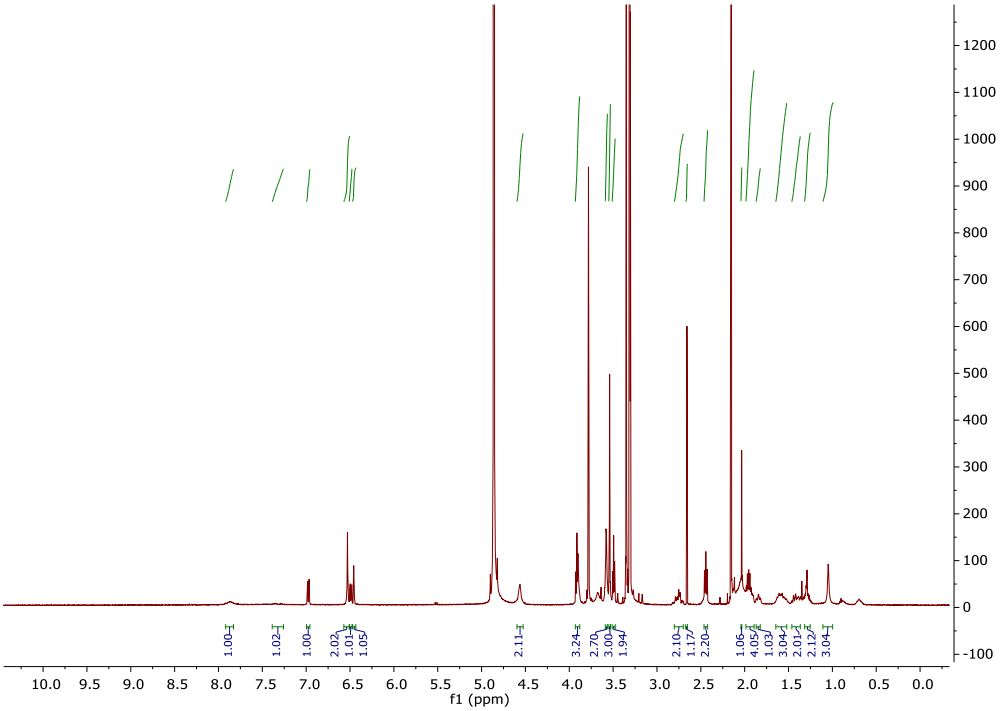

Supplementary Figure 19. NMR spectrum of trimethoprim-PEG-ethinylestradiol.

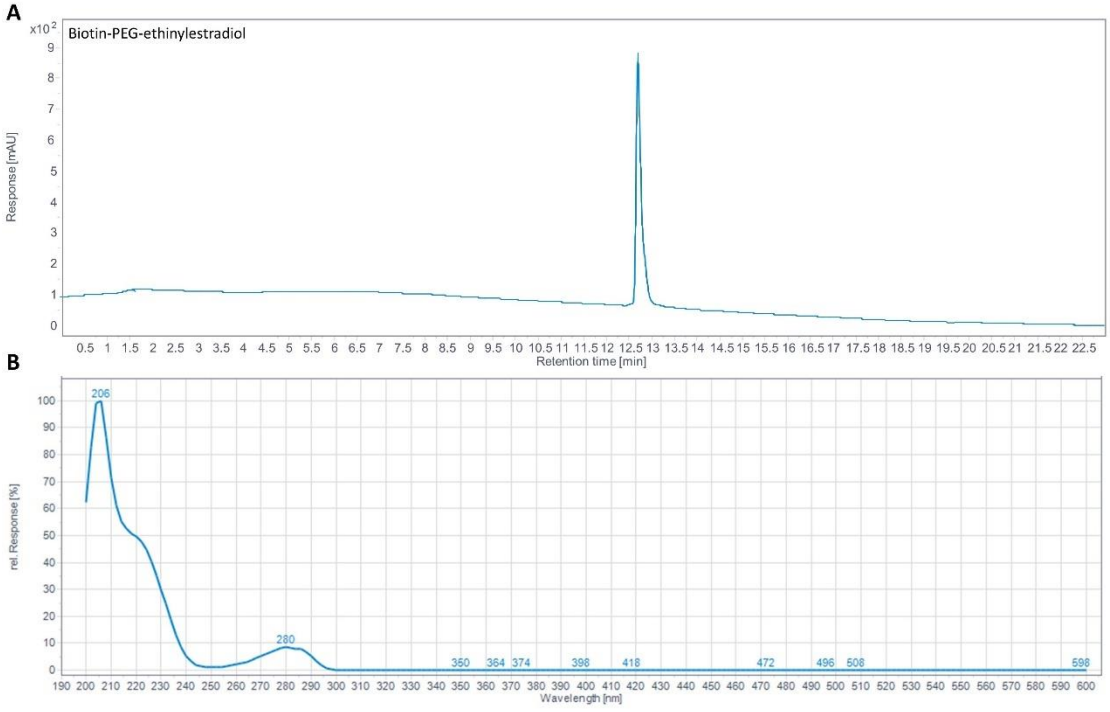

Supplementary Figure 20. Analytical HPL chromatogram and UV spectrum of biotin-PEG-ethinylestradiol.

A. HPLC analysis of biotin-PEG-ethinylestradiol at 220 nm indicated the retention time of its main peak at 12.7 min. B. UV/Vis online spectra of biotin-PEG-ethinylestradiol.

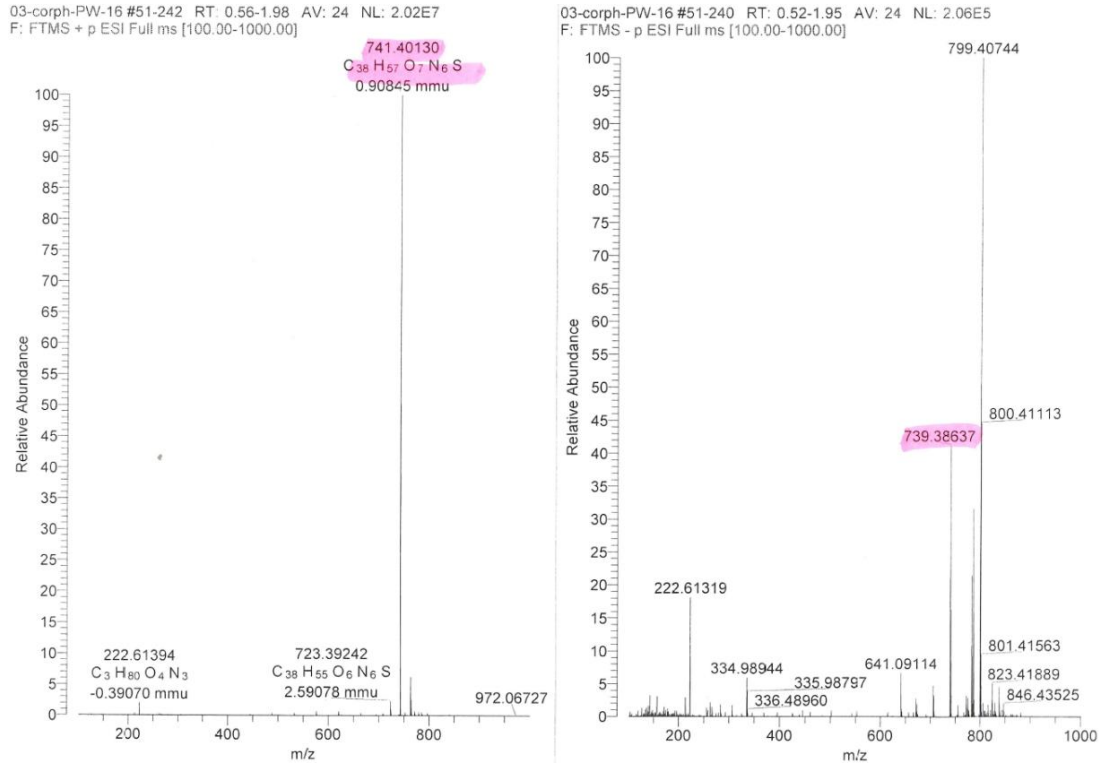

Supplementary Figure 21. HR-ESI-MS spectrum of biotin-PEG-ethinylestradiol.

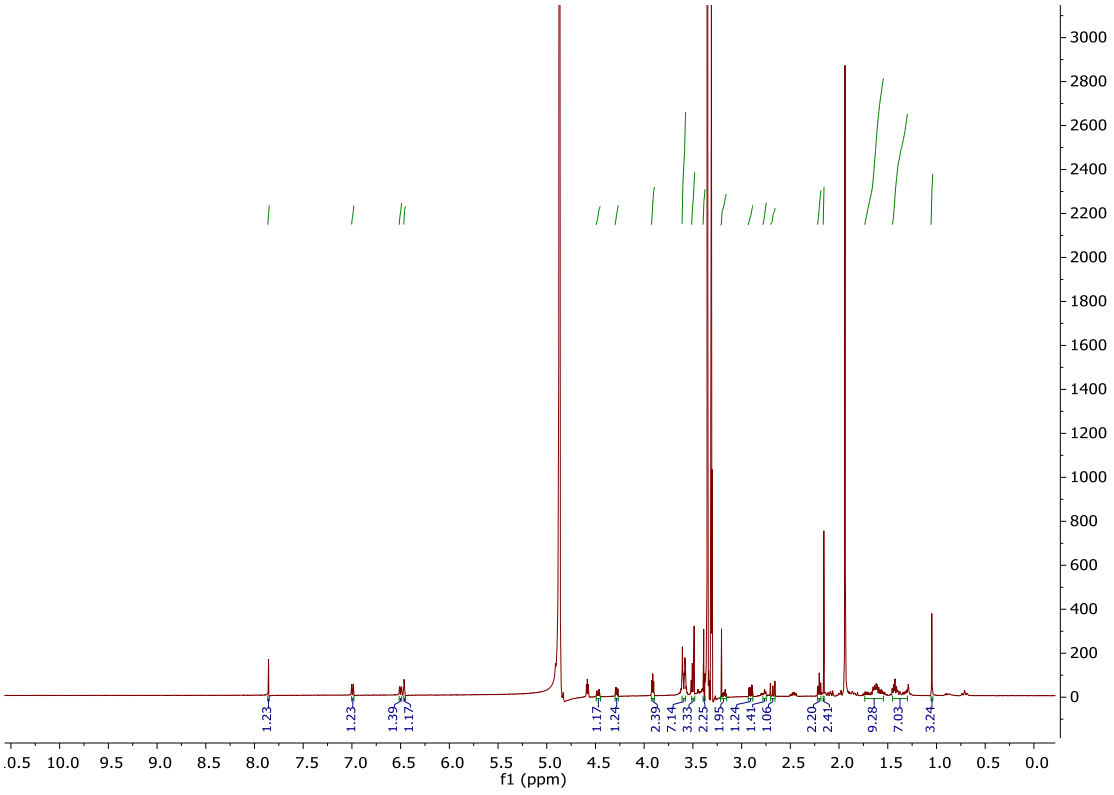

Supplementary Figure 22. NMR spectrum of biotin-PEG-ethinylestradiol.

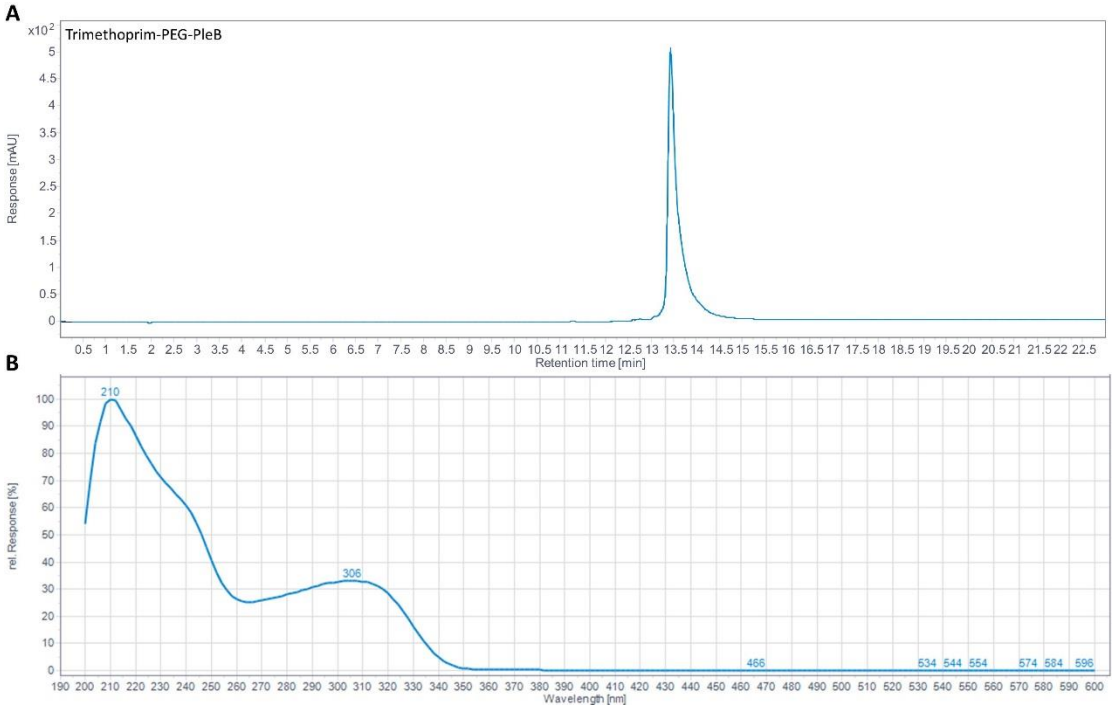

Supplementary Figure 23. Analytical HPL chromatogram and UV spectrum of trimethoprim-PEG-PleB.

A. HPLC analysis of trimethoprim-PEG-PleB at 220 nm indicated the retention time of its main peak at 13.4 min. B. UV/Vis online spectra of trimethoprim-PEG-PleB.

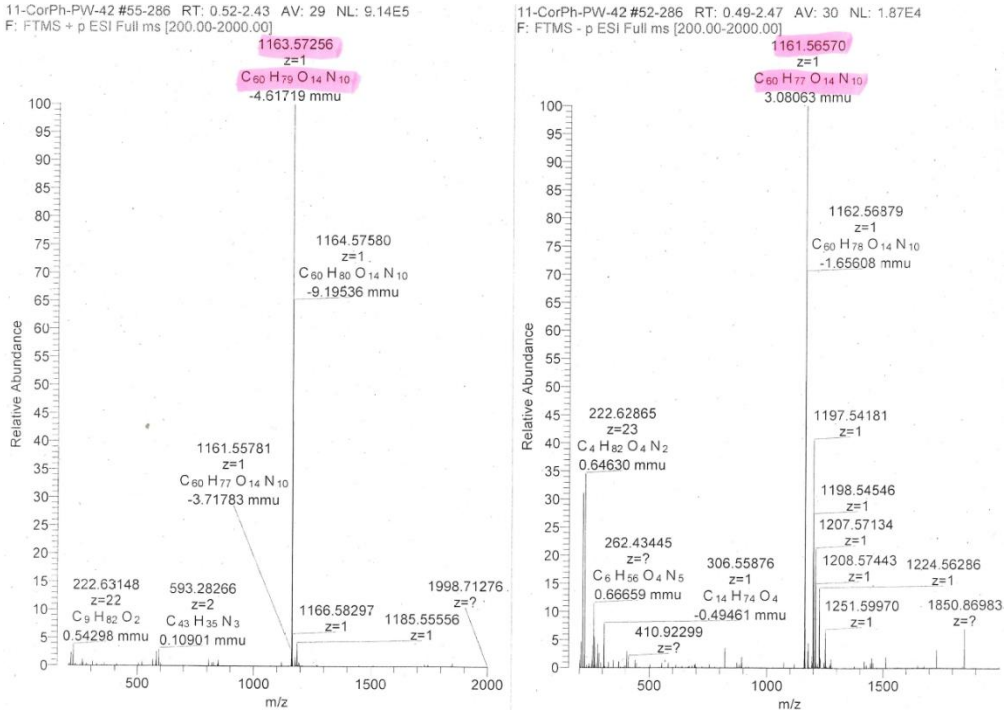

Supplementary Figure 24. HR-ESI-MS spectrum of trimethoprim-PEG-PleB.

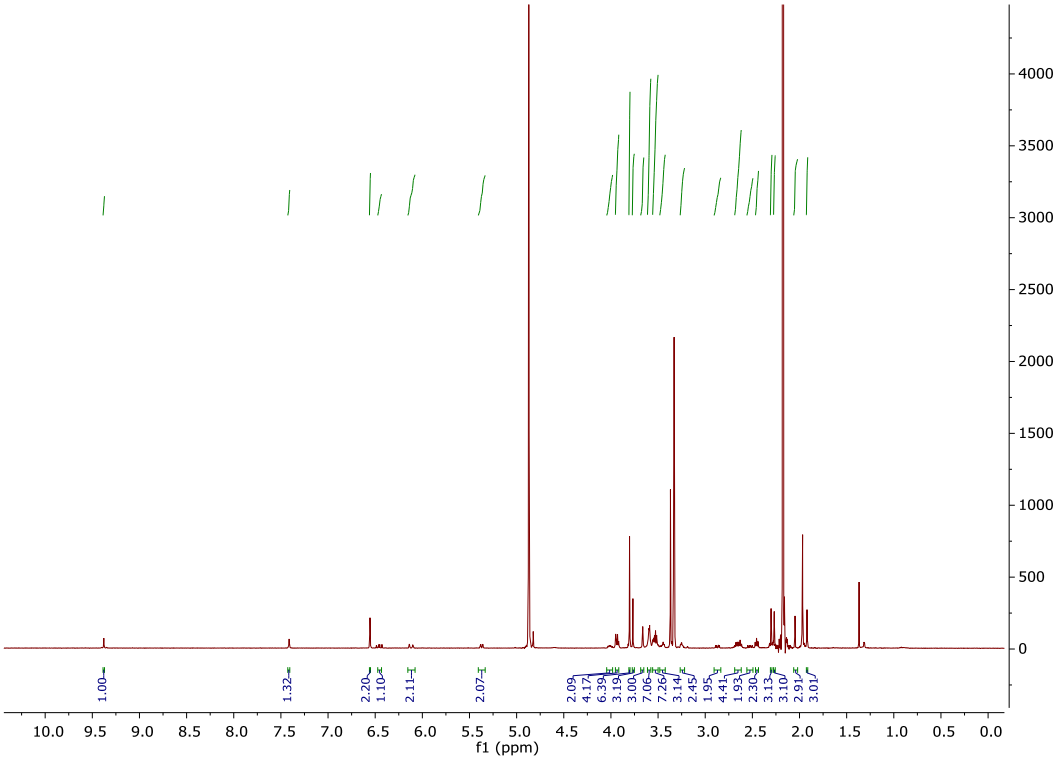

Supplementary Figure 25. NMR spectrum of trimethoprim-PEG-PleB.

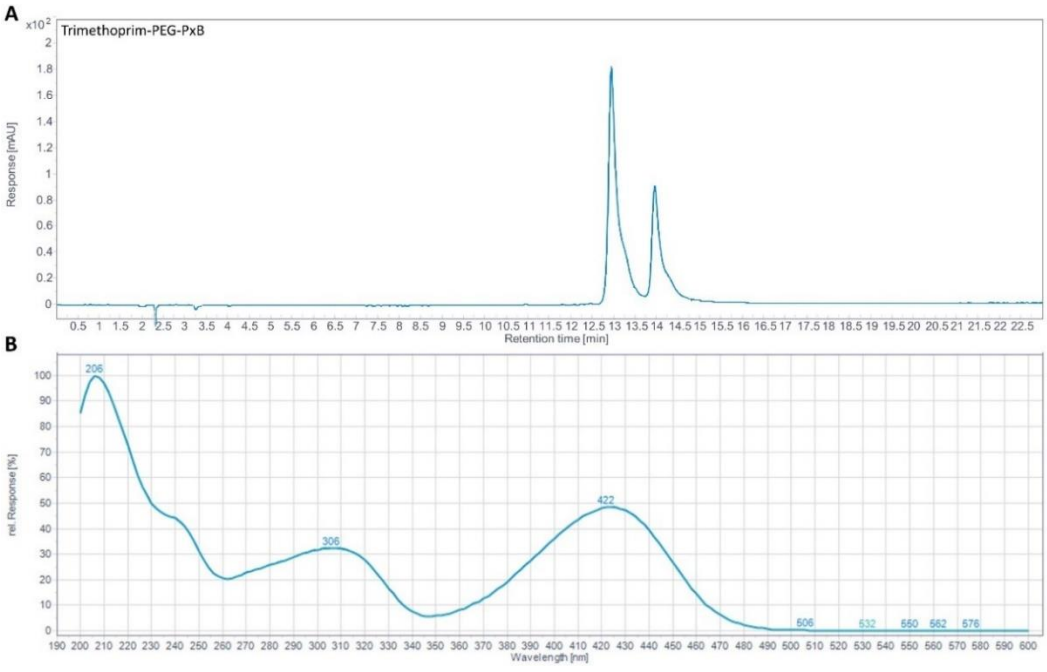

Supplementary Figure 26. Analytical HPL chromatogram and UV spectrum of trimethoprim-PEG-PxB.

A. HPLC analysis of trimethoprim-PEG-PxB at 420 nm indicated the retention time of its main peaks at 12.9 min and 13.9 min. B. UV/Vis online spectra of trimethoprim-PEG-PxB.

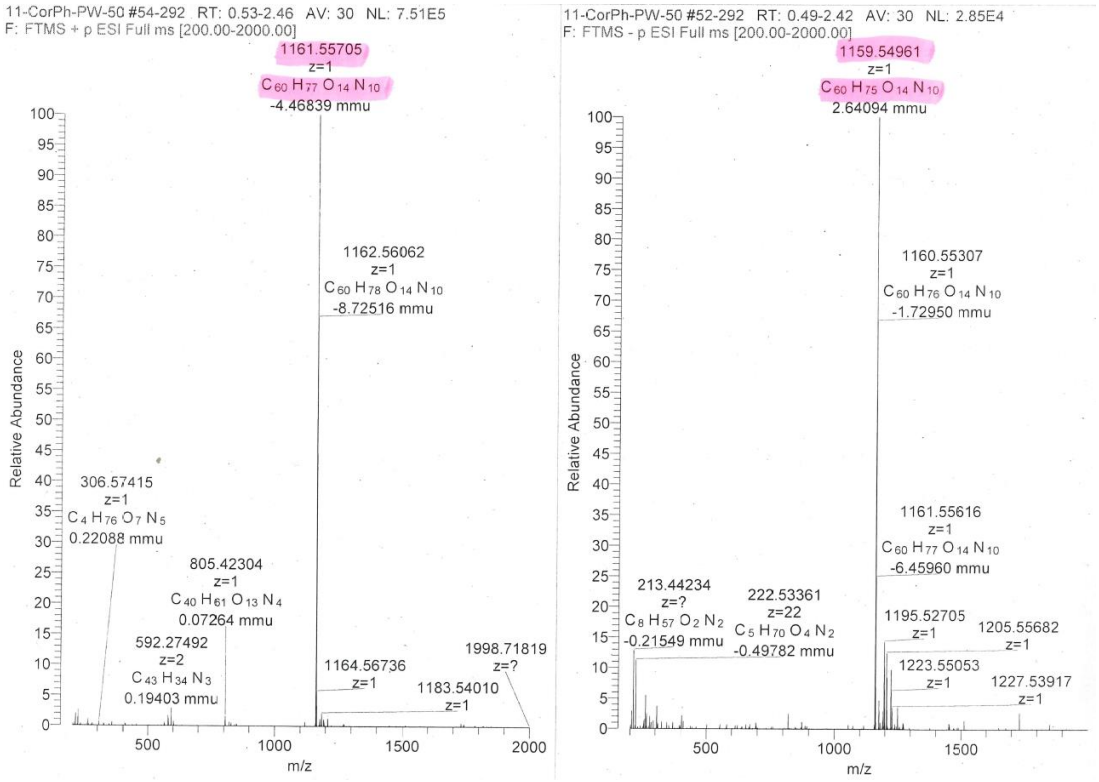

Supplementary Figure 27. HR-ESI-MS spectrum of trimethoprim-PEG-PxB.

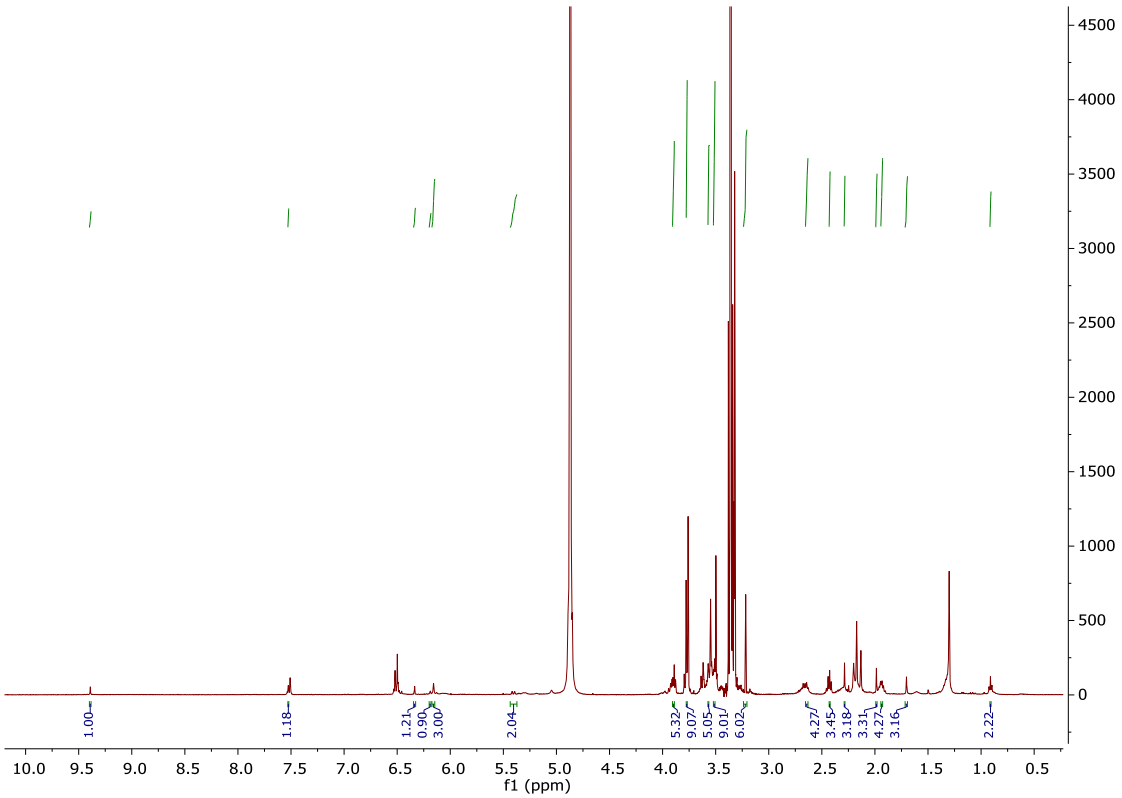

Supplementary Figure 28. NMR spectrum of trimethoprim-PEG-PxB.

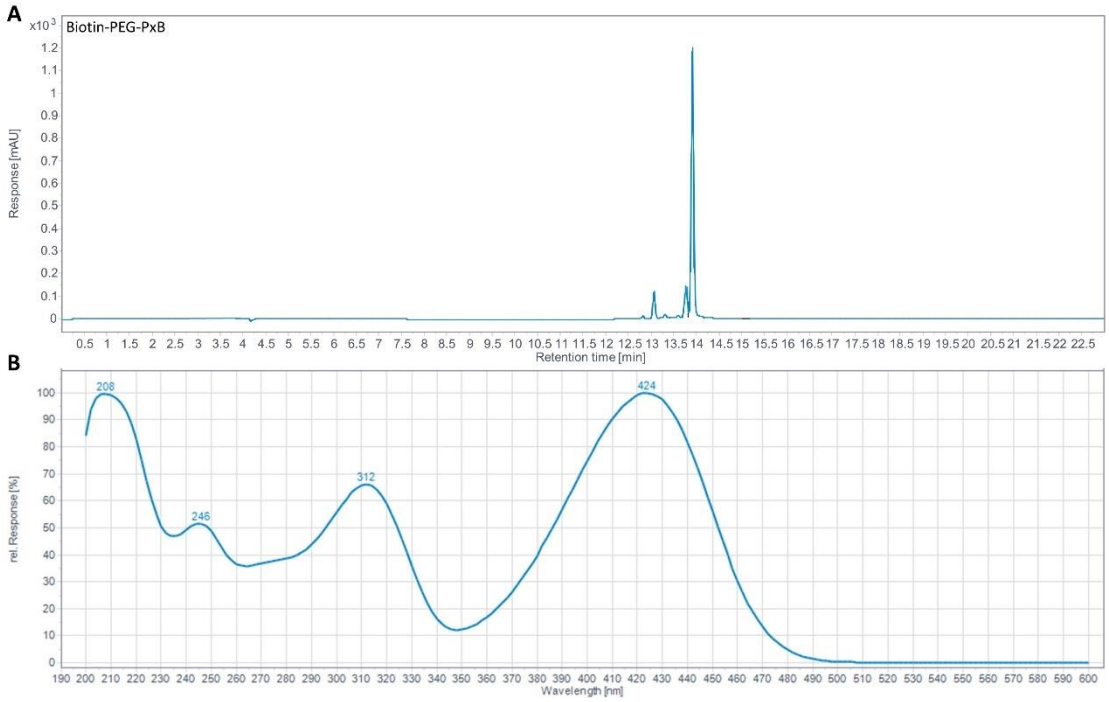

Supplementary Figure 29. Analytical HPL chromatogram and UV spectrum of biotin-PEG-PxB.

A. HPLC analysis of biotin-PEG-PxB at 420 nm indicated the retention time of its main peaks at 13.0 min and 13.9 min. B. UV/Vis online spectra of biotin-PEG-PxB.

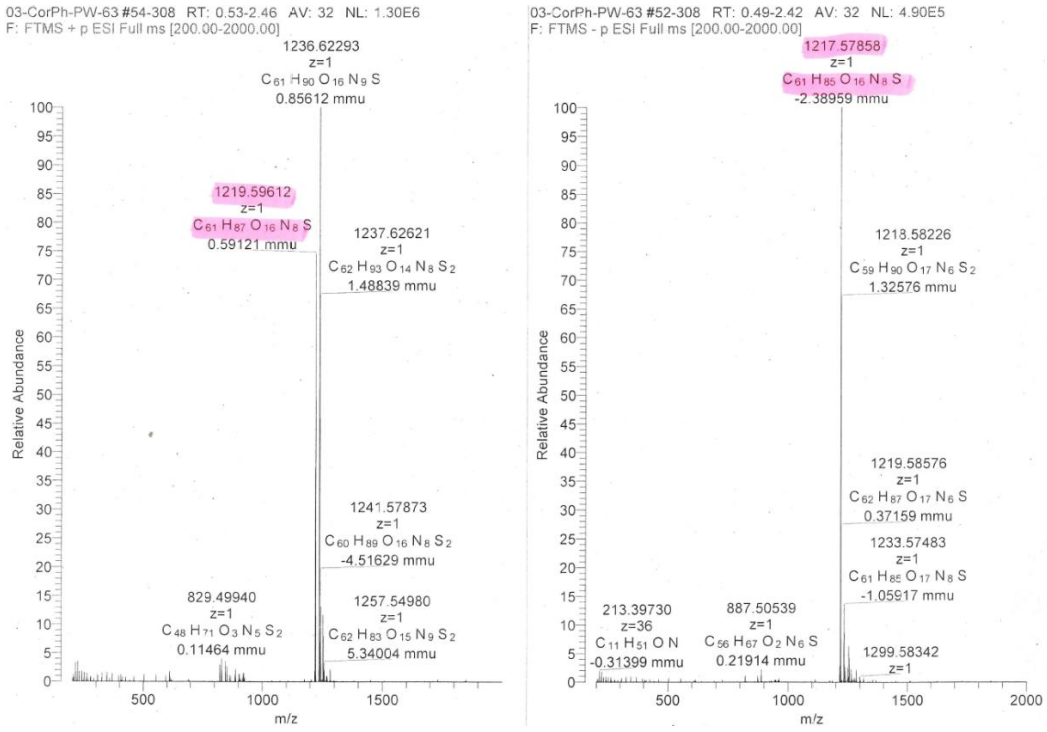

Supplementary Figure 30. HR-ESI-MS spectrum of biotin-PEG-PxB.

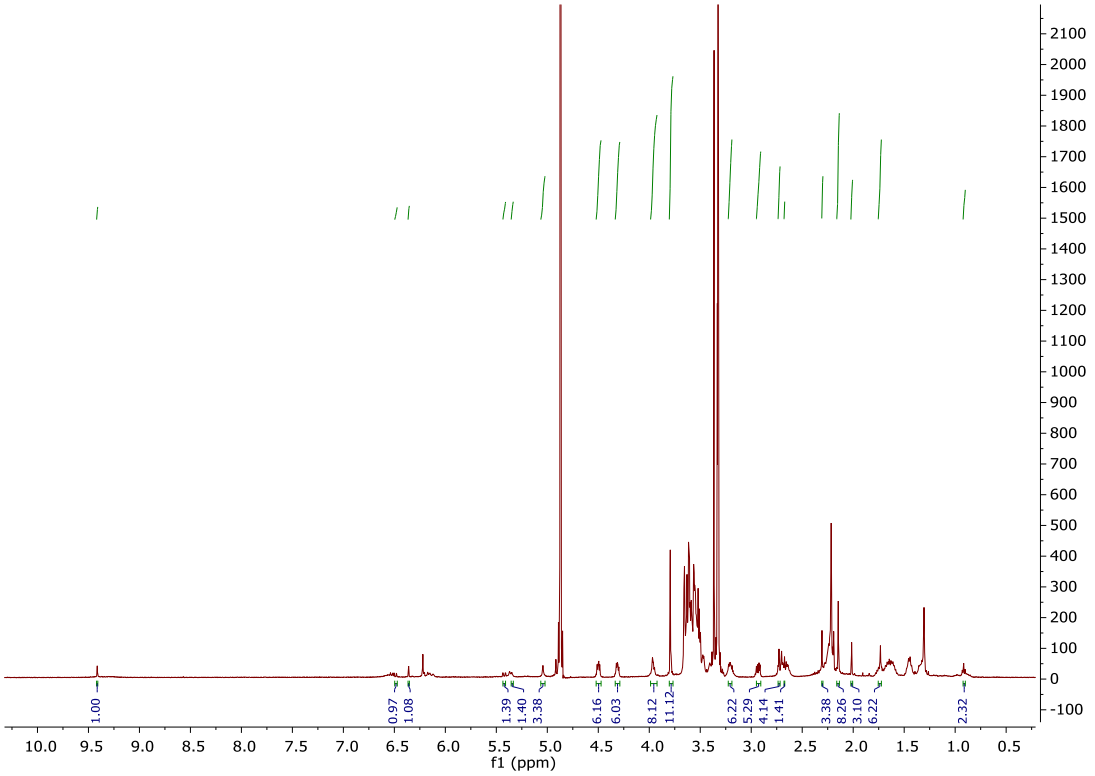

Supplementary Figure 31. NMR spectrum of biotin-PEG-PxB.

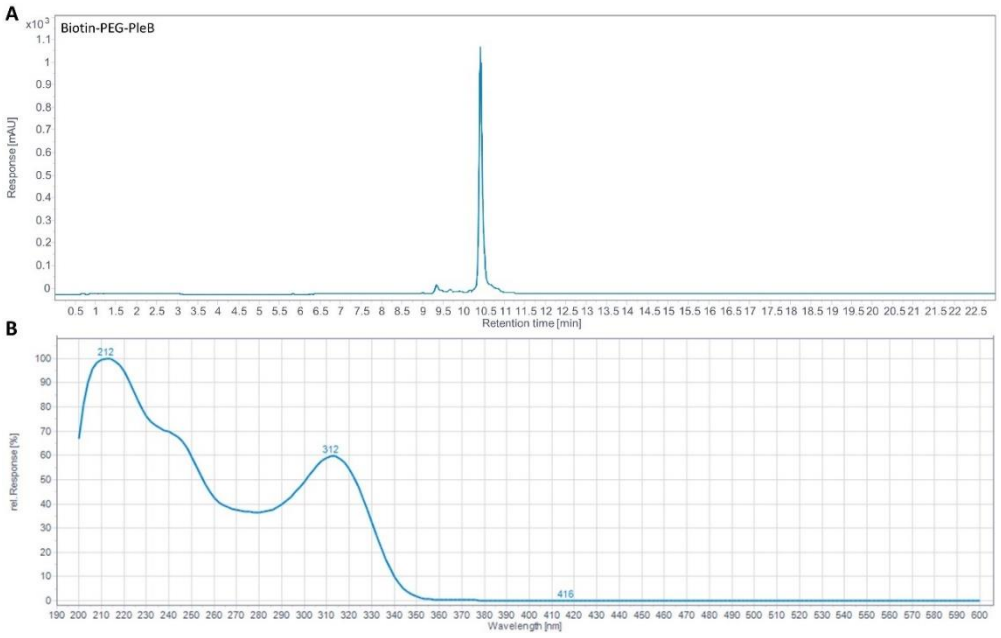

Supplementary Figure 32. Analytical HPL chromatogram and UV spectrum of biotin-PEG-PleB.

A. HPLC analysis of biotin-PEG-PleB at 320 nm indicated the retention time of its main peak at 10.4 min. B. UV/Vis online spectra of biotin-PEG-PleB.

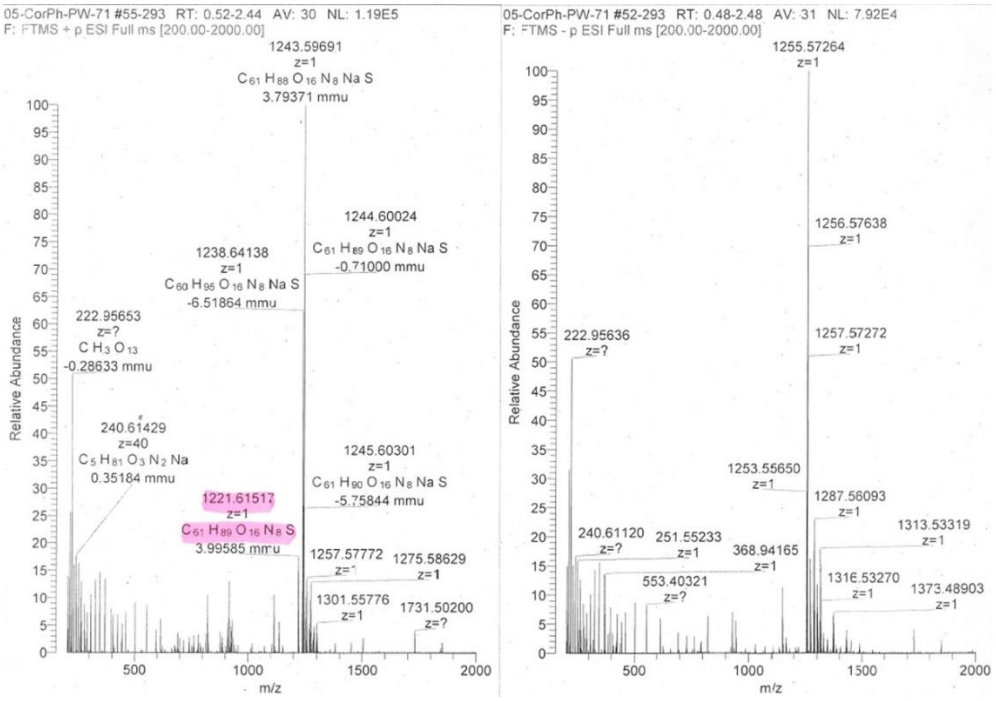

Supplementary Figure 33. HR-ESI-MS spectrum of biotin-PEG-PleB.

7.2 Abbreviations

Abbreviation	Term
°C	Degree celsius
ANOVA	Analysis of variance between groups
APS	Ammonium persulfate
BSA	Bovine serum albumin
cDNA	Complementary DNA
cm, cm^2	Centimetre, Square centimetre
Chl	Chlorophyll
Cj	*Cercidiphyllum japonicum*
DCM	Dichloromethane
DMEM	Dulbecco's Modified Eagle Medium
DMSO	Dimethyl sulfoxide
DNA	Deoxyribonucleic acid
DTT	Dithiothreithol
ECL	Enhanced chemiluminescence
EDTA	Ethylenediaminetetraacetic acid
EE	Ethinylestradiol

Abbreviation	Term
EGTA	Ethylene glycol-bis(2-aminoethylether)-N,N,N′,N′-tetraacetic acid
ESI	Electrospray ionization
et al.	And others
FCS	Fetal calf serum
FITC	Fluorescein isothiocyanate
g	Gram
h	Hour
HPLC	High-performance liquid chromatography
HR	High resolution
Hz	Hertz
IC50	Half maximal inhibitory concentration
kDa	Kilodalton
l	Liter
k	Kilo
M	Molar
mg, ml, mM, mm	Milligram, milliliter, millimolar, millimetre
min	Minute
MS	Mass spectrometry
nM, nm	Nanomolar, Nanometre
NMR	Nuclear magnetic resonance
ns	Not significant
PAGE	Polyacrylamide gel electrophoresis
PB	Phyllobilin
PBS	Phosphate-buffered saline
PCR	Polymerase chain reaction
PEG	Polyethylene glycol
pH	Potential of hydrogen
PleB	Phylloleucobilin
PluB	Phyllolumibilin
Po	*Platanus occidentalis*
PrB	Phylloroseobilin
PurB	Purvalanol B
PxB	Phylloxanthobilin
PVDF	Polyvinylidene difluoride

Abbreviation	Term
rpm	Revolutions per minute
RT	Room temperature
R_t	Retention time
s	Second
SEM	Standard error of the mean value
SD	Standard deviation
SDS	Sodium dodecyl sulfate
SDS-PAGE	Sodium dodecyl sulfate-polyacrylamide gel electrophoresis
TBS-T	Tris-buffered Saline with Tween 20
TBTA	Tris[(1-benzyl-1H-1,2,3-triazol-4-yl)methyl]amine
T/E	Trypsin/EDTA
TEMED	N, N, N', N' tetramethylethylene diamine
TIRF	Total internal reflection fluorescence
TLC	Thin layer chromatography
Tris	Trishydroxymethylaminomethane
UV	Ultraviolet
V	Volt
VIS	Visible
v/v	Volume per volume
w/v	Weight per volume
µg, µl, µM, µm	Microgram, microliter, micromolar, micrometre
Y2H	Yeast two-hybrid
Y3H	Yeast three-hybrid
3-AT	3-amino-1,2,4-triazole

Table 11. List of Abbreviations

7.3 Index of figures

7.4 Index of tables

7.5 List of publications

Wang, P., Klassmüller, T., Karg, C.A., Kretschmer, M., Zahler, S., Braig, S., Bracher, F., Vollmar, A.M. and Moser, S. (2022). Using the yeast three-hybrid system for the identification of small molecule-protein interactions with the example of ethinylestradiol. *Biological Chemistry*, *403*(4), 421-431.

Wang, P., Karg, C.A., Frey, N., Frädrich, J., Vollmar, A.M. and Moser, S. (2021). Phyllobilins as a challenging diverse natural product class: Exploration of pharmacological activities. *Archiv der Pharmazie*, *354*(10), 2100061.

Karg, C. A., **Wang, P.**, Kluibenschedl, F., Müller, T., Allmendinger, L., Vollmar, A.M., & Moser, S. (2020). Phylloxanthobilins are Abundant Linear Tetrapyrroles from Chlorophyll Breakdown with Activities Against Cancer Cells. *European Journal of Organic Chemistry, 2020*, 4499-4509.

Karg, C. A., **Wang, P.**, Vollmar, A. M., & Moser, S. (2019). Re-opening the stage for *Echinacea* research - Characterization of phylloxanthobilins as a novel anti-oxidative compound class in *Echinacea purpurea*. *Phytomedicine, 60*, 152969.

ACKNOWLEDGEMENT

8 Acknowledgement

First and foremost, I would like to express my deep and sincere gratitude to Frau Prof. Dr. Angelika M. Vollmar, for giving me the opportunity to do research in your group and providing invaluable guidance throughout my time here. It was a great privilege to work and study in your group, where you created such a wonderful environment for us to grow. Your vision, humanity, wisdom and extraordinary energy have deeply inspired me. I can't speak enough about how your smile calms me down and literally gives me hope every time I talk to you or even only see you. Thanks again for welcoming me and embracing me from my first day.

I want to give my biggest thanks to Frau Dr. Simone Moser for excellent supervision during my PhD study. Dear Simone, thanks for your continuous patience and support starting from our first call when I was still back in China. You led me to this fascinating world of natural products and helped me build my knowledge around it from scratch. As my supervisor and the leader of our group, you not only give me best advices on a daily basis but also care about me, about my work, my life and my future. Without you, I might not be able to survive abroad, let alone to finish a PhD. I can't ask for a better mentor than you, and I hope I didn't let you down.

I would also like to thank Herr Prof. Dr. Stefan Zahler. Thanks for all of your kind help and timely advices. Besides, if it weren't you that forwarded my email to Simone, I won't get the opportunity to come to Germany.

I want to sincerely acknowledge the time and interest of the members of my defense committee: Prof. Dr. Franz Bracher, Prof. Dr. Ulrich Lächelt, Prof. Dr. Olivia Merkel and Prof. Dr. Wolfgang Frieß. Thank you for accepting my invitation and spending your time on reviewing on my thesis.

I would like to give my special gratitude to Dr. Cornelia Karg. Dear Conny, although I almost thank you every day, I still think that's not enough. You are always there for me no matter what kind of stupid questions I asked you or what kind of help I needed from

you. You are so good at everything that you seem to be capable of doing everything perfectly. Therefore, it's really difficult for me to do something for you in return of your endless favor. I hope I still have some chances in the future.

Thanks to our phyllobilin team: Kerstin, Rita, Patricia, Elke and Christian. It's been a pleasure to work with you and learn from you. I want to thank all my colleagues in AK Vollmar. Themis, Flo G, Daniel, Martin, Karin, Olgo, Chrissi and Caro, thanks for welcoming me and helping me when I came to the lab. I still remember the first day we spent at Oktoberfest. Thanks to Shuaijun, Lucas, Yudong and Ling for being friends to me and helping each other far away from home. Thanks to Maibritt, Adrian, Franz, Flo L, Mehak, Julia, Jana, Christina, Amélie and Frau Schnegg for all your kind help and amazing days in the lab. I really enjoyed my four years in AK Vollmar.

I would like to thank the China Scholarship Council for offering me the opportunity to study abroad and support me financially.

I want to thank my friends for supporting me and keeping in touch with me. Although I haven't seen most of you for almost 4 years, I know we are still together.

More importantly, I want to thank my family. Thank my dad and my mom for all the incredible support and encouragement. You always take care of me and give me the best without asking anything in return. You are definitely the best parents. Thank my brother for looking after my parents while I'm away. I love you all.

At last, I would like to thank my dear Chang. I am so lucky and blessed that I could meet you. The love I received from you lighted up my life during my darkest hours. You gave me the strength and never doubted that I could finish my PhD. The support and encouragement you gave me is just beyond my wildest expectation. I will always remember and be grateful about the sacrifice you made for me, and it would be absolutely impossible for me to finish this thesis without you. Thank you from the bottom of my heart. I love you!